PROTEINS IN ENAMEL DEVELOPMENT: SECRETOME, TRANSPORT AND POSTTRANSLATIONAL FATE

A Dissertation

by

MIRALI GAURANG PANDYA

Submitted to the Office of Graduate and Professional Studies of
Texas A&M University
in partial fulfillment of the requirements for the degree of

DOCTOR OF PHILOSOPHY

Chair of Committee,	Thomas Diekwisch
Committee Members,	Xianghong Luan
	Phillip Kramer
	Reginald Taylor
Head of Department,	Larry Bellinger

August 2019

Major Subject: Oral Biology

ABSTRACT

Amelogenesis is a process involving formation of mineralized tooth enamel by ameloblast cells. During amelogenesis, ameloblasts secrete matrix consisting of enamel proteins that facilitate future enamel prism formation. In this study, we focused on understanding the transportation and fate of enamel proteins from the time of secretion in the enamel matrix to the stage where the fragments come in contact with the initial enamel prisms and thereafter. For the first part, we used focused on the transportation part of proteins using *Phospho1* knockout mice to understand the role of secretory vesicles in ameloblasts and the transportation of proteins through ameloblasts. Our study demonstrated the presence of PHOSPHO1 protein in ameloblasts including the enamel layer and the ameloblast Tomes' processes. The effect of disruption of the vesicular coat protein in *Phospho1 -/-* mice significantly affected physiological enamel mineralization. A loss of enamel prism organization was observed and a 25% increase in enamel layer was noted indicating the retention of enamel proteins in the matrix due to transportation failure. *Phospho1 -/-* mice indicated that the matrix vesicular protein PHOSPHO 1 is an integral part of enamel mineralization process. For the second part, our intent was to use a mouse molar model to establish a temporo-spatial correlation of the events occurring through the different stages of enamel development and document the consequential changes in the enamel matrix proteins. Our proteomic analysis identified some novel proteins which may also play a key role during amelogenesis. The final part of the study focuses on amelogenin and its fate once it is secreted in the matrix. Our data demonstrates that the protein matrix configuration changes substantially from the time it is transported through the ameloblasts and the amelogenin fragmentation plays a major role in enamel crystal growth. The Western blot analysis of enamel

matrix from different layers of porcine enamel tooth organ documented the close association of amelogenin C-terminus with the apatite crystal surface while the N-terminus fragments are likely retained in between the growing enamel crystals indicating perhaps the C-terminal fragments help with prism growth in C-axis direction while N-terminal fragments maintain the inter-prismatic distance.

DEDICATION

To my husband for his continued patience, love and support through this challenging and wonderful journey.

ACKNOWLEDGEMENTS

The last four years have been the most memorable of my life. My pivotal and defining growth as an individual, both personally and professionally, has been a result of the immense support and encouragement that I have received from Dr. Thomas Diekwisch, my guide and my mentor. His vision, guidance and invaluable inputs have been critical in shaping each and every step of this exciting and wonderful journey. Furthermore, his passion towards dental research and the zeal to empower his students have inspired me to be steadfast in the face of failure, provided the courage to transform dreams into reality and above all, instilled in me the confidence to pursue a career as a clinician scientist.

I would like to thank Dr. Xianghong Luan for sharing her experience and insights in enamel research, for helping me with my gene expression experiments and for providing valuable suggestions for all my research projects.

I would like to express my sincere gratitude towards Dr. Phillip Kramer and Dr. Reginald Taylor for being a part of my committee and for all their guidance throughout the years.

My sincere thanks to Dr. Kathy Svoboda, our program director, for her support and guidance. I also want to thank Dr. Yongbo Lu, Dr. Feng Tao, and the BMS faculty for the GSA meetings and Dr. Lynn Opperman for organizing the colloquium which significantly helped enhance my presentation skills and critical scientific thinking.

A special thanks to Dr. Larry Bellinger's office for organizing seminars with distinguished speakers and the graduate research staff, Kim, Marge, Nancy and everyone for their help throughout the program.

My thanks to Dr. Qin for being my cognate examiner and for generously allowing me to use the X-Ray machine in his lab.

The animal experiments for the studies would not have been possible without the help from Priscilla, Gerald, and Richard.

Words are not enough to express the help and support I received from my lab members, Connie, Dr. Gokul Gopinathan, and Ma Wei, without whom this journey would not have been the same, and my friends and colleagues Wedad, Qian, Sufang, Ke, Lily, Bei, Rajay, Mickey and all graduate students who made this experience truly remarkable.

Finally, my loving husband Hitesh, whom I can't thank enough for the encouragement to be fearless and follow my passion for science and research.

CONTRIBUTORS AND FUNDING SOURCES

Contributors

This work was supervised by a dissertation committee consisting of Dr. Thomas Diekwisch, Chair of Department of Periodontics, Dr. Xianghong Luan of the Department of Periodontics, Dr. Phillip Kramer of Department of Biomedical Sciences and Dr. Reginald Taylor of Department of Orthodontics.

The *Phospho1* knockout mice for Chapter 1 were a generous gift from Dr. José L. Millán of Sanford Children's Health Research Center, Sanford-Burnham institute for Medical Research, La Jolla, CA.

The proteomics and informatics services for Chapter 2 were performed at the CBC-UIC Research Resources Center Mass Spectroscopy, Metabolomics, and Proteomics facility.

M Pandya wrote the manuscripts and performed the majority of the experiments and TGHD designed the studies and edited the writing.

Funding Sources

Funding for the studies was provided by NIDCR grant DE18900 to TGHD and College of Dentistry start-up funds to TGHD.

TABLE OF CONTENTS

Page

ABSTRACT ii
DEDICATION iv
ACKNOWLEDGEMENTS v
CONTRIBUTORS AND FUNDING SOURCES vii
LIST OF FIGURES xi
1. INTRODUCTION - INTRAVESICULAR PHOSPHATASE PHOSPHO1 FUNCTION IN ENAMEL MINERALIZATION AND PRISM FORMATION 1
1.1. Overview 1
1.2. Introduction 2
1.3. Materials and Methods 4
1.3.1. Animal models and biosafety 4
1.3.2. Ultrathin ground sections of control and Phospho1$^{-/-}$ mouse mandibles 5
1.3.3. Radiographs 5
1.3.4. Micro-CT Analysis 5
1.3.5. Scanning Electron Microscopy (SEM) and Energy Dispersive X-ray Spectroscopy (EDS) 6
1.3.6. Transmission electron microscopy 6
1.3.7. Paraffin sections and immunohistochemistry 7
1.3.8. Western Blot 7
1.3.9. Statistical Analysis 8
1.4. Results 9
1.4.1. PHOSPHO1 protein localization in the enamel layer and the walls of secretory vesicles 9
1.4.2. Decreased enamel mineralization and loss of sharp incisal tips in Phospho1-/- mice 10
1.4.3. Disintegration and loss of enamel prism structure in Phospho1-/- mouse enamel 11
1.4.4. Presence of mineral precipitates in ameloblast secretory vesicles as revealed by transmission electron microscopy 11
1.5. Discussion 12
1.6. References 15
2. INTEGRATIVE TEMPORO-SPATIAL, MINERALOGIC, SPECTROSCOPIC AND PROTEOMIC ANALYSIS OF POSTNATAL ENAMEL DEVELOPMENT IN TEETH WITH LIMITED GROWTH 23

Page

2.1.Overview....23
2.2. Introduction....24
2.3. Materials and Methods....27
2.3.1. Vertebrate animals and tissue preparation....27
2.3.2. Enamel thickness measurements and polarized light microscopy....27
2.3.3. X-ray powder diffraction....28
2.3.4. Attenuated total reflectance Fourier transform infrared (ATR-FTIR) Spectroscopy....29
2.3.5. Proteomics sample preparation....29
2.3.6. Nano-scale liquid chromatography....30
2.3.7. Mass spectrometry....30
2.3.8. Proteomics data analysis....31
2.3.9. Western blot....31
2.3.10. Statistical analysis....32
2.4. Results....32
2.4.1. Increasing thickness and birefringence of the developing enamel matrix....32
2.4.2. Single-crystal powder sample X-ray diffraction analysis of the postnatal enamel matrix yields calcium phosphate diffraction patterns on postnatal days 1 and 2, and apatite diffraction patterns from postnatal day 4 onward ..33
2.4.3. Attenuated total reflectance spectra (ATR) demonstrated enhanced secondary structure and increased phosphate and carbonate incorporation into the enamel matrix....33
2.4.4. Proteomics demonstrated unique changes in the enamel organ/enamel matrix protein complex between postnatal days 2, 4, and 6....34
2.4.5. Western blot analysis of hydrophobic enamel proteins illustrated continuously increasing amelogenin levels from 1dpn until 8dpn, while enamelin peaked on days 1 and 2dpn, and ameloblastin on days 1-5dpn....36
2.5. Discussion....37
2.6. References....46
3. POSTTRANSLATIONAL AMELOGENIN PROCESSING AND CHANGES IN MATRIX ASSEMBLY DURING ENAMEL DEVELOPMENT....60
3.1. Overview....60
3.2. Introduction....61
3.3. Materials and Methods....69
3.3.1. Animal experiments and organ culture....69
3.3.2. Transmission electron microscopy....69
3.3.3. Proteins....70
3.3.4. Atomic force microscopy....70

Page

3.3.5. Fluorescent images of aqueous protein assemblies 71
3.3.6. Polyhistidine tag labeling and electron microscopy 72
3.3.7. Western Blot 72
3.3.8. Statistical Analysis 73
3.4. Results 74
3.4.1. Changes in matrix subunit compartment dimensions between secretory vesicle matrix, extracellular enamel protein matrix ("nanospheres"), and pericrystalline protein matrix ("crystal ghosts") 74
3.4.2. Key features of enamel crystal growth in organ culture: (i) granular mineral deposits associated with the enamel matrix framework, (ii) dot-like mineral deposits along elongating initial enamel crystallites, and (iii) "crystal ghost" organic matrix adjacent to forming enamel crystals 75
3.4.3. Linear and 20nm hexagonal/ring-shaped amelogenin protein assemblies on mica surfaces and 20nm globular amelogenin assemblies of Nickel-stained N92 amelogenins on carbon coated grids as revealed via AFM and TEM 76
3.4.4. Western blot analysis reveals parallels between amelogenin fragmentation and changes in matrix organization during enamel protein transport, "nanosphere" assembly, and crystal growth 77
3.5. Discussion 78
3.6. References 84
4. CONCLUSION 93
APPENDIX A 95

LIST OF FIGURES

Page

Figure 1- Chapter 1 : PHOSPHO1 localization in the ameloblast secretory vesicle walls. Reprinted with permission from Frontiers editorial office..... 95

Figure 2 - Chapter 1 : Decreased mineralization in the enamel layer of 30 days old *Phospho1-/-* mice. Reprinted with permission from Frontiers editorial office. 97

Figure 3 - Chapter 1 : Loss of enamel prism structure and crystal organization in *Phospho1-/-* mouse molars. Reprinted with permission from Frontiers editorial office. 99

Figure 4 - Chapter 1 : PHOSPHO1 as an intravesicular apatite nucleation enzyme in ameloblast secretory vesicles. Reprinted with permission from Frontiers editorial office..... 101

Figure 1 - Chapter 2 : First mandibular mouse molar development from postnatal days 1 to 8. Reprinted with permission from Frontiers editorial office..... 103

Figure 2 - Chapter 2 : Mouse molar enamel birefringence and enamel matrix layer dissection for mineral and protein analysis. Reprinted with permission from Frontiers editorial office..... 105

Figure 3 - Chapter 2 : Analysis of the postnatal mouse molar enamel mineral layer. Reprinted with permission from Frontiers editorial office. 107

Figure 4 - Chapter 2 : Comparison between spectral counts of individual proteins identified during postnatal mouse molar enamel development. Reprinted with permission from Frontiers editorial office. 109

Figure 5 - Chapter 2 : Changes in mouse molar enamel matrix protein levels from postnatal day 1 – 8. Reprinted with permission from Frontiers editorial office. 111

Figure 1 - Chapter 3 : Electron micrographs illustrating subunit assembly and structural transformation during initial enamel crystal formation *in vivo*. Reprinted with permission from Frontiers editorial office..... 112

Figure 2 - Chapter 3 : Constituents of first mandibular mouse molar enamel formation in organ culture as revealed by electron microscopy. Reprinted with permission from Frontiers editorial office. 114

Figure 3 - Chapter 3 : Amelogenin protein self-assembly *in vitro*. Reprinted with permission from Frontiers editorial office. 116

Figure 4 - Chapter 3 : Localization of amelogenin fragments in enamel organ, superficial, and deep enamel layers based on fractionated protein extraction and antibody recognition site. Reprinted with permission from Frontiers editorial office. 118

Figure 5 - Chapter 3 : Model explaining enamel crystal formation through matrix assembly and processing. Reprinted with permission from Frontiers editorial office. 120

1. INTRODUCTION - INTRAVESICULAR PHOSPHATASE PHOSPHO1 FUNCTION IN ENAMEL MINERALIZATION AND PRISM FORMATION*

1.1. Overview

The transport of mineral ions from the enamel organ-associated blood vessels to the developing enamel crystals involves complex cargo packaging and carriage mechanisms across several cell layers, including the ameloblast layer and the stratum intermedium. Previous studies have established PHOSPHO1 as a matrix vesicle membrane-associated phosphatase that interacts with matrix vesicles molecules phosphoethanolamine and phosphocholine to initiate apatite crystal formation inside of matrix vesicles in bone. In the present study, we sought to determine the function of Phospho1 during amelogenesis. PHOSPHO1 protein localization during amelogenesis was verified using immunohistochemistry, with positive signals in the enamel layer, ameloblast Tomes' processes, and in the walls of ameloblast secretory vesicles. These ameloblast secretory vesicle walls were also labeled for amelogenin and the exosomal protein marker HSP70 using immunohistochemistry. Furthermore, PHOSPHO1 presence in the enamel organ was confirmed by Western blot. Phospho1-/- mice lacked sharp incisal tips, featured a significant 25% increase in total enamel volume, and demonstrated a significant two-fold reduction in silver grain density of von Kossa stained ground sections indicative of reduced mineralization in the enamel layer when compared to wild-type mice ($p<0.001$). Scanning electron micrographs of Phospho1-/- mouse enamel revealed a loss of the prominent

* Reprinted with permission from Frontiers Editorial office - Pandya, M., Rosene, L., Farquharson, C., Millán, J. L., & Diekwisch, T. (2017). Intravesicular Phosphatase PHOSPHO1 Function in Enamel Mineralization and Prism Formation. *Frontiers in physiology*, *8*, 805.

enamel prism "picket fence" structure, a loss of parallel crystal organization within prisms, and a 1.56-fold increase in enamel prism width ($p < 0.0001$). Finally, EDS elemental analysis demonstrated a significant decrease in phosphate incorporation in the enamel layer when compared to controls ($p<0.05$). Together, these data establish that the matrix vesicle membrane-associated phosphatase PHOSPHO1 is essential for physiological enamel mineralization. Our findings also suggest that intracellular ameloblast secretory vesicles have unexpected compositional similarities with the extracellular matrix vesicles of bone, dentin, and cementum in terms of vesicle membrane composition and intravesicular ion assembly.

1.2. Introduction

Amelogenesis is a complex process that involves a multitude of proteins and proteinases to facilitate the orderly assembly of elongated calcium phosphate apatite crystals into enamel prisms. Early studies have established that proline/glutamine-rich enamel proteins such as amelogenin, ameloblastin, and enamelin control enamel crystal shape and habit by facilitating enamel crystal growth in c-axis dimension and limiting their expansion in width (Diekwisch, David et al. 1993, Masuya, Shimizu et al. 2005, Hatakeyama, Fukumoto et al. 2009, Gopinathan, Jin et al. 2014). During the secretion of these structural proteins, two enamel proteases, MMP20 and KLK4, are involved in the processing and degradation of the proline-rich enamel matrix (Ryu, Hu et al. 2002, Shin, Hu et al. 2014). Through the step-wise removal of the organic protein matrix, the MMP20 and KLK4 enamel proteases facilitate inorganic crystal nucleation and growth resulting in an overall increase of enamel hardness (Lu, Papagerakis et al. 2008). In addition, MMP20 appears to have additional functions related to the stability of the dentin-

enamel junction, ameloblast retreat during enamel thickening, and ameloblast differentiation (Hu, Smith et al. 2016).

Enamel proteases not only affect enamel crystal growth by processing matrix proteins such as amelogenins that are directly in contact with the growing crystal surface. Enzymes also play a role as components of the vesicular transport machinery that facilitates the orderly movement of ions, notably calcium and phosphate, from the blood vessels of the enamel organ into the enamel layer. The secretory cells of bone, dentin, and cartilage connective tissues contain small vesicles surrounded by a lipid bilayer that in addition to small calcium phosphate crystals contain a number of enzymes that are important for their function in tissue mineralization, including tissue non-specific alkaline phosphate, (TNAP), nucleotide pyrophosphatase phosphodiesterase (NPP1/PC-1), annexins (ANX), and other matrix metalloproteinases (MMPs)(Howard and Anderson 1978, Anderson 1984, Bonucci 1992, Dean, Schwartz et al. 1992, Wuthier, Wu et al. 1992). These unique proteases have been implicated in the mineralization of bone and dentin (Golub 2009).

One of the matrix vesicle enzymes involved in initiation of bone, dentin, and cartilage mineralization is the matrix vesicle phosphatase PHOSPHO1 (Millan 2013). PHOSPHO1 has been identified in the matrix vesicles of osteoblasts, odontoblasts, and chondrocytes (Houston, Stewart et al. 2004, Roberts, Narisawa et al. 2007, McKee, Yadav et al. 2013). Biochemical studies have characterized PHOSPHO1 as a haloacid dehalogenase family member that interacts with matrix vesicle molecules phosphoethanolamine and phosphocholine to initiate apatite crystal formation inside of matrix vesicles (Millan 2013, Cui, Houston et al. 2016). PHOSPHO1 has also been localized in ameloblasts (McKee, Yadav et al. 2013), and enzyme replacement therapy has verified the essential role of the matrix vesicle alkaline phosphate TNAP for enamel

formation (Yadav, de Oliveira et al. 2012), but according to textbook knowledge, enamel mineralization occurs without the involvement of matrix vesicles (Nanci 2008).

We thus conducted the present study to characterize the role of PHOSPHO1 during amelogenesis and to determine the function of PHOSPHO1 as a component of the ameloblast secretory vesicle wall in its effect on enamel structure and mineralization. We hypothesized that the loss of PHOSPHO1 would affect enamel structural integrity through a delay in intravesicular mineralization initiation, and we used light and electron microscopy as well as elemental mapping and von Kossa staining to characterize the effects of loss of PHOSPHO1 on the enamel layer. Our data not only provide a structural characterization of the *Phospho1* deficient enamel but also give insights into the function of the matrix vesicle phosphatase PHOSPHO1 related to enamel ion transport in vesicles.

1.3. Materials and Methods

1.3.1. Animal models and biosafety

Animals were sacrificed in accordance with guidelines of the Animal Care and Use Committee at the Sanford Burnham Prebys Medical Discovery Institute and National Institutes of Health (NIH). Breeding, genotyping, and characterization of Phospho1-/- mice has been described previously (Yadav, Simao et al. 2011, Zweifler, Ao et al. 2016). Eleven mandibles each from control and *Phospho1-/-* mice were chosen for histology and microscopy studies. All research involving biohazards and toxins has been carried out according to Texas A&M institutional biosafety standards.

1.3.2. Ultrathin ground sections of control and *Phospho1*$^{-/-}$ mouse mandibles

Thirty day old hemi-mandibles of control and *Phospho1-/-* were fixed in 10% formalin and processed for ground sections. The mandibles were subjected to a series of different gradients of alcohol as well as mixture of ethanol/technovit as per the EXAKT company standard protocol for preparation of tissue samples for ground sections. Once the samples were in 100% light cure technovit (Technovit 7200, EXAKT), they were polymerized and embedded. The samples were grossly sectioned using a diamond bandsaw (EXAKT 300 CP), ground and polished to produce 30µm thin sections (Liu, Reed et al. 2016). Two of the four ground sections were stained with alizarin red for 90 minutes and the other two for von Kossa staining.

1.3.3. Radiographs

Thirty day old hemi-mandibles were analyzed using a Faxitron MX-20 specimen radiography system (Faxitron X-ray Corp., IL) at 20 kV for 20s.

1.3.4. Micro-CT Analysis

Three WT and three *Phospho1-/-* mouse mandibles were imaged individually and analyzed using a Micro-CT 20 Scanco Medical Scanner (Zürich, Switzerland). Specimens were scanned in standard resolution mode, with *x*-, *y*- and *z*-axis resolution of approximately 10 µm. The level of X-ray exposure was 55 kVp energy and 800 ms exposure time. After the scanning was completed, 3-D data were generated by segmenting specimens at a threshold chosen to only include enamel tissue based on a morphological match with normal tooth histology. For each mandible, 70 slices were assembled and analyzed to perform a 3-D reconstruction of the

incisors, and the total enamel volume fractions of the incisors were calculated and compared between the WT and *Phospho1-/-* samples.

1.3.5. Scanning Electron Microscopy (SEM) and Energy Dispersive X-ray Spectroscopy (EDS)

Thirty day old hemi-mandibles for control and *Phospho1-/-* mice were fixed in 10% formalin and treated gently with 4.5% EDTA for 15 minutes. The etched samples were dried and sputter coated with Au/Pd alloy for 90 seconds. These mandibles were further analyzed using a scanning electron microscope (JEOL JSM-6010LA). For EDS analysis, the samples were fixed, dried and analyzed by selecting five random points in the enamel region. The elemental mapping at the selected points was recorded and the mass percent amount of calcium and phosphorous was compared between the control and PHOSPHO1 samples.

1.3.6. Transmission electron microscopy

E16 tooth organs were cultured for 12 days, and thereafter fixed in Karnovsky's fixative as previously described (Diekwisch 1998), dehydrated and embedded in Eponate 12 (Ted Pella, Redding, CA). Following polymerization of the Eponate, ultrathin sections were cut on a Leica Ultracut UCT ultramicrotome. After drying, sections were contrasted using uranyl acetate and Reynold's lead citrate for 15 min each. Stained sections were examined using a JEOL 1220EX transmission electron microscope at the UIC Research Resources Center (Chicago, IL).

1.3.7. Paraffin sections and immunohistochemistry

Three days old hemi-mandibles of three wild-type mice were fixed in 10% formalin, decalcified with 4.5% EDTA for one week, and then processed for regular paraffin sectioning after dehydrating through graded series of ethanol and xylene. Alternatively, a second set of 3-days old wildtype mandibles was fixed in Bouin's fixative and also processed into 5μm thin paraffin sections. For antigen retrieval, the paraffin fixed samples were incubated in 10mM sodium citrate buffer for 30 min at pH 6 and boiling temperature. Alternatively, the samples fixed in Bouin's fixative were treated with 8M guanidine HCl overnight at 4°C and pH 8 to unmask the PHOSPHO1 antigen sites as suggested by McKee et al. (2013). Following antigen retrieval, samples were incubated using human recombinant Fab monoclonal anti-PHOSPHO1 primary antibody (AbD Serotec, Morphosys AG) or polyclonal anti-PHOSPHO1 antibody (GeneTex, USA) for PHOSPHO1 identification. Other vesicle associated proteins such as amelogenin or HSP70 were labeled using a polyclonal anti-amelogenin antibody or a mouse monoclonal anti-HSP70 antibody (Abcam, Cambridge, MA). Immunohistochemistry was performed using a broad spectrum IHC staining kit and an AEC substrate kit (Life Technologies, Carlsbad, CA) and stained sections were analyzed using a Leica DMR light microscope (Nuhsbaum, IL).

1.3.8. Western Blot

Enamel organs were immediately harvested from unerupted mandibular molars of three months old pigs sacrificed at a local animal farm. The enamel organs were subjected to extraction with 0.5% sodium dodecyl sulfate (SDS) lysis buffer with subsequent extraction with 4M guanidine HCl (pH 7.4). Initially, the proteins from enamel organ were extracted using SDS

lysis buffer for five days. The supernatant was collected after centrifugation at 2400g and 4°C. The residue after SDS extraction was subjected to extraction with 4M guanidine (Gu) HCl buffer for five days. The supernatant from Gu-based extract was collected and processed following the same procedure as the SDS based extract. The extracted protein lysate from SDS and Gu-based extracts were dialyzed against double distilled water for 1 week. Equal amounts of protein extracts were loaded for both groups in a 10% SDS polyacrylamide gel and was subjected to gel electrophoresis at 150 V for 58 minutes. A semi-dry transfer system was used to transfer proteins from the gel to a polyvinylidine difluoride (PVDF) membrane at 18 V for 40 minutes. The PVDF membrane was blocked for 1 hour with 5% dry milk in tris buffered saline with tween 20 (TBST), incubated with human recombinant Fab monoclonal anti-PHOSPHO1 primary antibody (1:500, AbD Serotec, Morphosys AG) for one hour, followed by washing in TBST three times for fifteen minutes and incubation with anti-mouse IgG HRP conjugated secondary antibody (1:2000, cell signaling) for one hour. The signal was detected using a chemiluminescent substrate (Thermo Scientific, USA).

1.3.9. Statistical Analysis

The width and the inter-prism space of enamel prisms was measured based on three control and three *Phospho1-/-* samples. Measurement of prism width and interprismatic distance were obtained from scanning electron micrographs of etched mouse molar enamel cross sections. For our analysis, only mid-sagittal cross sections were chosen, and all samples were etched at identical times and concentrations, and rinsed for the same amount of time. Representative micrographs at 750x magnification from the distal interproximal enamel of the first molar were chosen for further analysis based on optimal prism pattern identification. Ten prisms were

randomly chosen from each micrograph, and their width and the inter-prism space were measured using the ImageJ software. To analyze the silver grain density in von Kossa stained sections, micrographs at 400x magnification were imported into the ImageJ software package, and three 100 x 100μm areas within the *Phospho1-/-* and WT cuspal tip molar enamel region were randomly chosen and pixel density was analyzed. For EDS analysis, ten points were randomly chosen in the enamel region of three *Phospho1-/-* and WT molars, and the values of calcium and phosphorus at the selected points was compared between both groups. All experiments were done in triplicates, the data analysis was conducted using student's T-test, and the significance value was set at $p < 0.05$.

1.4. Results

1.4.1. PHOSPHO1 protein localization in the enamel layer and the walls of secretory vesicles

Immunohistochemical and Western blot analysis were performed to verify whether the PHOSPHO1 protein was localized in the enamel organ. Our analysis of paraffin sections of three days old wildtype mice revealed PHOSPHO1 protein localization in the enamel layer, Tomes' processes, and in ameloblast secretory vesicles (Fig. 1). Positive signals for PHOSPHO1 were obtained using both antibodies available to us (GTX119275 from Genetex in Figs. 1A,C and AbD Serotec/Millán in Figs. 1B,D) and independent from the type of fixative employed (Formalin in Figs. 1A,C,E, and Bouin in Figs. 1B,D). In general, PHOSPHO1 expression levels were stronger in the mineralized enamel layer and at the ameloblast secretory pole (Figs. 1A,C), while there was no staining in the control section using the same technique without primary antibody (Fig. 1E). High magnification images revealed positive staining for PHOSPHO1 at the

periphery of circular organelles at the ameloblast secretory pole (Fig. 1C,D). A Western blot using the AbD Serotec antibody and performed on guanidine or SDS extracts of enamel organs demonstrated a characteristic 32KDa full-length PHOSPHO1 band and a 25kDa cleavage product, confirming the presence of PHOSPHO1 in the enamel organ.

1.4.2. Decreased enamel mineralization and loss of sharp incisal tips in *Phospho1-/-* mice

To determine how loss of PHOSPHO1 affects enamel quality, a number of physicochemical parameters such as total enamel volume, calcium and phosphate ratios, level of mineralization based on von Kossa sections, and sharpness of incisal tips were assessed and compared between *Phospho1-/-* and WT mice. Comparison of X-ray radiographs and alizarin red stained ground sections between thirty day old control and *Phospho1-/-* mouse teeth revealed a rounded incisal tip in the PHOSPHO1 null incisors compared to the sharp incisal tips of their wild-type counterparts (Fig. 2A-D). There was a significant two-fold reduction in silver grain density on von Kossa stained ground sections (1.44 +/-0.11 vs. 0.71 +/-0.04 pixel units) indicative of reduced mineralization in the enamel layer of the *Phospho1-/-* mice when compared to the WT mice (Figs. 2E,F,J). Von Kossa staining also demonstrated a substantial reduction in dentin mineralization in the *Phospho1-/-* mice versus controls (Fig. 2E,F). Total enamel volume as measured by micro-CT volumetric analysis was significantly higher in *Phospho1-/-* incisors compared to WT controls (Fig. 2G,I). EDS elemental analysis demonstrated a significant decrease in the amount of phosphorus in the *Phospho1-/-* mice when compared to controls ($p<0.05$), while calcium levels were only little affected by the loss of PHOSPHO1 (Fig. 2H).

1.4.3. Disintegration and loss of enamel prism structure in Phospho1-/- mouse enamel

Scanning electron microscopy comparisons between thirty days old *Phospho1-/-* and control mice demonstrated a complete loss of the prominent enamel prism "picket fence" structure on surface etched *Phospho1-/-* mouse enamel preparations when compared to controls (Fig. 3A-D). High magnification scanning electron micrographs at individual crystal resolution revealed a loss of individual prism boundaries as a result of a 45.3% reduction in the mineral-free inter-prism space between individual prisms in *Phospho1-/-* mice when compared to controls (Fig. 3C,D versus A,B). These micrographs also documented a loss of parallel crystal organization within prisms (Fig. 3D). Moreover, there was a 1.56-fold increase in enamel prism width in *Phospho1-/-* mutant mice ($p<0.0001$).

1.4.4. Presence of mineral precipitates in ameloblast secretory vesicles as revealed by transmission electron microscopy

Ameloblast secretory vesicles (sketch in Fig. 4A) were long considered to be protein-rich intracellular entities within ameloblasts. Micrographs presented in this study illustrate that following 12 days of organ culture, these secretory vesicles also contained numerous mineral precipitates at the outside of and within the secretory vesicles (Fig. 4B). Moreover, high magnification immunohistochemistry micrographs demonstrated the presence of half-moon shaped PHOSPHO1-positive signals in the walls of ameloblast secretory vesicles close to the developing enamel front (Fig. 4C). Supportive of their involvement in secretory processes during amelogenesis, vesicles also stained positively for amelogenin and the vesicular marker protein HSP70 on paraffin sections of secretory ameloblasts (Fig. 4D).

1.5. Discussion

The purpose of the present study was to determine the function of the matrix vesicle phosphatase PHOSPHO1 during amelogenesis and on the structural integrity of the enamel layer. In this study we compared the enamel layers of wild-type and *Phospho1-/-* mice using light and electron microscopy as well as elemental mapping and von Kossa staining. Three different models have been used to verify PHOSPHO1 expression and function during amelogenesis: (i) the *Phospho1-/-* mouse molar model for phenotype analysis and immunohistochemistry, (ii) E16 mouse molar organ culture to visualize secretory vesicles using electron microscopy, (iii) and porcine enamel organ protein extracts to verify the presence of PHOSPHO1 in the enamel organ. In general, our study demonstrated reduced enamel mineralization and prism formation as a results of loss of PHOSPHO1. Using immunohistochemistry, PHOSPHO1 was localized to the walls of ameloblast secretory vesicles and in the enamel layer. Together, these findings demonstrate that PHOSPHO1 is essential for physiological enamel ion transport and for the structure of the enamel layer.

Our immunochemical analysis using two different antibodies against PHOSPHO1 and two different types of fixation procedures demonstrated that PHOSPHO1 was localized in the enamel layer and adjacent to the walls of ameloblast secretory vesicles. The presence of PHOSPHO1 in the walls of ameloblast secretory vesicles was a surprise finding as ameloblast vesicles are commonly distinguished from the matrix vesicles involved in the mineralization of bone, dentin, and cartilage (Nanci 2008). The presence of PHOSPHO1 in ameloblast vesicles would suggest potential similarities between matrix vesicles and ameloblast secretory vesicles as PHOSPHO1 functions to facilitate initial mineralization inside of such vesicles. PHOSPHO1 presence in ameloblast vesicles was previously documented by McKee et al. (2013), and the

substantial enamel defects in mice lacking the PHOSPHO1 enzyme reported here support the concept of a putative function of PHOSPHO1 during amelogenesis. Similar to matrix vesicles, ameloblast secretory vesicles are surrounded by a distinct membrane and contain a mixture of protein matrix and small mineral crystallites (Diekwisch 1998, Brookes, Barron et al. 2014), even though they lack the double layer membrane commonly associated with matrix vesicles (Howard and Anderson 1978). There was also an obvious size difference between the ameloblast secretory vesicles described here (2-3µm) and the average diameter of typical matrix vesicles of the bone extracellular matrix (100nm, Anderson 2003), and this size difference may be explained by the function of ameloblasts to transport and deposit substantial amounts of protein and mineral within a relatively short period of time. Nevertheless, further studies will be needed to establish the similarities and differences between the matrix vesicles of the mesenchymal bone extracellular matrix and the secretory vesicles of ameloblast epithelial cells beyond the differences in localization, content, and size. Especially, cryoimmuno-electron microscopic techniques to map individual matrix components within individual vesicle components would further advance our understanding of the secretory machinery common to epithelial and mesenchymal mineral forming cells. While the presence of PHOSPHO1 in ameloblast secretory vesicles alone may not suffice to draw parallels between matrix vesicles and ameloblast vesicles, PHOSPHO1 as a common apatite nucleation enzyme in both types of vesicles suggests similar mechanisms of mineral growth related to early intravesicular apatite nucleation between mineralized tissues of ectodermal and ectomesenchymal origin (Fig. 4A).

Loss of *Phospho1* in our mouse model had a number of dramatic effects on enamel prism structure and mineralization, including reduced mineralization as indicated by von Kossa staining, rounded incisal tips, disrupted enamel prism pattern, and lack of individual crystal

integrity within their prismatic subunit. Together, this phenotype indicates that enamel biomineralization in *Phospho1-/-* mice was severely impaired. Based on the present phenotype it is not entirely clear whether the dramatic phenotype in the mature enamel was due to a failure of mineralization initiation or due to a failure of PHOSPHO1 to continuously function during enamel maturation within the enamel layer. It is also not clear whether PHOSPHO1 plays only a direct role in early crystal nucleation and growth, and the lack of sufficiently hardened crystals impairs their assembly into enamel prisms, or whether PHOSPHO1 has additional functions during prism organization. Nevertheless, the remarkable enamel phenotype reported in the present study confirms that a phosphatase so far only known for its role during the early phase of bone and dentin crystal growth is essential for physiological enamel mineralization and prism patterning. Moreover, our electron micrographs of intravesicular mineral precipitation within ameloblast secretory vesicles support the concept of PHOSPHO1 function during initial mineralization.

In addition to the mineralization defects discussed above, there was also a significant increase in overall enamel volume and in the thickness of the enamel layer. This is a remarkable finding as the thickness of the enamel layer is usually highly consistent within a species. Yet, the reduced level of mineralization might have caused a delayed onset of enzymatic degradation of the enamel matrix via enamel-related proteases such as MMP20 and KLK4. Alternatively, the higher level of mineralization in the wild-type mice might have been associated with a greater degree of protein compaction and a resulting thinner enamel layer. The less mineralized enamel layer also explains the rounded incisal tips of *Phospho1-/-* mice, where a different mineral content results in an altered wear pattern. Finally, the reduced level of underlying dentin

mineralization might have affected the mechanosensory control of the ameloblast secretory apparatus, resulting in an overcompensation through enhanced enamel secretion.

While our data revealed remarkable structural defects in the enamel layer of *Phospho1-/-* mice, our elemental analysis demonstrated that only phosphate incorporation into the enamel layer of *Phospho1-/-* mice was significantly reduced, and calcium levels were not significantly different between mutant and wild-type mice. Phosphate content is essential for normal bone health, and loss of phosphate is destined to set the physiological calcium/phosphate homeostasis out of balance (Penido and Alon 2012). However, the role of PHOSPHO1 is predominantly associated with early intravesicular mineral nucleation, suggesting the phenotype observed here is less due to a reduction in phosphate transport but rather because of the failure of early intravesicular crystals to form as precursors and templates for mature enamel crystals and subsequently enamel prisms.

1.6. References

- Anderson, H. C. (1984). "Mineralization by matrix vesicles." Scan Electron Microsc(Pt 2): 953-964.
- Bard, J. (2007). "Systems developmental biology: the use of ontologies in annotating models and in identifying gene function within and across species." Mammalian Genome **18**(6-7): 402-411.
- Bartlett, J. and J. Simmer (1999). "Proteinases in developing dental enamel." Critical Reviews in Oral Biology & Medicine **10**(4): 425-441.
- Bartlett, J. and C. Smith (2013). "Modulation of cell-cell junctional complexes by matrix metalloproteinases." Journal of dental research **92**(1): 10-17.

- Bartlett, J. D. (2013). "Dental enamel development: proteinases and their enamel matrix substrates." ISRN dentistry **2013**.
- Bonucci, E. (1992). "Comments on the ultrastructural morphology of the calcification process: an attempt to reconcile matrix vesicles, collagen fibrils, and crystal ghosts." Bone Miner **17**(2): 219-222.
- Brookes, S. J., M. J. Barron, R. Boot-Handford, J. Kirkham and M. J. Dixon (2014). "Endoplasmic reticulum stress in amelogenesis imperfecta and phenotypic rescue using 4-phenylbutyrate." Hum Mol Genet **23**(9): 2468-2480.
- Cui, L., D. A. Houston, C. Farquharson and V. E. MacRae (2016). "Characterisation of matrix vesicles in skeletal and soft tissue mineralisation." Bone **87**: 147-158.
- Deakins, M. (1942). "Changes in the Ash, Water, and Organic Content of Pig Enamel During Calcification." Journal of Dental Research **21**(5): 429-435.
- Dean, D. D., Z. Schwartz, O. E. Muniz, R. Gomez, L. D. Swain, D. S. Howell and B. D. Boyan (1992). "Matrix vesicles are enriched in metalloproteinases that degrade proteoglycans." Calcified tissue international **50**(4): 342-349.
- Diekwisch, T., S. David, P. Bringas, V. Santos and H. C. Slavkin (1993). "Antisense inhibition of AMEL translation demonstrates supramolecular controls for enamel HAP crystal growth during embryonic mouse molar development." Development **117**(2): 471-482.
- Diekwisch, T. G. (1998). "Subunit compartments of secretory stage enamel matrix." Connect Tissue Res **38**(1-4): 101-111; discussion 139-145.
- Eastoe, J. (1979). "Enamel protein chemistry-past, present and future." Journal of dental research **58**(2 suppl): 753-764.

- Edelman, L. B., S. Chandrasekaran and N. D. Price (2009). "Systems biology of embryogenesis." Reproduction, Fertility and Development **22**(1): 98-105.
- Gibson, C. W., Z.-A. Yuan, B. Hall, G. Longenecker, E. Chen, T. Thyagarajan, T. Sreenath, J. T. Wright, S. Decker and R. Piddington (2001). "Amelogenin-deficient mice display an amelogenesis imperfecta phenotype." Journal of Biological Chemistry **276**(34): 31871-31875.
- Golub, E. E. (2009). "Role of matrix vesicles in biomineralization." Biochim Biophys Acta **1790**(12): 1592-1598.
- Gopinathan, G., T. Jin, M. Liu, S. Li, P. Atsawasuwan, M.-T. Galang, M. Allen, X. Luan and T. G. Diekwisch (2014). "The expanded amelogenin polyproline region preferentially binds to apatite versus carbonate and promotes apatite crystal elongation." Frontiers in physiology **5**.
- Gopinathan, G., T. Jin, M. Liu, S. Li, P. Atsawasuwan, M.-T. Galang, M. Allen, X. Luan and T. G. H. Diekwisch (2014). "The expanded amelogenin polyproline region preferentially binds to apatite versus carbonate and promotes apatite crystal elongation." Frontiers in Physiology **5**: 430.
- Guan, X., F. B. Bidlack, N. Stokes and J. D. Bartlett (2014). "E-Cadherin can replace N-cadherin during secretory-stage enamel development." PloS one **9**(7): e102153.
- Hatakeyama, J., S. Fukumoto, T. Nakamura, N. Haruyama, S. Suzuki, Y. Hatakeyama, L. Shum, C. W. Gibson, Y. Yamada and A. B. Kulkarni (2009). "Synergistic roles of amelogenin and ameloblastin." J Dent Res **88**(4): 318-322.
- Houston, B., A. J. Stewart and C. Farquharson (2004). "PHOSPHO1-A novel phosphatase specifically expressed at sites of mineralisation in bone and cartilage." Bone **34**(4): 629-637.

- Howard, H. T. H. and H. C. Anderson (1978). "Calcification of Isolated Matrix Vesicles and Reconstituted Vesicles from Fetal Bovine Cartilage." Proceedings of the National Academy of Sciences of the United States of America **75**(8): 3805-3808.
- Hu, J. C.-C., Y. Hu, Y. Lu, C. E. Smith, R. Lertlam, J. T. Wright, C. Suggs, M. D. McKee, E. Beniash and M. E. Kabir (2014). "Enamelin is critical for ameloblast integrity and enamel ultrastructure formation." PloS one **9**(3): e89303.
- Hu, Y., C. E. Smith, A. S. Richardson, J. D. Bartlett, J. C. C. Hu and J. P. Simmer (2016). "MMP20, KLK4, and MMP20/KLK4 double null mice define roles for matrix proteases during dental enamel formation." Molecular Genetics & Genomic Medicine **4**(2): 178-196.
- Hubbard, M. J. (2000). "Calcium transport across the dental enamel epithelium." Critical Reviews in Oral Biology & Medicine **11**(4): 437-466.
- Iijima, M. and J. Moradian–Oldak (2004). "Interactions of amelogenins with octacalcium phosphate crystal faces are dose dependent." Calcified tissue international **74**(6): 522-531.
- Jin, T., Y. Ito, X. Luan, S. Dangaria, C. Walker, M. Allen, A. Kulkarni, C. Gibson, R. Braatz and X. Liao (2009). "Elongated polyproline motifs facilitate enamel evolution through matrix subunit compaction." PLoS Biol **7**(12): e1000262.
- Lacruz, R. S. (2017). "Enamel: Molecular identity of its transepithelial ion transport system." Cell Calcium.
- Lacruz, R. S., A. Nanci, I. Kurtz, J. T. Wright and M. L. Paine (2010). "Regulation of pH during amelogenesis." Calcified tissue international **86**(2): 91-103.
- Lagerström, M., N. Dahl, Y. Nakahori, Y. Nakagome, B. Bäckman, U. Landegren and U. Pettersson (1991). "A deletion in the amelogenin gene (AMG) causes X-linked amelogenesis imperfecta (AIH1)." Genomics **10**(4): 971-975.

- Liu, M., D. A. Reed, G. M. Cecchini, X. Lu, K. Ganjawalla, C. S. Gonzales, R. Monahan, X. Luan and T. G. Diekwisch (2016). "Varanoid Tooth Eruption and Implantation Modes in a Late Cretaceous Mosasaur." Front Physiol **7**: 145.
- Lu, X., Y. Ito, A. Kulkarni, C. Gibson, X. Luan and T. G. Diekwisch (2011). "Ameloblastin-rich enamel matrix favors short and randomly oriented apatite crystals." European journal of oral sciences **119**(s1): 254-260.
- Lu, Y., P. Papagerakis, Y. Yamakoshi, J. C. C. Hu, J. D. Bartlett and J. P. Simmer (2008). "Functions of KLK4 and MMP-20 in dental enamel formation." Biological chemistry **389**(6): 695-700.
- Masuya, H., K. Shimizu, H. Sezutsu, Y. Sakuraba, J. Nagano, A. Shimizu, N. Fujimoto, A. Kawai, I. Miura and H. Kaneda (2005). "Enamelin (Enam) is essential for amelogenesis: ENU-induced mouse mutants as models for different clinical subtypes of human amelogenesis imperfecta (AI)." Human molecular genetics **14**(5): 575-583.
- Masuya, H., K. Shimizu, H. Sezutsu, Y. Sakuraba, J. Nagano, A. Shimizu, N. Fujimoto, A. Kawai, I. Miura, H. Kaneda, K. Kobayashi, J. Ishijima, T. Maeda, Y. Gondo, T. Noda, S. Wakana and T. Shiroishi (2005). "Enamelin (Enam) is essential for amelogenesis: ENU-induced mouse mutants as models for different clinical subtypes of human amelogenesis imperfecta (AI)." Hum Mol Genet **14**(5): 575-583.
- McKee, M. D., M. C. Yadav, B. L. Foster, M. J. Somerman, C. Farquharson and J. L. Millan (2013). "Compounded PHOSPHO1/ALPL deficiencies reduce dentin mineralization." J Dent Res **92**(8): 721-727.
- Millan, J. L. (2013). "The role of phosphatases in the initiation of skeletal mineralization." Calcif Tissue Int **93**(4): 299-306.

- Mochida, K. and K. Shinozaki (2011). "Advances in omics and bioinformatics tools for systems analyses of plant functions." Plant and Cell Physiology **52**(12): 2017-2038.
- Moradian-Oldak, J. (2012). "Protein-mediated enamel mineralization." Frontiers in bioscience: a journal and virtual library **17**: 1996.
- Nanci, A. (2008). Ten Cate's Oral Histology: Development, Structure, and Function, Elsevier Health Sciences.
- Paine, M. L., S. N. White, W. Luo, H. Fong, M. Sarikaya and M. L. Snead (2001). "Regulated gene expression dictates enamel structure and tooth function." Matrix Biology **20**(5): 273-292.
- Penido, M. G. M. G. and U. S. Alon (2012). "Phosphate homeostasis and its role in bone health." Pediatric Nephrology (Berlin, Germany) **27**(11): 2039-2048.
- Roberts, S., S. Narisawa, D. Harmey, J. L. Millan and C. Farquharson (2007). "Functional involvement of PHOSPHO1 in matrix vesicle-mediated skeletal mineralization." J Bone Miner Res **22**(4): 617-627.
- Robinson, C. (2014). "Enamel maturation: a brief background with implications for some enamel dysplasias." Frontiers in physiology **5**.
- Robinson, C., H. Briggs, P. Atkinson and J. Weatherell (1979). "Matrix and mineral changes in developing enamel." Journal of Dental Research **58**(2_suppl): 871-882.
- Robinson, C., P. Fuchs, D. Deutsch and J. Weatherell (1978). "Four chemically distinct stages in developing enamel from bovine incisor teeth." Caries research **12**(1): 1-11.

- Robinson, C., J. Kirkham and A. Hallsworth (1988). "Volume distribution and concentration of protein, mineral and water in developing bovine enamel." Archives of oral biology **33**(3): 159-162.
- Ryu, O., J. C. Hu, Y. Yamakoshi, J. L. Villemain, X. Cao, C. Zhang, J. D. Bartlett and J. P. Simmer (2002). "Porcine kallikrein-4 activation, glycosylation, activity, and expression in prokaryotic and eukaryotic hosts." Eur J Oral Sci **110**(5): 358-365.
- Shin, M., Y. Hu, C. E. Tye, X. Guan, C. C. Deagle, J. V. Antone, C. E. Smith, J. P. Simmer and J. D. Bartlett (2014). "Matrix metalloproteinase-20 over-expression is detrimental to enamel development: a Mus musculus model." PLoS One **9**(1): e86774.
- Simmer, J. P. and J. C.-C. Hu (2002). "Expression, structure, and function of enamel proteinases." Connective tissue research **43**(2-3): 441-449.
- Stack, M. (1960). Changes in the organic matrix of enamel during growth. Journal of bone and Joint Surgery - Bristish Editorial Soc Editorial Volume.
- Takagi, Y., H. Fujita, H. Katano, H. Shimokawa and T. Kuroda (1998). "Immunochemical and biochemical characteristics of enamel proteins in hypocalcified amelogenesis imperfecta." Oral Surgery, Oral Medicine, Oral Pathology, Oral Radiology, and Endodontology **85**(4): 424-430.
- Wuthier, R. E., L. N. Wu, G. R. Sauer, B. R. Genge, T. Yoshimori and Y. Ishikawa (1992). "Mechanism of matrix vesicle calcification: characterization of ion channels and the nucleational core of growth plate vesicles." Bone Miner **17**(2): 290-295.
- Yadav, M. C., R. C. de Oliveira, B. L. Foster, H. Fong, E. Cory, S. Narisawa, R. L. Sah, M. Somerman, M. P. Whyte and J. L. Millan (2012). "Enzyme replacement prevents enamel defects in hypophosphatasia mice." J Bone Miner Res **27**(8): 1722-1734.

- Yadav, M. C., A. M. Simao, S. Narisawa, C. Huesa, M. D. McKee, C. Farquharson and J. L. Millan (2011). "Loss of skeletal mineralization by the simultaneous ablation of PHOSPHO1 and alkaline phosphatase function: a unified model of the mechanisms of initiation of skeletal calcification." J Bone Miner Res **26**(2): 286-297.
- Zweifler, L. E., M. Ao, M. Yadav, P. Kuss, S. Narisawa, T. N. Kolli, H. F. Wimer, C. Farquharson, M. J. Somerman, J. L. Millan and B. L. Foster (2016). "Role of PHOSPHO1 in Periodontal Development and Function." J Dent Res **95**(7): 742-751.

2. INTEGRATIVE TEMPORO-SPATIAL, MINERALOGIC, SPECTROSCOPIC AND PROTEOMIC ANALYSIS OF POSTNATAL ENAMEL DEVELOPMENT IN TEETH WITH LIMITED GROWTH*

2.1.Overview

Tooth amelogenesis is a complex process beginning with enamel organ cell differentiation and enamel matrix secretion, transitioning through changes in ameloblast polarity, cytoskeletal and matrix organization, that affects crucial biomineralization events such as mineral nucleation, enamel crystal growth, and enamel prism organization. Here we have harvested the enamel organ including the pliable enamel matrix of postnatal first mandibular mouse molars during the first eight days of tooth enamel development to conduct a step-wise cross-sectional analysis of the changes in the mineral and protein phase. Mineral phase diffraction pattern analysis using single-crystal, powder sample X-ray diffraction analysis indicated conversion of calcium phosphate precursors to partially fluoride substituted hydroxyapatite from postnatal day 4 (4 dpn) onwards. Attenuated total reflectance spectra (ATR) revealed a substantial elevation in phosphate and carbonate incorporation as well as structural reconfiguration between postnatal days 6 and 8. Nanoscale liquid chromatography coupled with tandem mass spectrometry (nanoLC-MS/MS) demonstrated highest protein counts for ECM/cell surface proteins, stress/heat shock proteins, and alkaline phosphatase on postnatal

* Reprinted with permission from Frontiers Editorial office - Pandya, M., Liu, H., Dangaria S.J., Zhu, W., Li, L.L. Pan, S., Abufarwa, M., Davis, R.G., Guggenheim, S., Keiderling, T., Luan, X., and Diekwisch, T.G.H. (2017). Integrative temporo-spatial, mineralogic, spectroscopic, and proteomic analysis of postnatal enamel development in teeth with limited growth. Front. Physiol. 8:793. doi: 10.3389/fphys.2017.00793

day 2, high counts for ameloblast cytoskeletal proteins such as tubulin β5, tropomyosin, β-actin, and vimentin on postnatal day 4, and elevated levels of cofilin-1, calmodulin, and peptidyl-prolyl cis-trans isomerase on day 6.

Western blot analysis of hydrophobic enamel proteins illustrated continuously increasing amelogenin levels from 1dpn until 8dpn, while enamelin peaked on days 1 and 2dpn, and ameloblastin on days 1-5dpn. In summary, these data document the substantial changes in the enamel matrix protein and mineral phase that take place during postnatal mouse molar amelogenesis from a systems biological perspective, including (i) relatively high levels of matrix protein expression during the early secretory stage on postnatal day 2, (ii) conversion of calcium phosphates to apatite, peak protein folding and stress protein counts, and increased cytoskeletal protein levels such as actin and tubulin on day 4, as well as (iii) secondary structure changes, isomerase activity, highest amelogenin levels, and peak phosphate/carbonate incorporation between postnatal days 6 and 8. Together, this study provides a baseline for a comprehensive understanding of the mineralogic and proteomic events that contribute to the complexity of mammalian tooth enamel development.

2.2. Introduction

Enamel development is an integral process of symphonic dimensions that is characterized by a continuous interplay between cells, matrices, minerals, proteins, and signals over the entire period of amelogenesis. Allegorically speaking, the key players in this symphony have been known for decades, including a mineral section that undergoes a transition from amorphous calcium phosphate and a protein section made up by classic enamel proteins such as amelogenins, ameloblastin, and enamelin, as they are further processed by enamel-related

enzymes, including MMP20 and KLK4. As amelogenesis progresses, the volume percentage of proteins and water decreases, while the mineral content increases, resulting in a 96% mineral content in the mature enamel layer of adult mammals (Deakins 1942, Stack 1960, Robinson, Fuchs et al. 1978, Robinson, Briggs et al. 1979, Robinson, Kirkham et al. 1988). Changes in the metastable enamel matrix that result from the loss of water and proteins have even been described as a "kind of crisis" (Eastoe 1979), referring to the multiple effects of water and protein resorption on the interface between remaining proteins and maturing enamel crystals.

For decades, the effect of individual enamel proteins such as amelogenin on enamel crystal growth have been a most intriguing and rewarding subject of study (Lagerström, Dahl et al. 1991, Diekwisch, David et al. 1993, Gibson, Yuan et al. 2001, Iijima and Moradian–Oldak 2004, Jin, Ito et al. 2009, Gopinathan, Jin et al. 2014). In addition to deciphering individual aspects of amelogenin function, much progress has been made elucidating the role of the less prominent enamel-related proteins ameloblastin and enamelin on enamel crystal growth and habit (Masuya, Shimizu et al. 2005, Lu, Ito et al. 2011, Hu, Hu et al. 2014). Moreover, it has been demonstrated that enamel proteins undergo posttranslational processing by the enamel proteinases MMP20 and KLK4 (Bartlett and Simmer 1999, Simmer and Hu 2002, Bartlett 2013).

While much is known about the major proteins and minerals involved in tooth enamel formation, it has become increasingly obvious that amelogenesis is more complex than a mixture of an aqueous enamel protein solution with a combination of calcium and phosphate ions, subjected to enzymatic protein digestion and gradual removal of water over time. Recent studies have illustrated the importance of ion transport mechanisms for mineral transport (Hubbard 2000, Paine, White et al. 2001, Lacruz 2017), the effect of pH modulation through regulatory molecules (Takagi, Fujita et al. 1998, Lacruz, Nanci et al. 2010, Moradian-Oldak 2012,

Robinson 2014) and the role of junctional proteins such as cadherins for ameloblast movement (Bartlett and Smith 2013, Guan, Bidlack et al. 2014). These molecules and events are only one part of a process that ensures a gradual deposition of minerals at the dentin-enamel junction throughout amelogenesis and their step-wise conversion into hydroxyapatite crystals and alignment into enamel prisms into one of the most fascinating biomaterials found in nature.

Development of a synthetic or mimetic model of amelogenesis would greatly benefit from a temporo-spatial integration of the multitude of processes involved in mammalian amelogenesis. Such multi-level and multi-scale data mining commonly requires a systems biology approach. Systems biology of development seeks to integrate bioinformatic data analysis with other molecular, cellular, and tissue-related information to reach a higher-level, multifaceted, and integrative understanding of developmental processes (Bard 2007, Edelman, Chandrasekaran et al. 2009). Integrative approaches toward biological problems have become possible as a result of recent advances in bioinformatics and omics technologies, including proteomics, transcriptomics, and metabolomics (Mochida and Shinozaki 2011). In mineralized tissue biology, systems biology would need to integrate genetic and proteomic data with mineralogic, structural, and spectroscopic data to develop a multi-dimensional understanding of a complex process such as amelogenesis.

In the present study we have employed first mandibular mouse molar amelogenesis as a model system to systematically map proteomic, spectroscopic, temporo-spatial, and mineralogic events during the first eight days of postnatal enamel development. The benefit of a model based on teeth with limited growth is the synchronicity of developmental events leading up to maturation of the entire tooth surface by the time of tooth eruption and providing a homogeneous enamel matrix at each stage ideally suited for proteomic and spectroscopic analysis. During the

course of this study we have generated sets of spectroscopic, proteomic, and mineralogic data and integrated related events through their common timescale of development. Our analysis provides timing of events, novel proteomic and spectroscopic data, and identification of novel non-hydrophobic groups of proteins and individual proteins that may contribute toward amelogenesis. Future studies will enhance our understanding of the interconnectedness between these processes during the progression of amelogenesis as they contribute to the formation of highly organized tooth enamel.

2.3. Materials and Methods

2.3.1. Vertebrate animals and tissue preparation

First mandibular molars of 1, 2, 3, 4, 5, 6, 7, and 8 day postnatal mice (Fig. 1A-H) were dissected from alveolar bone crypts (Fig. 2E) to characterize the developing enamel matrix. Postnatal days 1 -8 were used for for Western blot. Days 2, 4, and 6 were selected for proteomics analysis. Days 1, 2, 4, 6, and 8 were used for X-ray powder diffraction, tissue dissection and polarized microscopy. All animal experiments were approved by the IACUC committees at the University of Illinois, Chicago and Texas A&M College of Dentistry.

2.3.2. Enamel thickness measurements and polarized light microscopy

Enamel thickness was measured on enlarged micrographs generated by a Leica stereo microscope. Enamel thickness was determined by calibration against a metric scale bar imaged at the same magnification. Birefringence of the enamel matrix was assessed by placing the enamel organs between crossed polarizers. The first polarizer was placed between the light source and the tooth organ and the second polarizer was placed between the tooth organ and the

camera. The second polarizer was rotated in 45^0 intervals, and birefringence was identified based on the color changes within the enamel matrix.

2.3.3. X-ray powder diffraction

For this study, the tooth enamel matrices of molars from days 1 to 8 postnatal mice were analyzed using X-ray powder diffraction in one-day intervals (excluding samples from 3 day postnatal mice). For each day of analysis, the enamel matrix of four different mouse molars was harvested in distilled water, and samples from all four teeth at each developmental stage were pooled for further analysis. Samples were stored for about 24 h at < 0^o C until analyzed at room temperature. Debye-Scherrer data simulations were obtained using a Bruker three-circle (transmission-mode) diffractometer using Mo radiation (0.7107 Å, APEX CCD detector, graphite monochromator, 0.3 mm Monocap capillary collimator, at operating conditions of 45 kV, 25 mA). Analyzed samples were approximately 0.1 mm^3 in volume, with each sample mounted on the end of a glass fiber, placed in the X-ray beam and rotated 360^o about the glass-fiber axis. Detector positions were at two theta = 0, 20, and 35^o using a frame resolution of 1024 x 1024 pixels, sample-to-detector distance of 120 mm, and each exposure was for 1200 s. Data collection using the SMART collection software (Braintree, MA) and initial data processing using the Bruker GADDS software package (Bruker, Billerica, MA). Integration along the Debye rings was performed after data collection with a step (bin) size of 0.02, followed by construction of intensity vs two-theta plots for each of the three detector positions, followed by a merger of the three plots based on the overlap of adjacent exposures to produce a traditional powder diffraction pattern. Additional pattern processing and phase identification using the Internal Center for Diffraction Data (ICDD, Newtown Square, PA, 2010) powder diffraction file

was applied using the JADE software (Materials Data, Inc., Livermore, CA, 2009). Details of the Debye-Scherrer technique have been published in Klug and Alexander (1954) (Klug and Alexander, 1954) and the use of the Bruker three-circle diffractometer to simulate the Debye-Scherrer technique have been previously reported (Guggenheim, 2005).

2.3.4. Attenuated total reflectance Fourier transform infrared (ATR-FTIR) Spectroscopy

For FTIR analysis, mice molar enamel matrix samples were transferred to an ATR crystal (PIKE MIRacle single reflection diamond ATR) accessory placed in an FTIR (Bruker Vertex 80) sample compartment. Samples were pressed against the crystal surface with a pressure clamp to form a better contact covering most of the crystal surface. Sample absorbance spectra over the range 4500 cm^{-1} to 600 cm^{-1} were collected as an average of 2048 scans (10 kHz scan speed with a DTGS detector) and processed with 3-term Blackman-Harris apodization and zero filling of 2. Background spectra, collected with same measurement parameters but without sample on the ATR crystal surface, were subtracted as a baseline correction.

2.3.5. Proteomics sample preparation

Distal slope enamel matrices of 50 first mouse mandibular molars were prepared from 2dpn, 4dpn, and 6dpn mice, and four sets of samples per time point were chosen. Enamel matrices from mice earlier than 2dpn were not harvested due to a lack of overall quantity and enamel matrices from mice later than 6dpn were omitted due to the advanced mineralization of those samples. Following cold acetone/trichloric acid precipitation, samples were redissolved in fifty microliters of 8 M urea. Reduction and alkylation of cysteines was accomplished by adding 1/10 volume of 45mM DTT to the sample, followed by 45 minutes incubation at 37ºC. After

samples were cooled to room temperature, 1/10 volume of 100mM iodoacetamide were added to the solution and samples were placed in dark at room temperature for 30 minutes. To equilibrate the sample for trypsin digestion, sufficient water was added to dilute the original 8M urea/ 0.4 M ammonium bicarbonate solution four fold. A total of 1μg trypsin was added and the sample was incubated at 37°C for 18-24 hours. The trypsin digest was stopped by freezing until nanoLC-MS/MS analysis.

2.3.6. Nano-scale liquid chromatography

Nano-scale liquid chromatography was performed using a Dionex Ultimate 3000 system. Mobile phase A was water/acetonitrile (95:5) with 0.1% formic acid. Mobile phase B was water: acetonitrile (5:95) with 0.1% formic acid. Digested sample was loaded offline onto a Thermo Scientific C18 PepMap100 peptide trap (300 μm ID x 5 mm, 5 μm, 100 A) with 100% mobile phase A flowing at 50 μL per minute. After allowing the peptides to concentrate and desalt for 10 min., the trap was switched inline with an Agilent Zorbax 300SB C18 nanoLC column (3.5 μm, 150 mm x 75 μm ID). The peptides were then resolved using a linear gradient from 5% B to 35% B over 60 minutes. The flow rate through the column was 250 nL per minute.

2.3.7. Mass spectrometry

The instrument used for mass spectrometry was an LTQ Orbitrap Velos Pro (Thermo Fisher) equipped with a Thermo LTQ nanospray source, which was operated at an ion spray voltage of 1.8 kV and a heated capillary temperature of 275°C. Full scan mass data were obtained between 400 – 1800 Da and the Orbitrap resolution was 30,000. The Orbitrap was operated in data dependent acquisition mode with dynamic exclusion (120 seconds). Twenty

most intense ions above the minimum signal threshold with charge states greater than or equal to 2 were selected for low-energy CID in the ion trap. Other operating parameters included a minimum signal threshold of 25000 and an activation time of 30.0 milliseconds.

2.3.8. Proteomics data analysis

Raw data files were processed using the Mass Matrix Conversion tool to generate Mascot generic files (MGFs) for the protein database search. Mascot 2.2 was used as a search engine and NCBI Mascot search results were imported into Scaffold.

2.3.9. Western blot

Cheesy enamel matrix from 1 day to 8 days postnatal mouse molars was scraped off and the proteins were homogenized and extracted using sodium dodecyl sulfate-polyacrylamide gel electrophoresis (SDS-PAGE) sample buffer. Equal amounts of the extracted proteins were loaded and separated on a 10% SDS-PAGE gel. From the gel, proteins were transferred to a polyvinylidene difluoride (PVDF) membrane in a semi-dry blotting apparatus at 18V for 40 minutes. The membrane was blocked for 1 hour with 5% milk powder after which it was incubated with anti-AMEL (1:200, custom made full-length), anti-AMBN (ab72776 1:200, Abcam), anti-ENAM (sc-33107, 1:100, Santa Cruz), anti-MMP20 (ab84737, 1:50, Abcam) and anti-carbonic anhydrase 2 (ab191343, 1:100, Abcam) primary antibodies for 1 hour. Following primary antibody incubation, the membrane was washed 3 times with washing buffer (TBS-T) for 15 minutes each and then incubated with HRP conjugated secondary anti-chicken, anti-mouse or anti-rabbit antibodies. To detect HRP, a chemiluminescent substrate (Thermo

Scientific) was used. Positive bands were quantitatively assessed using densitometry analysis using the Image J software.

2.3.10. Statistical analysis

For X-ray diffraction and ATR-FTIR studies, enamel matrix from four different mice of the same position and developmental stage was pooled, and pooled enamel matrix was used for further analysis. Mass-spectroscopy data and proteomics analysis were based on separately collected biological quadruplicates. All other data (thickness measurements and Western blot analyses) were based on triplicates. Data analysis was performed using SPSS software. Statistical significance was assessed using the non-parametric Mann-Whitney U test, and the significance level was set at $p < 0.05$.

2.4. Results

2.4.1. Increasing thickness and birefringence of the developing enamel matrix

First mandibular molars of 1, 2, 3, 4, 5, 6, 7, and 8 day postnatal mice (Fig. 1A-H) were dissected from alveolar bone crypts (Fig. 2E) to characterize the developing enamel matrix. Stereo micrographs documented a continuous increase in enamel matrix thickness from 1-2µm (1 day postnatal) to 75µm (6 days – 8 days postnatal) based on measurements of the enamel matrix thickness of the distal slope of the central major cusp, while the overall length of the tooth did not increase (Fig. 1A-H, 2F). Analysis of eight days postnatal molars between crossed polarizers revealed changes in matrix color pattern when analyzers were rotated in 90 degree intervals indicative of birefringence (Fig. 2A-D). The soft and pliable consistency of the enamel

matrix allowed for mechanical separation from the underlying dentin layer using a scalpel (Fig. 2G, H).

2.4.2. Single-crystal powder sample X-ray diffraction analysis of the postnatal enamel matrix yields calcium phosphate diffraction patterns on postnatal days 1 and 2, and apatite diffraction patterns from postnatal day 4 onward

Previous studies have indicated that the mineral phase of mouse molar enamel transitions from calcium carbonate, tri- and octacalcium phosphate precursors to partially fluoride substituted hydroxyapatite (Diekwisch et al., 1995;Diekwisch, 1998;Gopinathan et al., 2014). To determine at what stage the mineral phase of the entire postnatal mouse molar enamel matrix converts from calcium phosphate precursor stages to apatite, dried enamel matrix preparations from developing mouse molars were subjected to single-crystal, powder sample X-ray diffraction analysis. Mineral phase analysis on days 1 and 2 revealed well-defined, weak-intensity peaks that only partially matched those of the apatite standard pattern and were indicative of a calcium phosphate precursor (Fig. 3B). In contrast, samples from postnatal days 4-8 yielded partially fluoride substituted hydroxyapatite diffraction patterns based on powder diffraction standards (Hughes et al., 1991)(PDF# 73-9797)(Fig. 3B). Four peaks labeled as X could not be matched to any ICDD data base pattern (Fig. 3B).

2.4.3. Attenuated total reflectance spectra (ATR) demonstrated enhanced secondary structure and increased phosphate and carbonate incorporation into the enamel matrix

The ATR spectra were measured for teeth obtained at four stages of development (2, 4, 6, and 8 days postnatal, labeled as 2dpn, 4dpn, 6dpn and 8dpn) of which 2, 6 and 8 dpn are shown

in Figure 3C. The 4dpn spectrum exhibited spectral characteristics similar to the 2dpn and 6dpn spectra. The large band at ~1650 cm^{-1} and the following one at ~1540 cm^{-1} represent the amide I and II bands of enamel matrix proteins. The peak at ~1237 cm^{-1} included the amide III band and likely other sources such as PO_2 type modes due to its intensity. The strong peaks at 1018 cm^{-1} with a shoulder at 1105 cm^{-1} and 958 cm^{-1} that emerged after 6 days was assigned to characteristic phosphate peaks (ν_3 PO_4 mode and ν_1 PO_4 stretching IR mode) (Antonakos et al., 2007;Leventouri et al., 2009). The peak at 872 cm^{-1} was representative of the ν_2 CO_3 band. Based on previous studies, we have assigned the weak shoulders at 1520 cm^{-1} and 880 cm^{-1} that appear after 6 days of development to A-type carbonate substitution (Elliot, 1994) and the increased peaks at 1405 cm^{-1} and 1445 cm^{-1} to B-type carbonate substitution (ν_3 CO_3 mode) (Vignoles-Montrejaud, 1984). The major developmental changes in the spectrum when comparing 2dpn, 4dpn, 6dpn, and 8dpn enamel included the substantial elevation of the phosphate and carbonate bands (800 to 1100 cm^{-1} and 1400 to 1480 cm^{-1}) and the increased peak height of the amide I and II bands (1650 and 1540 cm^{-1}, respectively), between postnatal day 6 to day 8.

2.4.4. Proteomics demonstrated unique changes in the enamel organ/enamel matrix protein complex between postnatal days 2, 4, and 6

Enamel organ proteomics analysis by nanoLC-MS/MS resulted in discrete peptide identification patterns distinguished between enamel organ/enamel matrix protein complex samples from postnatal days 2, 4, and 6. In these samples, individual proteins were identified using the Mascot search software and ranked based on quantitative Orbitrap counts. Mascot data analysis yielded five protein groups with high spectral counts (Fig. 4), including (i)

mineralization proteins, (ii) cytoskeletal proteins, (iii) extracellular matrix/cell surface proteins, (iv) stress proteins, and (v) isomerases. Within each group, individual proteins were ranked based on spectral count, and individual counts per day for each postnatal day (postnatal days 2, 4, and 6) were subjected to statistical analysis and displayed in Fig. 4.

Among the biomineralization proteins, alkaline phosphatase 2 peaked on day 2 and significantly decreased by 0.9 fold ($p < 0.05$) from day 2 to day 4 while there was no alkaline phosphatase detected on day 6. Calmodulin was detected on day 2, decreased below the detection threshold on day 4, but once more rose to a significant peak on day 6. There was a 36-fold increase of reticulocalbin 3 levels from day 2 to day 4 ($p < 0.05$) but thereafter the reticulocalbin counts decreased significantly ($p < 0.05$) from day 4 to day 6. Calnexin levels decreased continuously from day 2 through day 6, including a significant decrease ($p < 0.05$) between days 4 to day 6. No expression for cathepsin B was observed at day 2, however the expression significantly peaked at day 4 ($p < 0.05$) and decreased again at day 6. In addition to the proteins displayed in Fig. 4, peaks for the major enamel protein amelogenin continuously increased from day 2 to day 4 and day 6 ($p<0.05$).

Four cytoskeleton related proteins displayed an increase in expression levels between days 2 and 4 and then decreased on day 6. Tubulin β5, β–actin and vimentin were detected at high levels on day 4 with a significant 10-fold ($p < 0.05$), 22-fold ($p < 0.05$) and 17-fold ($p < 0.05$) increase from day 2 to day 4, respectively, and a subsequent decrease between days 4 to 6 by 0.9-fold ($p < 0.05$). Cytoskeleton associated protein 4 on the other hand peaked on day 2, followed by a 0.9-fold ($p < 0.05$) decrease from day 2 to day 4, while cofilin-1 increased significantly from day 4 to day 6 ($p < 0.05$). Tropomyosin was not detected on days 2 and 6 but rose to significant levels on day 4 ($p < 0.05$).

All of the proteins related to extracellular matrix/cell surface displayed an identical trend of high levels on day 2, followed by a steep decrease through day 6. Catenin α1, vinculin, integrin β1, laminin B1, cadherin 1, and cadherin 2 all exhibited a significant decrease from day 2 to day 4 by 0.9-fold ($p < 0.05$), 0.9-fold ($p < 0.05$), 1-fold ($p < 0.05$) and 1-fold ($p < 0.05$), respectively. Vinculin and integrin β1 significantly decreased from day 4 to day 6 ($p < 0.05$). Laminin B1, cadherin 1 and cadherin 2 were only counted on day 2 and were not detected on days 4 and 6.

High levels of stress proteins 60kDa heat shock protein and 78kDa glucose regulated protein were detected on day 2, and then gradually decreased through day 6 with a 0.8 fold ($p < 0.05$) and 1 fold ($p < 0.05$) decrease, respectively, from day 2 to day 4 and a 1 fold ($p < 0.05$) decrease from day 4 to day 6 for both proteins. Chaperone stress 70 protein was present at high levels on day 2 but its expression level dropped significantly as it was not expressed either on day 4 ($p < 0.05$) or day 6. Protein disulfide isomerase A6 displayed a significant 7 fold ($p < 0.05$) increase from 2dpn to 4dpn and a 1 fold decrease between days 4 and 6 ($p < 0.05$), while protein disulfide isomerase A3 peaked on day 4 and significantly decreased one fold ($p < 0.05$) on day 6. There was a remarkable 61 fold increase of peptidyl-propyl cis-trans isomerase between days 4 and 6 ($p < 0.05$).

2.4.5. Western blot analysis of hydrophobic enamel proteins illustrated continuously increasing amelogenin levels from 1dpn until 8dpn, while enamelin peaked on days 1 and 2dpn, and ameloblastin on days 1-5dpn.

As an alternative strategy and because of the hydrophilic bias of our proteomics technology, known enamel organ/enamel matrix protein complex samples were assayed using

classic Western blot methodology (Fig. 5A,B). There was a continuous increase in the 26kDa amelogenin band in our enamel organ extracts from postnatal days 1 to 8. Ameloblastin levels were high and unchanged between postnatal days 1 to 5, featuring both 50kDa and 55kDa bands. Beginning with day 6, overall ameloblastin levels were reduced, only the upper 55kDa band was present, and several bands of lesser molecular weight than the 50kDa band were detected in addition to the 55kDa band. Enamelin levels (130kDa band) were relatively high on postnatal days 1 and 2, and gradually diminished thereafter. The 46kDa band specific for the enamel protease MMP20 was present at relatively high levels from days 1-3 postnatal, and intensity decreased from 4 days postnatal onward. The pH regulator carbonic anhydrase II peaked between postnatal days 2 and 4, reaching a maximum on postnatal day 3 on our Western blot, while it was present at lesser quantities on postnatal days 1 and 5-8 (all Western blot data illustrated in Fig. 5A,B).

2.5. Discussion

Here we have used the developing mouse mandibular molar as a model system to track changes in protein and mineral composition during postnatal amelogenesis and to correlate findings from individual protein and mineral analyses to synthesize an integrated systems perspective of enamel formation in the mouse molar. The key benefit of the postnatal mouse molar model was the suitability of the distal slopes of first molar cusps to harvest sufficient quantities of fresh enamel matrix for proteomic and mineral composition analysis in daily increments. Moreover, the mouse mandibular molar has a long history as a model for morphogenesis, cytodifferentiation, and tissue specific biomineralization (Gaunt, 1955;Slavkin et al., 1976;Slavkin et al., 1988), allowing for cross-referencing between classic developmental

biology data, mouse genetics models of amelogenesis, proteomics analysis databases, and the present systems biological study. The mouse molar model owes its popularity to its resemblance to the human molar in terms of completion of enamel formation following eruption and to the ubiquitous availability of mice and mouse genetic tools for experimental studies. In general, the mouse incisor would be equally attractive for studies of mammalian amelogenesis. However, for historical reasons and because of its larger size, the continuously erupting rat incisor has provided an alternative model for the study of enamel matrix and mineral composition during development (Schour and Massler, 1949;Robinson et al., 1979;Robinson et al., 1981;Smith and Nanci, 1989). The rat incisor model relies on the preparation of sequential segments along the rat incisor labial surface representative of the entire sequence of amelogenesis from the youngest enamel at the root apex to the oldest enamel at the incisal edge (Robinson et al., 1997). We expect that amelogenesis in the continuously erupting rat incisor and in mouse molars of limited growth are highly similar because of the known similarities in the rat and mouse genomes, overall developmental patterns, and enamel mineral composition. In the present study, the mouse molar amelogenesis model was chosen because of the availability of mouse proteomics analysis tools and the feasibility of fresh enamel matrix preparation on successive days of postnatal amelogenesis.

We began our study by documenting the daily incremental increase in the thickness of enamel covering the distal slopes of the molar cusps between 1dpn until 8dpn. During this time, the semi-transparent enamel layer increased in thickness from 1µm covering to 75µm. Throughout those eight days, the matrix was pliable and ideally suited for further biochemical analysis as it allowed for harvesting of the matrix and the attached enamel organ in bulk and in daily increments. The pliable nature of the developing enamel matrix has impressed naturalists

and early biochemists since John Hunter's time (Hunter, 1778;Eastoe, 1979;Termine et al., 1980), and as a result has been termed cheesy or cheese-like by the early enamel biochemists (Alan Fincham, personal communication). The mouse molar enamel matrix retained its opaque, soft, and cheese-like consistency throughout postnatal development, with the exception of postnatal day 8, when the hardening of the matrix began. At that stage, matrix birefringence was at its peak, causing the enamel matrix to appear in alternating polarization colors depending on the angle between polarizing and analyzing filters. Earlier studies have focused on the anisotropy of the enamel matrix during the secretory stage (Keil, 1935;Schmidt, 1959;Spears et al., 1993;do Espirito Santo et al., 2006). The highly polarized structure of the enamel matrix is evidence of the highly ordered enamel matrix structure as it provides a template for the highly ordered enamel mineral layer as a biomechanical buffer to occlusal loads and stresses.

X-ray diffraction analysis unambiguously identified enamel matrix diffraction patterns from day 4 to day 8 postnatal as partially fluoride substituted hydroxyapatite, and apatite electron diffraction patterns of 6dpn and 7dpn mouse molar enamel were confirmed in the present study and in earlier electron diffraction studies (Diekwisch et al., 1995;Diekwisch, 1998). In contrast, X-ray diffraction patters from 1dpn and 2dpn samples contained less prominent peaks that nevertheless matched the same overall partially fluoride substituted hydroxyapatite pattern of the samples from older enamel, and similarly, our earlier electron diffractions studies revealed fewer and less pronounced diffraction rings, suggesting that these earlier stages of enamel matrix maturation contain precursor phases of apatite maturation, such as octacalcium phosphate or tricalcium phosphate (Diekwisch et al., 1995;Aoba et al., 1998;Diekwisch, 1998). There were several non-identified peaks present in the 2dpn sample, which were neither found in the 1dpn sample nor in the 4-8dpn samples, suggesting the presence of unusual intermediate phases during

the transition from apatite precursors to fully mature hydroxyapatite. Together, these data demonstrate that the bulk of the distal slope first mandibular mouse molar enamel matrix converts from a lesser order of crystallinity into crystalline partially fluoride substituted hydroxyapatite between 2 and 4dpn.

Our ATR data were interpreted according to previously published band assignments (Vignoles-Montrejaud, 1984;Elliot, 1994;Gadaleta et al., 1996;Boskey et al., 2006;Antonakos et al., 2007;Leventouri et al., 2009) and provide spectroscopic evidence for the structural conversion of the mouse molar enamel matrix from a mixed amorphous calcium phosphate/protein layer at 2dpn to a crystalline hydroxyapatite structure featuring highly elongated crystals at 8dpn. On a protein level, this change was accompanied by increased peak heights of the amide I and II bands, especially from postnatal day 6 to day 8, indicative of changes in protein secondary structure and increased rigidity of the peptide bonds between the carboxyl and the amino groups of two adjacent amino acids through an increase in the double bond character of the peptide bond, resulting in increased structural rigidity of the enamel protein matrix.

Our ATR data revealed dramatic changes in the phosphate region (800 to 1100 cm^{-1}) in the postnatal mouse molar develop enamel matrix. Specifically, our data demonstrated a transition from a contoured plateau (1000 to 1100 cm^{-1}) indicative of amorphous calcium phosphate at 2dpn to a single sharp and highly elevated peak (1015 cm^{-1}) with shoulders at 1105 cm^{-1} and 958 cm^{-1} at 8dpn representative of high crystalline hydroxyapatite with crystals featuring long c-axis dimensions (Gadaleta et al., 1996). These findings are in congruence with our previous studies suggestive of a gradual transition from amorphous calcium phosphate to highly ordered and

elongated apatite crystals during amelogenesis through a process called Ostwald ripening (Diekwisch et al., 1995;Aoba et al., 1998;Diekwisch, 1998).

Moreover, there was strong evidence for carbonate substitution in the enamel matrix between postnatal days 6 and 8, as the peaks at 880 cm^{-1} (A-type carbonate) and 1405 cm^{-1} and 1445 cm^{-1} (B-type carbonate) indicated. Carbonate is known to replace phosphate in biological apatites (Zapanta-LeGeros, 1965;Wopenka and Pasteris, 2005), affects its physical properties, including decreased crystallinity and increased c-axis length (Fleet et al., 2004;Wopenka and Pasteris, 2005;Boskey et al., 2006) and mechanical properties, such as decreased hardness and Young's modulus (Morgan et al., 1997;Xu et al., 2012).

Our proteomic analysis provided only low counts for classic enamel proteins, which are known to be of hydrophobic nature (Eastoe, 1965), even though its most prominent member, amelogenin, comprises 80-90% of the developing enamel matrix protein composition (Fincham et al., 1999). This result is characteristic for unmodified proteomic studies, which have a systematic bias against hydrophobic proteins and membrane proteins and favor hydrophilic components instead (Santoni et al., 2000;Chandramouli and Qian, 2009;Josic, 2014). To address the systematic scarcity of hydrophobic proteins in proteomic datasets, classic Western blot studies of enamel protein expression from days 1 – 8 postnatal were performed. These studies demonstrated a continuous increase in amelogenin from day 1 – 8, relatively high levels of ameloblastin from days 1 – 5, peak enamelin protein level peaks on day 1 and 2, relatively high levels of MMP20 from days 1 – 3, and relatively high levels of carbonic anhydrase between postnatal days 2 and 4. These data underscore the continuous presence of amelogenin during the secretory stages of amelogenesis (Termine et al., 1980), while ameloblastin, enamelin, and MMP20 are only prominent during early secretory stage enamel development, possibly

establishing a patterning template for enamel crystal and prism growth (Bartlett, 2013;Pugach et al., 2013;Zhu et al., 2014;Prajapati et al., 2016). Our Western blot data provided evidence for relatively high levels of carbonic anhydrase during early enamel development (days 1-4), indicative of a role for pH adjustment during initial crystal nucleation, while other regulators may be involved in the pH regulation during the massive elevation of phosphate and carbonate during late-stage crystal growth. In addition, the continuous increase in amelogenin during postnatal enamel development was also verified by our proteomics study, albeit at a lower level of counts due to its hydrophobicity. Three of the proteins analyzed in Fig. 4 (Calmodulin, Cofilin-1, and Peptidyl-prolyl cis-trans isomerase) featured higher levels of expression on days 2 and 6, and a substantial decline in protein counts on day 4. We interpret these data to indicate that such proteins may have dual functions during enamel ion transport and enamel crystal growth.

Disregarding the moderate counts for classic enamel proteins such as amelogenin, ameloblastin, and enamelin, our proteomics analysis detected a number of other proteins relevant for enamel mineralization during our 2 – 6 days postnatal mouse molar enamel matrix sampling window. Among these was the protein with the highest number of counts in our analysis, alkaline phosphatase, which peaked at day 2 during the early secretory stage. At the onset of amelogenesis, alkaline phosphatase may be involved in transporting phosphate from blood vessels near the stratum intermedium into the enamel organ by increasing local phosphate concentrations in the stratum intermedium via hydrolysis of phosphorylated substrates. Phosphatase mediated hydrolysis of pyrophosphate may also be involved in the generation of other phosphorylated macromolecules (Woltgens et al., 2003;Liu et al., 2016). The other mineralization-related protein with an early peak at 2 days postnatal was the protein folding

chaperone calnexin, which may play a role in the prevention of endoplasmic reticulum stress due to misfolded enamel proteins or in calcium transport (Wang et al., 2005;Brookes et al., 2014). Calreticulin, which peaked at postnatal day 4, is another enamel protein with a dual function misfolded protein processing and calcium transport (Somogyi et al., 2003) that was detected in our proteomics analysis. Two other calcium transport proteins, calmodulin and reticulocalbin-3, peaked on day 6 (maturation stage, calmodulin) or on day 4 (late secretory stage, reticulocalbin-3). Calmodulin and reticulocalbin are capable of binding calcium using an EF-hand motif, and this function may be related to the protein-mediated transport of calcium ions through the ameloblast cell layer. The most prominent enzyme in our proteomics analysis of mouse molar enamel organs was the lysosomal cysteine protease cathepsin B, which peaked on day 4 postnatal. Cathepsin B is an important lysosomal enzyme of the enamel matrix (Al Kawas et al., 1996;Tye et al., 2009) that has been shown to enhance the activity of other proteases such as metalloproteinases and cathepsin D (Hammarström et al., 1971;Blair et al., 1989). As such, cathepsin B may promote the proteolytic degradation of the enamel matrix by enhancing the activity of MMP20 and cathepsin D.

Four of the six high-scoring cytoskeletal proteins in the enamel organ, including actin, tubulin, tropomyosin, and vimentin isoforms, peaked at postnatal day 4 during the late secretory stage. Increased presence of cytoskeletal proteins during the late secretory stage is likely indicative of their role in cell polarization and vesicular secretion (Manneville et al., 2003;Neco et al., 2003;De Lisle, 2015). Highly specific actin and tubulin immunoreactivity in secretory ameloblasts has been reported earlier (Diekwisch, 1988;Kero et al., 2014). Cytoskeleton associated protein 4 (CLIMP63) is actually a transmembrane protein that is instrumental in anchoring the endoplasmic reticulum to microtubules (Vedrenne et al., 2005), and its early

secretory stage expression matches that of other transmembrane proteins reported here (cadherin, catenin). In contrast, Cofilin-1 levels only became elevated during the resorptive maturation stage (6dpn), which may be explained by its role in actin depolymerization (Maciver and Hussey, 2002;Morita et al., 2016). Vimentin has long been hailed as an intermediate filament protein marker of mesenchymal tissues (Kidd et al., 2014). However, our present study reports strong evidence for vimentin signals in the enamel organ, lending support to earlier studies about transitory vimentin expression in the stellate reticulum (Kasper et al., 1989;Kero et al., 2014). Together, our proteomic data provide strong evidence for high levels of cytoskeletal proteins at the late secretory stage, likely related to their role in ameloblast polarization and enamel matrix secretion.

Our proteomics data indicated that six high-scoring extracellular matrix/cell surface molecules identified in the present study all peaked on day 2 postnatal at the onset of the secretory stage. This group included the classic extracellular matrix molecule laminin, the integrin β1 cell surface receptor, the β-integrin binding extracellular matrix adhesion molecule vinculin, and three cell adhesion molecules of the catenin/cadherin complex. The presence of laminin as part of the ameloblast basal lamina at the dentin-enamel junction has been demonstrated to play a role in terminal odontoblast differentiation (Lesot et al., 1981), and this basal lamina is removed during further ameloblast differentiation, presumably facilitating enamel deposition in sarcopterygian vertebrates (Diekwisch et al., 2002). Based on previous studies, we speculate that both the adherens junction protein vinculin and its binding partner β-integrin function to establish the sliding interface between secretory ameloblasts that allows for ameloblast cell movements during prism formation (Kubler et al., 1988;Nishikawa et al., 1988;Nishikawa et al., 1990;Xu et al., 1998;Saito et al., 2015). Three of the six significantly

upregulated proteins belonged to the cadherin-based adherens junction complex, namely catenin α1 and cadherins 1 and 2. Catenins are known to interact with cadherins (Rangarajan and Izard, 2013) and provide a link between adherens junctions and the actin cytoskeleton (McCrea and Gu, 2010). In ameloblasts, E-cadherin appears to be involved in ameloblast polarization (Terling et al., 1998) and β-catenin is essential for ameloblast movement (Guan et al., 2016). A switch between E-cadherin and N-cadherin has been documented in ameloblasts that slide by each other to form decussating enamel rod patterns (Guan et al., 2014). Together, the high levels of adherens junction and matrix proteins in the early enamel organ are indicative of the involvements of these proteins at the early secretory stage of amelogenins.

Three heat shock/stress proteins also were among the high-scoring proteins that peaked at the onset of the secretory stage. These proteins included the 60kDa heat shock protein (Hspd1), the 78kDa glucose regulated protein (Grp-78), and the chaperone stress 70 protein (Hsp70). All three of these proteins are involved in macromolecular assembly, the prevention of misfolding, as well as the prevention of aggregation. One of the major challenges of amelogenesis is the transport of amelogenin, a protein prone to self-assembly (Zhang et al., 2011), through the ameloblast cells. It is likely that both Grp-78 and Hsp70 may be involved in the prevention of amelogenin self-assembly inside of the ameloblast cell body, as both proteins are known to prevent protein aggregation (Wegele et al., 2004;Mayer and Bukau, 2005), while Hspd1 might rather function to prevent amelogenin misfolding (Xu et al., 2006).

Three isomerases joined the list of high-scoring enamel proteins, including the protein disulfide isomerases A3 and A6, and the peptidyl-prolyl cis-trans isomerase. Disulfide isomerases (PDIs) catalyze protein folding by facilitating disulfide bond formation and arrangement (Kersteen and Raines, 2003), a process that apparently takes place during the entire

secretory stage, as PDI peaks in our proteomics data indicate. In contrast, peptidyl-prolyl cis-trans isomerase interconverts the trans-isomers of newly synthesized peptide bonds into cis-isomers of higher biological activity (Herzberg and Moult, 1991;Pal and Chakrabarti, 1999;Balbach and Schmid, 2000;Shaw, 2002). Peptidyl-prolyl cis-trans isomerase function may play a role in the conformational modification of amelogenin and enable its role as a molecular hinge in the promotion of crystal growth (Delak et al., 2009).

In conclusion, this integrative proteomic/cell biological analysis of postnatal mouse molar enamel development identifies many of the substantial changes in the enamel matrix protein and mineral phase that take place during postnatal mouse molar amelogenesis, including (i) relatively high levels of matrix protein secretion during the early secretory stage on postnatal day 2, (ii) conversion of calcium phosphates to apatite, peak protein folding and stress protein counts, and increased cytoskeletal protein levels such as actin and tubulin on day 4, as well as (iii) secondary structure changes, isomerase activity, highest amelogenin levels, and peak phosphate/carbonate incorporation between postnatal days 6 and 8 (Fig. 5C).

2.6. References

- Al Kawas, S., Amizuka, N., Bergeron, J., and Warshawsky, H. (1996). Immunolocalization of the cation-independent mannose 6-phosphate receptor and cathepsin B in the enamel organ and alveolar bone of the rat incisor. Calcified Tissue International 59, 192-199.
- Antonakos, A., Liarokapis, E., and Leventouri, T. (2007). Micro-Raman and FTIR studies of synthetic and natural apatites. Biomaterials 28, 3043-3054.
- Aoba, T., Komatsu, H., Shimazu, Y., Yagishita, H., and Taya, Y. (1998). Enamel mineralization and an initial crystalline phase. Connective Tissue Research 38, 129-137.

- Balbach, J., and Schmid, F.X. (2000). Proline isomerization and its catalysis in protein folding. Mechanisms of Protein Folding 2, 212-249.
- Bard, J. (2007). Systems developmental biology: the use of ontologies in annotating models and in identifying gene function within and across species. Mammalian Genome 18, 402-411.
- Bartlett, J., and Simmer, J. (1999). Proteinases in developing dental enamel. Critical Reviews in Oral Biology & Medicine 10, 425-441.
- Bartlett, J., and Smith, C. (2013). Modulation of cell-cell junctional complexes by matrix metalloproteinases. Journal of Dental Research 92, 10-17.
- Bartlett, J.D. (2013). Dental enamel development: proteinases and their enamel matrix substrates. ISRN Dentistry 2013.
- Blair, H.C., Teitelbaum, S.L., Ghiselli, R., and Gluck, S. (1989). Osteoclastic bone resorption by a polarized vacuolar proton pump. Science 245, 855-858.
- Boskey, A.L., Goldberg, M., Kulkarni, A., and Gomez, S. (2006). Infrared imaging microscopy of bone: Illustrations from a mouse model of Fabry disease. Biochimica et Biophysica Acta (BBA)-Biomembranes 1758, 942-947.
- Brookes, S.J., Barron, M.J., Boot-Handford, R., Kirkham, J., and Dixon, M.J. (2014). Endoplasmic reticulum stress in amelogenesis imperfecta and phenotypic rescue using 4-phenylbutyrate. Human Molecular Genetics 23, 2468-2480.
- Chandramouli, K., and Qian, P.-Y. (2009). Proteomics: challenges, techniques and possibilities to overcome biological sample complexity. Human Genomics and Proteomics 1.

- De Lisle, R.C. (2015). Role of the actin cytoskeleton in acinar cell protein secretion. Pancreapedia: The Exocrine Pancreas Knowledge Base.
- Deakins, M. (1942). Changes in the ash, water, and organic content of pig enamel during calcification. Journal of Dental Research 21, 429-435.
- Delak, K., Harcup, C., Lakshminarayanan, R., Sun, Z., Fan, Y., Moradian-Oldak, J., and Evans, J.S. (2009). The tooth enamel protein, porcine amelogenin, is an intrinsically disordered protein with an extended molecular configuration in the monomeric form. Biochemistry 48, 2272-2281.
- Diekwisch, T. (1988). Localization of microfilaments and microtubules during dental development in the rat. Acta Histochemica. Supplementband 37, 209-212.
- Diekwisch, T., David, S., Bringas, P., Santos, V., and Slavkin, H.C. (1993). Antisense inhibition of AMEL translation demonstrates supramolecular controls for enamel HAP crystal growth during embryonic mouse molar development. Development 117, 471-482.
- Diekwisch, T.G. (1998). Subunit compartments of secretory stage enamel matrix. Connective Tissue Research 38, 101-111.
- Diekwisch, T.G., Berman, B.J., Anderton, X., Gurinsky, B., Ortega, A.J., Satchell, P.G., Williams, M., Arumugham, C., Luan, X., and Mcintosh, J.E. (2002). Membranes, minerals, and proteins of developing vertebrate enamel. Microscopy Research and Technique 59, 373-395.
- Diekwisch, T.G., Berman, B.J., Gentner, S., and Slavkin, H.C. (1995). Initial enamel crystals are not spatially associated with mineralized dentine. Cell and Tissue Research 279, 149-167.
- Do Espirito Santo, A.R., Novaes, P.D., and Line, S.R. (2006). Anisotropic properties of the enamel organic extracellular matrix. European Journal of Oral Sciences 114, 333-337.

- Eastoe, J. (1965). Methods for the determination of phosphate, calcium and protein in small portions of mineralized tissues. Calcified Tissue (edited by Richelle, LJ and Dallemagne, MJ), 265-274.
- Eastoe, J. (1979). Enamel protein chemistry-past, present and future. Journal of Dental Research 58, 753-764.
- Edelman, L.B., Chandrasekaran, S., and Price, N.D. (2009). Systems biology of embryogenesis. Reproduction, Fertility and Development 22, 98-105.
- Elliot, J. (1994). Mineral, synthetic and biological carbonate apatites. Structure and Chemistry of the Apatites and Other Calcium Orthophosphates, 191-304.
- Fincham, A., Moradian-Oldak, J., and Simmer, J. (1999). The structural biology of the developing dental enamel matrix. Journal of Structural Biology 126, 270-299.
- Fleet, M.E., Liu, X., and King, P.L. (2004). Accommodation of the carbonate ion in apatite: An FTIR and X-ray structure study of crystals synthesized at 2–4 GPa. American Mineralogist 89, 1422-1432.
- Gadaleta, S., Paschalis, E., Betts, F., Mendelsohn, R., and Boskey, A. (1996). Fourier transform infrared spectroscopy of the solution-mediated conversion of amorphous calcium phosphate to hydroxyapatite: new correlations between X-ray diffraction and infrared data. Calcified Tissue International 58, 9-16.
- Gaunt, W.A. (1955). The development of the molar pattern of the mouse (Mus musculus). Cells Tissues Organs 24, 249-268.
- Gibson, C.W., Yuan, Z.-A., Hall, B., Longenecker, G., Chen, E., Thyagarajan, T., Sreenath, T., Wright, J.T., Decker, S., and Piddington, R. (2001). Amelogenin-deficient mice display an amelogenesis imperfecta phenotype. Journal of Biological Chemistry 276, 31871-31875.

- Gopinathan, G., Jin, T., Liu, M., Li, S., Atsawasuwan, P., Galang, M.-T., Allen, M., Luan, X., and Diekwisch, T.G. (2014). The expanded amelogenin polyproline region preferentially binds to apatite versus carbonate and promotes apatite crystal elongation. Frontiers in Physiology 5.
- Griffin, N.M., and Schnitzer, J.E. (2011). Overcoming key technological challenges in using mass spectrometry for mapping cell surfaces in tissues. Molecular & Cellular Proteomics 10, R110. 000935.
- Guan, X., Bidlack, F.B., Stokes, N., and Bartlett, J.D. (2014). E-Cadherin can replace N-cadherin during secretory-stage enamel development. PloS One 9, e102153.
- Guan, X., Xu, M., Millar, S.E., and Bartlett, J.D. (2016). Beta-catenin is essential for ameloblast movement during enamel development. European Journal of Oral Sciences 124, 221-227.
- Guggenheim, S. (2005). Simulations of Debye-Scherrer and Gandolfi patterns using a Bruker SMART/APEX Diffractometer system. Bruker-AXS Application Notes Series 373, 1-8.
- Hammarström, L., Wade, C.W., Hanker, J., and Toverud, S. (1971). Cellular differences in acid phosphatase isoenzymes in bone and teeth. Clinical Orthopaedics and Related Research 78, 151-167.
- Herzberg, O., and Moult, J. (1991). Analysis of the steric strain in the polypeptide backbone of protein molecules. Proteins: Structure, Function, and Bioinformatics 11, 223-229.
- Hu, J.C.-C., Hu, Y., Lu, Y., Smith, C.E., Lertlam, R., Wright, J.T., Suggs, C., Mckee, M.D., Beniash, E., and Kabir, M.E. (2014). Enamelin is critical for ameloblast integrity and enamel ultrastructure formation. PloS One 9, e89303.

- Hubbard, M.J. (2000). Calcium transport across the dental enamel epithelium. Critical Reviews in Oral Biology & Medicine 11, 437-466.
- Hughes, J.M., Cameron, M., and Mariano, A.N. (1991). Rare-earth-element ordering and structural variations in natural rare-earth-bearing apatites. American Mineralogist 76, 1165-1173.
- Hunter, J. (1778). The natural history of the human teeth: explaining their structure, use, formation, growth, and diseases. Illustrated with Copper-plates. By John Hunter. J. Johnson.
- Iijima, M., and Moradian–Oldak, J. (2004). Interactions of amelogenins with octacalcium phosphate crystal faces are dose dependent. Calcified Tissue International 74, 522-531.
- Jin, T., Ito, Y., Luan, X., Dangaria, S., Walker, C., Allen, M., Kulkarni, A., Gibson, C., Braatz, R., and Liao, X. (2009). Elongated polyproline motifs facilitate enamel evolution through matrix subunit compaction. PLoS Biol 7, e1000262.
- Josic, D. (2014). Strategies for complete proteomic analysis of hydrophobic proteins in complex biological samples-hyde-and seek. Journal of Data Mining in Genomics & Proteomics 5, 1.
- Kasper, M., Karsten, U., Stoslek, P., and Moll, R. (1989). Distribution of intermediate-filament proteins in the human enamel organ: unusually complex pattern of coexpression of cytokeratin polypeptides and vimentin. Differentiation 40, 207-214.
- Keil, A. (1935). Über den wandel der doppelbrechung des zahnschmelzes bei entkalkung, wärmeeinwirkung und karies. Cell and Tissue Research 22, 633-649.
- Kero, D., Govorko, D.K., Vukojevic, K., Cubela, M., Soljic, V., and Saraga-Babic, M. (2014). Expression of cytokeratin 8, vimentin, syndecan-1 and Ki-67 during human tooth development. Journal of Molecular Histology 45, 627-640.

- Kersteen, E.A., and Raines, R.T. (2003). Catalysis of protein folding by protein disulfide isomerase and small-molecule mimics. Antioxidants and Redox Signaling 5, 413-424.
- Kidd, M.E., Shumaker, D.K., and Ridge, K.M. (2014). The role of vimentin intermediate filaments in the progression of lung cancer. American Journal of Respiratory Cell and Molecular Biology 50, 1-6.
- Klug, H.P., and Alexander, L.E. (1954). X-ray diffraction procedures. Wiley-Interscience, Ch.9.
- Kubler, M.-D., Lesot, H., and Ruch, J.V. (1988). Temporo-spatial distribution of matrix and microfilament components during odontoblast and ameloblast differentiation. Development Genes and Evolution 197, 212-220.
- Lacruz, R.S. (2017). Enamel: Molecular identity of its transepithelial ion transport system. Cell Calcium.
- Lacruz, R.S., Nanci, A., Kurtz, I., Wright, J.T., and Paine, M.L. (2010). Regulation of pH during amelogenesis. Calcified Tissue International 86, 91-103.
- Lagerström, M., Dahl, N., Nakahori, Y., Nakagome, Y., Bäckman, B., Landegren, U., and Pettersson, U. (1991). A deletion in the amelogenin gene (AMG) causes X-linked amelogenesis imperfecta (AIH1). Genomics 10, 971-975.
- Lesot, H., Osman, M., and Ruch, J.V. (1981). Immunofluorescent localization of collagens, fibronectin, and laminin during terminal differentiation of odontoblasts. Developmental Biology 82, 371-381.
- Leventouri, T., Antonakos, A., Kyriacou, A., Venturelli, R., Liarokapis, E., and Perdikatsis, V. (2009). Crystal structure studies of human dental apatite as a function of age. International Journal of Biomaterials 2009.

- Liu, H., Yan, X., Pandya, M., Luan, X., and Diekwisch, T.G. (2016). Daughters of the enamel organ: development, fate, and function of the stratum intermedium, stellate reticulum, and outer enamel epithelium. Stem Cells and Development 25, 1580-1590.
- Lu, X., Ito, Y., Kulkarni, A., Gibson, C., Luan, X., and Diekwisch, T.G. (2011). Ameloblastin-rich enamel matrix favors short and randomly oriented apatite crystals. European Journal of Oral Sciences 119, 254-260.
- Maciver, S.K., and Hussey, P.J. (2002). The ADF/cofilin family: actin-remodeling proteins. Genome Biology 3, reviews3007. 3001.
- Manneville, J.-B., Etienne-Manneville, S., Skehel, P., Carter, T., Ogden, D., and Ferenczi, M. (2003). Interaction of the actin cytoskeleton with microtubules regulates secretory organelle movement near the plasma membrane in human endothelial cells. J Cell Sci 116, 3927-3938.
- Masuya, H., Shimizu, K., Sezutsu, H., Sakuraba, Y., Nagano, J., Shimizu, A., Fujimoto, N., Kawai, A., Miura, I., and Kaneda, H. (2005). Enamelin (Enam) is essential for amelogenesis: ENU-induced mouse mutants as models for different clinical subtypes of human amelogenesis imperfecta (AI). Human Molecular Genetics 14, 575-583.
- Mayer, M., and Bukau, B. (2005). Hsp70 chaperones: cellular functions and molecular mechanism. Cellular and Molecular Life Sciences 62, 670.
- Mccrea, P.D., and Gu, D. (2010). The catenin family at a glance. J Cell Sci 123, 637-642.
- Mochida, K., and Shinozaki, K. (2011). Advances in omics and bioinformatics tools for systems analyses of plant functions. Plant and Cell Physiology 52, 2017-2038.
- Moradian-Oldak, J. (2012). Protein-mediated enamel mineralization. Frontiers in Bioscience: a Journal and Virtual Library 17, 1996.

- Morgan, E., Yetkinler, D., Constantz, B., and Dauskardt, R. (1997). Mechanical properties of carbonated apatite bone mineral substitute: strength, fracture and fatigue behaviour. Journal of Materials Science: Materials in Medicine 8, 559-570.
- Morita, R., Kihira, M., Nakatsu, Y., Nomoto, Y., Ogawa, M., Ohashi, K., Mizuno, K., Tachikawa, T., Ishimoto, Y., and Morishita, Y. (2016). Coordination of cellular dynamics contributes to tooth epithelium deformations. PloS One 11, e0161336.
- Neco, P., Giner, D., Del Mar Frances, M., and Gutiérrez, L.M. (2003). Differential participation of actin-and tubulin-based vesicle transport systems during secretion in bovine chromaffin cells. European Journal of Neuroscience 18, 733-742.
- Nishikawa, S., Fujiwara, K., and Kitamura, H. (1988). Formation of the tooth enamel rod pattern and the cytoskeletal organization in secretory ameloblasts of the rat incisor. European Journal of Cell Biology 47, 222-232.
- Nishikawa, S., Tsukita, S., Tsukita, S., and Sasa, S. (1990). Localization of adherens junction proteins along the possible sliding interface between secretory ameloblasts of the rat incisor. Cell Structure and Function 15, 245-249.
- Paine, M.L., White, S.N., Luo, W., Fong, H., Sarikaya, M., and Snead, M.L. (2001). Regulated gene expression dictates enamel structure and tooth function. Matrix Biology 20, 273-292.
- Pal, D., and Chakrabarti, P. (1999). Cis peptide bonds in proteins: residues involved, their conformations, interactions and locations. Journal of Molecular Biology 294, 271-288.
- Prajapati, S., Tao, J., Ruan, Q., De Yoreo, J.J., and Moradian-Oldak, J. (2016). Matrix metalloproteinase-20 mediates dental enamel biomineralization by preventing protein occlusion inside apatite crystals. Biomaterials 75, 260-270.

- Pugach, M., Suggs, C., Li, Y., Wright, J.T., Kulkarni, A., Bartlett, J., and Gibson, C. (2013). M180 amelogenin processed by MMP20 is sufficient for decussating murine enamel. Journal of Dental Research 92, 1118-1122.
- Rangarajan, E.S., and Izard, T. (2013). Dimer asymmetry defines α-catenin interactions. Nature Structural & Molecular Biology 20, 188-193.
- Robinson, C. (2014). Enamel maturation: a brief background with implications for some enamel dysplasias. Frontiers in Physiology 5.
- Robinson, C., Briggs, H., Atkinson, P., and Weatherell, J. (1979). Matrix and mineral changes in developing enamel. Journal of Dental Research 58, 871-882.
- Robinson, C., Brookes, S.J., Bonass, W.A., Shore, R.C., and Kirkham, J. (1997). Enamel maturation. Ciba Foundation Symposium: John Wiley & sons Ltd, 156-174.
- Robinson, C., Fuchs, P., Deutsch, D., and Weatherell, J. (1978). Four chemically distinct stages in developing enamel from bovine incisor teeth. Caries Research 12, 1-11.
- Robinson, C., Fuchs, P., and Weatherell, J. (1981). The appearance of developing rat incisor enamel using a freeze fracturing technique. Journal of Crystal Growth 53, 160-165.
- Robinson, C., Kirkham, J., and Hallsworth, A. (1988). Volume distribution and concentration of protein, mineral and water in developing bovine enamel. Archives of Oral Biology 33, 159-162.
- Saito, K., Fukumoto, E., Yamada, A., Yuasa, K., Yoshizaki, K., Iwamoto, T., Saito, M., Nakamura, T., and Fukumoto, S. (2015). Interaction between fibronectin and β1 integrin is essential for tooth development. PloS One 10, e0121667.

- Santoni, V., Molloy, M., and Rabilloud, T. (2000). Membrane proteins and proteomics: un amour impossible? Electrophoresis 21, 1054-1070.
- Schmidt, W. (1959). Texturdoppelbrechung der organischen Matrix fertigen menschlichen schmelzes nebst bemerkungen zur optik entkalkten dentins. Cell and Tissue Research 49, 319-329.
- Schour, I., and Massler, M. (1949). The teeth. The Rat in Laboratory Investigation 2, 104-165.
- Shaw, P.E. (2002). Peptidyl-prolyl isomerases: A new twist to transcription. EMBO Reports 3, 521-526.
- Simmer, J.P., and Hu, J.C.-C. (2002). Expression, structure, and function of enamel proteinases. Connective Tissue Research 43, 441-449.
- Slavkin, H.C., Bessem, C., Bringas, P., Zeichner-David, M., Nanci, A., and Snead, M.L. (1988). Sequential expression and differential function of multiple enamel proteins during fetal, neonatal, and early postnatal stages of mouse molar organogenesis. Differentiation 37, 26-39.
- Slavkin, H.C., Mino, W., and Bringas, P. (1976). The biosynthesis and secretion of precursor enamel protein by ameloblasts as visualized by autoradiography after tryptophan administration. The Anatomical Record 185, 289-312.
- Smith, C., and Nanci, A. (1989). A method for sampling the stages of amelogenesis on mandibular rat incisors using the molars as a reference for dissection. The Anatomical Record 225, 257-266.

- Somogyi, E., Petersson, U., Hultenby, K., and Wendel, M. (2003). Calreticulin—an endoplasmic reticulum protein with calcium-binding activity is also found in the extracellular matrix. Matrix Biology 22, 179-191.
- Spears, I., Van Noort, R., Crompton, R., Cardew, G., and Howard, I. (1993). The effects of enamel anisotropy on the distribution of stress in a tooth. Journal of Dental Research 72, 1526-1531.
- Stack, M. (1960). Changes in the organic matrix of enamel during growth. Journal of Bone and Joint Surgery - Bristish Volume : British Editorial Soc Bone Joint Surgery, 853-853.
- Takagi, Y., Fujita, H., Katano, H., Shimokawa, H., and Kuroda, T. (1998). Immunochemical and biochemical characteristics of enamel proteins in hypocalcified amelogenesis imperfecta. Oral Surgery, Oral Medicine, Oral Pathology, Oral Radiology, and Endodontology 85, 424-430.
- Terling, C., Heymann, R., Rozell, B., Öbrink, B., and Wroblewski, J. (1998). Dynamic expression of E-cadherin in ameloblasts and cementoblasts in mice. European Journal of Oral Sciences 106, 137-142.
- Termine, J., Belcourt, A., Christner, P., Conn, K., and Nylen, M. (1980). Properties of dissociatively extracted fetal tooth matrix proteins. I. Principal molecular species in developing bovine enamel. Journal of Biological Chemistry 255, 9760-9768.
- Tye, C.E., Lorenz, R.L., and Bartlett, J.D. (2009). Lysosomal protease expression in mature enamel. Cells Tissues Organs 189, 111-114.
- Vedrenne, C., Klopfenstein, D.R., and Hauri, H.-P. (2005). Phosphorylation controls CLIMP-63–mediated anchoring of the endoplasmic reticulum to microtubules. Molecular Biology of the Cell 16, 1928-1937.

- Vignoles-Montrejaud, M. (1984). Contibution a l'etude des apatites carbonate es de type B. [These d'Etat], Institut National Polytechnique de Toulouse, France.
- Wang, H., Tannukit, S., Zhu, D., Snead, M.L., and Paine, M.L. (2005). Enamel matrix protein interactions. Journal of Bone and Mineral Research 20, 1032-1040.
- Wegele, H., Müller, L., and Buchner, J. (2004). Hsp70 and Hsp90—a relay team for protein folding. Reviews of Physiology, Biochemistry and Pharmacology. Springer), 1-44.
- Woltgens, J., Lyaruu, D.M., Bronckers, A., Bervoets, T., and Van Duin, M. (2003). Biomineralization during early stages of the developing tooth in vitro with special reference to secretory stage of amelogenesis. International Journal of Developmental Biology 39, 203-212.
- Wopenka, B., and Pasteris, J.D. (2005). A mineralogical perspective on the apatite in bone. Materials Science and Engineering: C 25, 131-143.
- Xu, C., Reed, R., Gorski, J.P., Wang, Y., and Walker, M.P. (2012). The distribution of carbonate in enamel and its correlation with structure and mechanical properties. Journal of Materials Science 47, 8035-8043.
- Xu, W., Coll, J.-L., and Adamson, E.D. (1998). Rescue of the mutant phenotype by reexpression of full-length vinculin in null F9 cells; effects on cell locomotion by domain deleted vinculin. Journal of Cell Science 111, 1535-1544.
- Xu, X.-H., Zhang, H.-L., Han, R., Gu, Z.-L., and Qin, Z.-H. (2006). Enhancement of neuroprotection and heat shock protein induction by combined prostaglandin A 1 and lithium in rodent models of focal ischemia. Brain Research 1102, 154-162.
- Zapanta-Legeros, R. (1965). Effect of carbonate on the lattice parameters of apatite. Nature 206, 403-404.

- Zhang, X., Ramirez, B.E., Liao, X., and Diekwisch, T.G. (2011). Amelogenin supramolecular assembly in nanospheres defined by a complex helix-coil-PPII helix 3D-structure. PLoS One 6, e24952.
- Zhu, L., Liu, H., Witkowska, H.E., Huang, Y., Tanimoto, K., and Li, W. (2014). Preferential and selective degradation and removal of amelogenin adsorbed on hydroxyapatites by MMP20 and KLK4 in vitro. Frontiers in Physiology 5.

3. POSTTRANSLATIONAL AMELOGENIN PROCESSING AND CHANGES IN MATRIX ASSEMBLY DURING ENAMEL DEVELOPMENT*

3.1. Overview

The extracellular tooth enamel matrix is a unique, protein-rich environment that provides the structural basis for the growth of long and parallel oriented enamel crystals. Here we have conducted a series of in vivo and in vitro studies to characterize the changes in matrix shape and organization that take place during the transition from ameloblast intravesicular matrices to extracellular subunit compartments and pericrystalline sheath proteins, and correlated these changes with stages of amelogenin matrix protein posttranslational processing. Our transmission electron microscopic studies revealed a 2.5-fold difference in matrix subunit compartment dimensions between secretory vesicle and extracellular enamel protein matrix as well as conformational changes in matrix structure between vesicles, stippled materials, and pericrystalline matrix. Enamel crystal growth in organ culture demonstrated granular mineral deposits associated with the enamel matrix framework, dot-like mineral deposits along elongating initial enamel crystallites, and dramatic changes in enamel matrix configuration following the onset of enamel crystal formation. Atomic force micrographs provided evidence for the presence of both linear and hexagonal/ring-shaped full-length recombinant amelogenin protein assemblies on mica surfaces, while Nickel-staining of the N-terminal amelogenin N92 His-tag revealed 20nm diameter oval and globular amelogenin assemblies in N92 amelogenin

* Reprinted with permission from Frontiers Editorial office - Pandya, M., Lin, T., Li, L., Allen, M., Jin, T., Luan, X., and Diekwisch, T.G.H. (2017). Posttranslational amelogenin processing and changes in matrix assembly during enamel development. Front. Physiol. 8:790. doi: 10.3389/fphys.2017.00790.

matrices. Western blot analysis comparing loosely bound and mineral-associated protein fractions of developing porcine enamel organs, superficial and deep enamel layers demonstrated (i) a single, full-length amelogenin band in the enamel organ followed by 3kDa cleavage upon entry into the enamel layer, (ii) a close association of 8-16kDa C-terminal amelogenin cleavage products with the growing enamel apatite crystal surface, and (iii) a remaining pool of N-terminal amelogenin fragments loosely retained between the crystalline phases of the deep enamel layer. Together, our data establish a temporo-spatial correlation between amelogenin protein processing and the changes in enamel matrix configuration that take place during the transition from intracellular vesicle compartments to extracellular matrix assemblies and the formation of protein coats along elongating apatite crystal surfaces. In conclusion, our study suggests that enzymatic cleavage of the amelogenin enamel matrix protein plays a key role in the patterning of the organic matrix framework as it affects enamel apatite crystal growth and habit.

3.2. Introduction

Tooth enamel is a remarkable bioceramic characterized by extraordinary hardness, resilience and fracture resistance. The formation of this extremely hard biomineral within the soft and gel-like extracellular enamel matrix remains an enigma in biomedical research to this day. In-depth understanding and visualization of the biological processes and mechanisms involved in amelogenesis are hampered by the limitations of conventional imaging techniques and artifacts introduced because of sample preparation. Specifically, optical *in vitro* and i*n vivo* imaging are limited by the resolution of conventional light microscopy; scanning and transmission electron microscopy are limited by sample preparation for near-vacuum electron beam imaging conditions, contrasting procedures for organic matrix visualization, and beam

damage to the mineral phase; atomic force microscopy provides high resolution but is restricted to surface topographies; and nuclear magnetic resonance spectroscopy lacks the topographical information provided by electro-optical imaging techniques. Yet, disregarding the weaknesses of individual strategies, the combination of information derived from complimentary approaches has yielded much progress toward a comprehensive understanding of the many aspects contributing to early enamel biomineralization. The combination of imaging and analytical techniques together with a plethora of individual approaches has resulted in a number of model systems that explain various aspects of enamel biomineralization.

Early enamel researchers thought of the enamel matrix as a "concentrated amorphous gel structure, rather than a more highly oriented assembly of fibres"(Fearnhead, 1963)and believed that the concept of the **enamel matrix as a thixotropic gel** would explain its "potential mobility as the protein would flow from regions where rapid growth of apatite crystallites caused a local increase in pressure to adjacent, relatively unmineralized regions, where it could initiate further crystals" (Eastoe, 1963). John E. Eastoe fathomed that the enamel proteins should be considered "as the true matrix of enamel in which the apatite crystallites are laid down, by a process which is not yet explored by which may be analogous to the epitactic mechanism believed to occur in collagenous mineralized tissues"(Glimcher, 1959;Eastoe, 1963). Thus, Eastoe imagined the enamel matrix as a homogeneous gel in which the enamel proteins freely float between further crystallized regions close to the dentin-enamel junction to the sites of early apatite crystallization at the ameloblast cell membrane, readily aiding each crystal to be initiated and grown "until they come into contact with their neighbours" (Eastoe, 1963). Notwithstanding this insightful speculation related to the function of the enamel matrix, Eastoe deserves much credit for the

discovery of amelogenins as tissue-specific enamel proteins rich in proline, glutamic acid, and histidine (Eastoe, 1960).

Eastoe's contemporaries, the electron microscopists Dorothy F. Travis and Marie U. Nylen, pioneered an ultrastructural perspective of the developing enamel matrix by recognizing the **stippled or finely granular materials** located at the mineralization front **as morphological building blocks of the enamel matrix** (Frank et al., 1964;Travis and Glimcher, 1964;Reith, 1967;Nylen, 1979). They and others reported the presence of 5-7 nm granules in sectioned material and in suspensions of developing enamel (Fearnhead, 1965;Nylen, 1979). The existence of stippled materials was briefly called into question when the effect of fixative temperature on matrix structure was discovered (Lyaruu et al., 1982;Lyaruu et al., 1984). Changes in enamel suprastructure at 4^0C temperature had been described earlier and attributed to the high proline content of the enamel matrix (Nikiforuk and Simmons, 1965). Needless to say, faithful ultrastructural examination of the enamel matrix requires fixation at 37^0C or room temperature as the mammalian body temperature does not drop to 4^0C (Diekwisch et al., 1993;Diekwisch et al., 1995). The functional significance of the **enamel matrix stippled materials as supramolecular subunit compartments responsible for the control of enamel crystal growth** became evident in study in which the translation of the key enamel matrix protein amelogenin was inhibited using an antisense strategy (Diekwisch et al., 1993). The concept of enamel matrix supramolecular assemblies as the basis for enamel crystal spacing and growth was thereafter confirmed using organ culture data (Diekwisch et al., 1995) and atomic force microcroscopy of unfixed freshly prepared enamel matrix (Diekwisch et al., 1993;Diekwisch et al., 1995;Diekwisch, 1998).

Inversely interpreted transmission electron micrographs together with atomic force microscopy images and dynamic light scattering data helped to advance the **nanosphere theory of enamel crystal growth** (Fincham et al., 1994;Fincham et al., 1995;Paine et al., 2001). A simplified sketch (Fincham et al., 1999) illustrates beaded rows of amelogenin nanospheres surrounding growing enamel crystals, and begs for the question as to how the needle-shaped thin enamel crystals would possibly grow while surrounded by densely packed globular structures. Indeed, the task of reconciling the rounded globes of amelogenin nanospheres with the sharp-edged hexagonal cross-sections of enamel apatite crystals resembles the fitting of a square peg in a round hole. Today, none of the three pillars of the nanosphere theory clearly provides evidence for the presence of spherical subunits in the enamel matrix: (i) light scattering data simply reference radii and not necessarily imply the presence of spherical assemblies, (ii) atomic force micrographs visualize the surface topographies of enamel proteins assembled on mica sheets and not in three dimensions, and (iii) the electron micrographs initially recruited to support the nanosphere theory incorrectly refer to the circular spaces in between nanospheres as protein assemblies instead of the electron dense protein coats associated with the growing enamel crystals (Diekwisch, 1998), a reversal of stained and unstained matrix compartments analogous to Edgar Rubin's young girl/old woman optical illusion. Moreover, the concept of self-assembly of amelogenins into spherical subunits is not universally accepted, as some investigators have argued that the organic enamel matrix organizes into fibrillar (Frank et al., 1960), lamellar (Ronnholm, 1962), or helical structures (Smales, 1975), or filaments and ribbons (Martinez-Avila et al., 2012;Carneiro et al., 2016). Recent small angle X-ray scattering (SAXS) studies propose that amelogenins self-assemble as nano-oblates with a 1:2 aspect ratio (Aichmayer et al., 2005;Margolis et al., 2006). Nevertheless, the nanosphere theory has established a model for the

role of globular enamel protein assemblies as structural entities involved in enamel hydroxyapatite crystal growth.

The ubiquitous presence of the amelogenin-rich extracellular enamel matrix throughout all stages of enamel crystal formation infers an involvement in multiple aspects of matrix-mediated enamel crystal growth, including (i) matrix assembly, (ii) enamel crystal nucleation, (iii) initial crystal fusion of apatite precursors into apatite ribbons, and (iv) eventual crystal elongation and growth of true apatite crystals. Three **models have been established to explain amelogenin nanosphere assembly and interaction among nanospheres**. A first model based on SAXS data postulates that amelogenin nanospheres assemble into nanospheres with a dense hydrophobic core and a shell of hydrophilic and negatively charged chain segments (Aichmayer et al., 2005;Margolis et al., 2006). A second model, the **amelogenin micelle model**, focuses on the distribution of hydrophilic and hydrophobic regions within the amelogenin molecule and hypothesize that amelogenins aggregate into micelles through the ionic interactions between positively and negatively charged mini-domains and the complementary domain of another amelogenin molecule in reverse orientation (Fukae et al., 2007). A third model based on heteronuclear single quantum coherence nuclear magnetic resonance (HSQC NMR) spectra and analytical ultracentrifugation proposes that **amelogenins self-assemble as donut-shaped entities** through ipsilateral interactions at the α-helical N-terminus of the molecule, while the hydrophilic C-termini point toward the outside of the assembly (Zhang et al., 2011). Together, these studies provide a good understanding of the *in vitro* self-assembly capacity of amelogenin into nanoscale subunits. However, a universally accepted model explaining the *in vivo* structural entities of protein-mediated enamel crystal growth and their transformation throughout

development is still lacking and in need of further investigation (Ruan and Moradian-Oldak, 2015).

Three recent *in vitro* studies have shed light on the possible **protein/mineral interactions that take place during the onset of enamel crystal growth**. The first of these three studies took advantage of a constant composition crystallization system, allowing for the control of ion concentration changes at the nanomolar level (Tomson and Nancollas, 1978). When used in combination with recombinant porcine amelogenin, this constant composition crystallization approach yielded hierarchically organized amelogenin and amorphous calcium phosphate (ACP) nanorod microstructures involving the **coassembly of amelogenin-ACP particles** (Yang et al., 2010). Second, a cryoelectron microscopy-based study has further confirmed that amelogenin undergoes stepwise hierarchical self-assembly, and that these assemblies are involved in the stabilization of mineral prenucleation clusters and their arrangement into linear chains (Fang et al., 2011). This study also demonstrated that the prenucleation clusters subsequently fused to form needle-shaped mineral particles and subsequently apatite crystallites (Fang et al., 2011). Finally, a combined circular dichroism/nuclear magnetic resonance (CD/NMR), dynamic light scattering, and fluorescence spectroscopy study resulted in a model for **nanosphere formation via oligomers**, suggesting that nanospheres disassemble to form oligomers in mildly acidic environment via histidine protonation (Bromley et al., 2011). In their model, amelogenins undergo stepwise self-assembly from monomers at pH3.5 to oligomers at pH5.5 and to nanospheres at pH8, while subsequent nanosphere breakdown would increase the amelogenin binding surface area to interact with the apatite crystal surface (Bromley et al., 2011). All three of these models postulate a very close interaction between the mineral and the protein phase at the site of initial calcium phosphate

crystal growth. Such an intimate relationship between the organic protein matrix and the growing crystal phase goes back to earlier concepts proposed as part of Ermanno Bonucci's **crystal ghost theory** (Bonucci et al., 1988;Bonucci, 2014).

A number of morphological findings have helped to further expand our understanding of enamel crystal growth beyond the nanosphere stage, including the visualization of rows of globular assemblies on the surface of developing enamel hydroxyapatite crystal planes via freeze fracture electron microscopy (Moradian-Oldak and Goldberg, 2005), reports of **nanosphere disassembly and "shedding" of amelogenins onto apatite surfaces** and associated changes in amelogenin secondary structure (Tarasevich et al., 2009a;Tarasevich et al., 2009b;Tarasevich et al., 2010;Lu et al., 2013), and the binding of globular matrix protein assemblies to developing enamel crystals *in vitro* (Robinson et al., 1981;Wallwork et al., 2001). Together, these findings lend support for a classic **model of matrix mediated enamel crystal growth**, henceforth dubbed the **beehive model**, which is comprised of strings of mineral/matrix nuclei that form a mantle of hexagonally arranged enamel mineral precursor deposits on the surface of growing enamel apatite crystals (Robinson et al., 1990).

Most recent reports about **filamentous amelogenin nanoribbon self-assembly** and their potential impact on enamel crystal formation add a unique dimension to the many shapes and forms resulting from amelogenin intermolecular associations (Martinez-Avila et al., 2011;Martinez-Avila et al., 2012;Carneiro et al., 2016). Originally, these filamentous amelogenin nanoribbons were detected at water-oil interfaces (Martinez-Avila et al., 2011) or in the presence of calcium and phosphate ions (Martinez-Avila et al., 2011). Similarities between amelogenin nanoribbons and the amyloid polyglutamine fibrillar aggregates as they occur in neurodegenerative diseases (Chen et al., 2002;Tanaka et al., 2002;Schneider et al.,

2011;Lyubchenko et al., 2012;Buchanan et al., 2014) have been invoked to explain the concept of nanoribbons templating apatite growth in human enamel (Carneiro et al., 2016). However, elongated enamel protein matrix ribbons without a close association to the adjacent mineral do not occur during enamel development *in vivo* (Diekwisch et al., 1995;Diekwisch et al., 2002), and the protein assemblies generated in the filamentous nanoribbon studies are rather evidence of the unique propensity of amelogenins to form elongated assemblies *in vitro* than a physiological occurrence during mammalian amelogenesis.

The present contribution seeks to introduce a developmental approach toward the relationship between enamel ions and proteins during enamel crystal formation and growth. Here we hypothesize that enamel ions and proteins are intimately associated with each other throughout the course of amelogenesis, starting from ion transport until advanced crystal growth, and that changes in mineral habit and protein conformation are caused by amelogenin enamel protein fragmentation. To verify our **dynamic three-phase model of enamel matrix transformation and crystal growth (Fig. 4)** we have interrogated electron micrographs of developing mouse molar enamel *in vivo* and *in vitro* and analyzed amelogenin self-assemblies using atomic force microscopy, fluorescence microscopy, and Nickel-labeling of the amelogenin N-terminus. To ask whether stage-specific changes in enamel matrix configuration were related to the presentation of amelogenin cleavage products within the matrix and adjacent to the crystal surface, we have separated porcine tooth molars into enamel organ, superficial and deep enamel preparations and performed a two-step protein extraction procedure separating loosely bound and mineral bound enamel proteins and probed protein extracts using N- and C-terminal amelogenin antibodies on Western blots. Together, these data provide new insights into the conformational

changes of enamel matrix structure and related effects of amelogenin processing that take place during enamel matrix assembly, enamel crystal nucleation, and enamel crystal growth.

3.3. Materials and Methods

3.3.1. Animal experiments and organ culture

For the preparation of two days postnatal mouse molars, mice were sacrificed according to UIC animal care regulation, molars were dissected from mandibles and immersed into Karnovsky's fixative as previously described (Diekwisch et al., 1995). For tooth organ culture studies, E16 timed-pregnant Swiss-Webster mice were sacrificed and mandibular first molars were dissected.

El6 cap stage tooth organs were cultured for 12 days in BGJb+ medium (Fitton-Jackson's modified BGJ medium) supplemented with 100 g/ml L-ascorbic acid and 100 U/ml penicillin/streptomycin as previously described (Diekwisch et al., 1995). Explanted molars were cultured at 37^0C with 95% air and 5% CO_2. Initial pH was adjusted to 7.4 and the medium was changed every other day.

3.3.2. Transmission electron microscopy

Three days postnatal mouse molar tooth organs as well as E16 tooth organs cultured for 12 days were fixed in Karnovsky's fixative as previously described (Diekwisch, 1998), dehydrated and embedded in Eponate 12 (Ted Pella, Redding, CA). Sections were cut on a Leica Ultracut UCT ultramicrotome. After drying, sections were contrasted in 1% uranyl acetate followed by Reynold's lead citrate for 15 min each. Observations were made on a JEOL 1220EX transmission electron microscope at the UIC Research Resources Center (Chicago, IL).

3.3.3. Proteins

The full length mouse amelogenin (M179), the N-terminal amelogenin N92 coding sequence, and the C-terminal amelogenin C86 were cloned into pASK-43(+) with EcoR I and XhoI restriction sites at the 5' and 3' end respectively as previously described(Jin et al., 2009;Zhang et al., 2011). M179 is the full-length mouse amelogenin protein lacking the N-terminal methionine (Simmer et al. 1994), while the terms N92 and C86 denote recombinant proteins based on the N-terminal amelogenin 92 amino acid fragment or the C-terminal amelogenin 86 amino acid fragment (Zhang et al., 2011). For Nickel staining of the N-terminal polyhistidine tag, an N-terminal MRGSHHHHHHGAGDRGPE HIS-tag was inserted at N-terminus of the protein. BL21-DM* host bacteria were cultured at 37^0C until the OD_{600} reached 0.8 and then were induced at 32^0C for 4 hours. The expressed proteins were absorbed onto a Ni-NTA agarose column and washed with 10 column volumes of PBS and 3 column volumes of 40mM imidazole in PBS, followed by protein elution with a pH 5.0 gradient (from 50mM to 500mM) imidazole PBS solution and dialysis against H_2O. Subsequently, the purified proteins were concentrated to about 10mg/ml using a Centriprep YM-3 column. Finally, the polyproline repeat amelogenin PXX33 peptide (>99% purity, sequence PMQPQPPVHPMQPLPPQPPLPPMFPMQPLPPML) was synthesized by Genescript (Piscataway, NJ).

3.3.4. Atomic force microscopy

The atomic force microscope (AFM) measurements were carried out using an extended MultiMode AFM (MMAFM) integrated with a NanoScope IIIa controller (Veeco Instruments,

Santa Barbara, CA) and a Q-Control Module (nanoAnalytics, Muenster, Germany) as previously described (Jin et al., 2009). The MMAFM was equipped with a calibrated E-type piezoelectric scanner and a glass cell for fluid TappingMode AFM (both from Veeco). The silicon AFM cantilever/probe used in this study was rectangular in shape, 130 µm in length and 35 µm in width (NSC36, MikroMasch). The advertised typical force constant and resonant frequency of this cantilever/probe is 0.6 N/m and 75 kHz respectively. Nominal sharpness of the probe-tip end radius is ≤10 nm. The cantilever/probes were oscillated near 30 kHz at low amplitude for fluid tapping mode AFM. Fluid damping reduces the resonant frequency of rectangular AFM cantilevers in air by approximately 50%. The AFM substrate used for protein adsorption was Grade V5, Pelco mica (10 x 40 mm) purchased from Ted Pella (Redding, CA). The mica was freshly cleaved using adhesive tape prior to use. Stock solutions of 10-20 mg/ml protein (either amelogenin M179 or C86) in 40 mM Tris (pH 8.0) were mixed and stored at 4º C and analyzed by AFM. Stock solutions were diluted typically at 1:100 into the blank AFM imaging buffer (40 mM Tris, pH 8.0) during scanning and adsorption to mica was monitored. Typical AFM scan rates were 1.0 - 1.25 Hz for 512 data points x 256 lines. The AFM images were planefit to correct for background sloping errors.

3.3.5. Fluorescent images of aqueous protein assemblies

Lyophilized recombinant M179 full-length mouse amelogenin and synthesized PXX polyproline repeat peptide were immersed in DDW (pH 7.4) overnight and allowed to self-assemble on a glass slide kept within a humid chamber. Same amounts of each protein were used in this study. After 24 hours, 1% fluorescein was added to the aqueous solution for 1 hour.

Subsequently protein solutions on glass slides were examined under a cover slip using a Leica fluorescent microscope with a 100x oil immersion lens.

3.3.6. Polyhistidine tag labeling and electron microscopy

Droplets containing 100µl of diluted (1mg/ml) pH7.5-8.0 His-tagged recombinant N92 amelogenin were placed on carbon coated copper TEM grids (Ted Pella, Redding, CA) and incubated in a moisturized container at 37^0C for 2hours. Thereafter, TEM grids were quickly rinsed with DDW, immersed into 100µl of freshly prepared 1% $NiSO_4$ (Sigma, St. Louis, MO) solution for 30 minutes, quickly rinsed with DDW again, air dried, and analyzed using a JEOL 1220EX transmission electron microscope at the UIC Research Resources Center (Chicago, IL).

3.3.7. Western Blot

Three months old porcine mandibles were obtained from a local animal farm, and enamel organ epithelium and enamel matrix proteins were collected immediately after slaughter from unerupted mandibular molars. As a first step, the epithelial enamel organ (EO) was collected separately from the matrix and subjected to protein extraction. As a second step, two successive layers of the protein rich enamel matrix were scraped off the tooth surface: (i) a superficial enamel matrix layer that was soft in consistency and easily removable without application of force (SEL), and (ii) a deeper enamel matrix layer that was already hardened and required mechanical force to be separated from the underlying and already mineralized dentin surface (DEL). Tissue and matrix from all three groups were then subjected to protein extraction for 5 days with SDS lysis buffer containing 0.5% sodium dodecyl sulfate, 0.05M TRIS-Cl, 1mMol dithiothreitol (DTT) with a pH of 8.0. After lysis, samples were dialyzed for one week at 4°C

against DDH_2O, and centrifuged for 15 min at 2400g and 4°C. As a first step, the SDS soluble supernatant from all three groups was collected for Western blot. After removal of the supernatant, the pellet of all three extracts was subject to a second round of extraction with 4M guanidine HCl. After five days of extraction in 4M guanidine HCL, the extraction solution was once more centrifuged, and the supernatant of the 4M guanidine group of each group was collected and dialyzed for 1 week at 4°C. Thereafter, proteins were concentrated using Amicon spin columns (3kDa cut-off, Millipore, Billerica, MA), and re-suspended in RIPA buffer for Western blot detection.

For Western blot analysis, equal amounts of protein were loaded onto a 10% SDS polyacrylamide gel, subjected to SDS gel electrophoresis and then transferred onto a polyvinylidine difluoride (PVDF) membrane using a semi dry transfer system. The membrane was blocked with 5% dry milk in TBST, probed either with primary antibody against the C-terminal amelogenin fragment or against the N-terminal amelogenin fragment (1:1000), followed by anti-rabbit IgG HRP conjugated secondary antibody (1:2000; cell signaling) incubation. Primary antibodies were based on the following amelogenin-derived peptides: LPPHP GSPGY INLSY EVLTP LKWYQ SMIRQ P (N-terminal antibody) and PLSPI LPELP LEAWP ATDKT KREEV D (C-terminal antibody) and generated in collaboration with Zymed (South San Francisco, CA). A chemiluminescent substrate (Thermo Scientific) was used to reveal the HRP signal.

3.3.8. Statistical Analysis

For this analysis, fifteen subunit compartments located either in secretory vesicles or within the enamel matrix were selected using a random generator and average subunit size and

standard deviations were calculated and reported for both groups. Student's t-test was used to determine statistically significant differences between the two groups and the significance level was set at $\alpha \leq 0.05$.

3.4. Results

3.4.1. Changes in matrix subunit compartment dimensions between secretory vesicle matrix, extracellular enamel protein matrix ("nanospheres"), and pericrystalline protein matrix ("crystal ghosts")

Transmission electron micrographs of developing mouse molar enamel revealed three stages involved in matrix mediated enamel crystal growth (Fig. 1A): (i) initial matrix assembly in ameloblast secretory vesicles, (ii) deposition of an extracellular enamel matrix consisting of stippled materials, and (iii) formation of initial enamel crystallites within this extracellular matrix. Comparison between Figs. 1B and 1C illustrates the remarkable subunit size differences between the enamel matrix of the stippled materials (Fig. 1C) and the matrix within the secretory vesicles (Fig. 1B). Subunit dimensions were 7.07nm+/-1.61nm for the secretory vesicle matrix and 17.47nm+/-3.44nm in the extracellular enamel matrix of the stippled materials (Fig. 1B versus Fig. 1C). The 2.5-fold difference in subunit size was statistically highly significant ($p<0.0001$). Transmission electron micrographs also demonstrated the less than parallel alignment of the earliest enamel crystallites (Fig. 1D) in comparison to the fairly parallel aligned crystal needles at a further advanced state of crystal growth (Fig. 1E). In terms of matrix assembly, these images revealed electron dense globular organic enamel matrix subunits closely associated with growing enamel crystallites (Fig. 1D) and beaded or helical arrangement of organic nanoribbons in close proximity to the elongating apatite crystals (Fig. 1E). Exposure of

isolated and free-standing enamel protein nanoribbons (arrows) was likely due to the thin plane of section on these 400Å diameter ultrathin sections (Fig. 1).

3.4.2. Key features of enamel crystal growth in organ culture: (i) granular mineral deposits associated with the enamel matrix framework, (ii) dot-like mineral deposits along elongating initial enamel crystallites, and (iii) "crystal ghost" organic matrix adjacent to forming enamel crystals

Organ culture models are unique experimental systems in which the loss of circulation and the reduced access to nutrients allows for enhanced morphological insights into key events of mineralized tissue formation (Diekwisch et al., 1993;Diekwisch et al., 1995;Diekwisch, 1998). Here, our tooth organ culture study revealed granular electron dense mineral deposits onto the organic matrix framework of the enamel matrix stippled materials (Fig. 2C), suggestive of a high mineral content in the pre-crystalline enamel extracellular matrix. Initial crystallites were surrounded by a fairly electron dense organic matrix (Fig. 2D). These initial mineral protein/mineral assemblies were separated from each other by electron-lucent zones in between discrete mineral assembly deposits (Fig. 2D). Elongated crystals were surrounded by an electron dense coat of mineral granules in immediate proximity to the crystal surface, indicative of epitaxial crystal growth (Fig. 2E). Finally, transmission electron micrographs of the enamel matrix/initial crystallization interface demonstrated an almost linear separation between the subunit compartments of the non-mineralized matrix and the crystal-associated matrix of the early crystalline phase, suggestive of an *en block* conversion of matrix assemblies from crystal-free to crystal-rich matrix (Fig. 2F).

3.4.3. Linear and 20nm hexagonal/ring-shaped amelogenin protein assemblies on mica surfaces and 20nm globular amelogenin assemblies of Nickel-stained N92 amelogenins on carbon coated grids as revealed via AFM and TEM

Three different types of experiments were conducted to visualize modes of amelogenin self-assembly and address the question as to which amelogenin motifs were involved in self-assembly and protein elongation. In a first set of experiments, recombinant full-length mouse amelogenin (M179) and C-terminal C86 amelogenin were placed on freshly cleaved mica and allowed to self-assemble (Fig. 3A,B). Tapping mode AFM images revealed parallel rows of globular amelogenin protein as well as circular/hexagonal inter-row assemblies (Fig. 3A) indicative of a propensity of full-length amelogenins to self-assemble either in linear rows or as hexagonal patterned subunit compartments when exposed to flat mica surfaces at pH 7.4 without the addition of additional proteins or ions. The C-terminal amelogenin alone without the helical N-terminus did not form any detectable surface patterns (Fig. 3B). To ask whether the amelogenin N-terminus was involved in self-assemblies, our previously generated N-terminally His-tagged N92 amelogenin (Zhang et al., 2011) was incubated on carbon-coated mesh wire grids and subjected to Nickel staining. Transmission electron micrographs of stained N92 matrices revealed oval or donut-shaped electron-dense assemblies measuring approximately 20nm in diameter (Fig. 3C). Fluorescent labeling of overnight incubated amelogenins in aqueous solution at pH 7.4 resulted in complex large scale assemblies measuring several micrometers in length (Fig. 3D). In contrast, self-assemblies of PXX33 polyproline-rich amelogenin peptides incubated under the same conditions were substantially thinner and smaller (Fig. 3E).

3.4.4. Western blot analysis reveals parallels between amelogenin fragmentation and changes in matrix organization during enamel protein transport, "nanosphere" assembly, and crystal growth

Here we asked whether changes in enamel matrix configuration as they occur during amelogenesis coincide with the gradual processing of the full-length amelogenin into enzymatically cleaved fragments. In addition, we employed two successive stages of protein extraction to separate loosely-bound and crystal-associated matrix proteins. First, loosely bound intercrystalline proteins were harvested using a sodium dodecyl sulfate (SDS)-based extraction procedure that functions similar to a detergent. Thereafter, crystal-bound enamel matrix proteins were extracted via 4M guanidine (modified after (Termine et al., 1980)). Individual SDS-based or guanidine (Gu)-based extracts from enamel organ, superficial or deep enamel matrix were then subjected to gel electrophoresis and Western blot (Fig. 4A). We postulated that our layer- and binding-level based analysis would provide new insights into relationship between amelogenin processing, matrix assembly, and protein-mediated crystal growth.

Our C-terminal amelogenin antibody recognized a distinct 28kDa band indicative of the full-length amelogenin on the SDS-based enamel organ extract (Fig. 4C, lane 1). This antibody identified two strong bands at 28 and 25kDa and a less intense band at 15kDa on the SDS-based extract of the superficial enamel matrix, while there was a single 26kDa band on the SDS-based extract of the deep enamel matrix (Fig. 4C, lanes 2 and 3). There was a 23kDa amelogenin positive band on the Gu-based extract of the enamel organ and a series of three amelogenin positive bands ranging from 8kDa to 16kDa on the Gu-based extract of the deep enamel matrix (Fig. 4C, lanes 4 and 6). In opposite to the strong amelogenin signal in the SDS extract of the superficial enamel layer, the amelogenin signal in the Gu extract of the superficial enamel was

below detection threshold (Fig. 4C, lane 5). In contrast, our N-terminal amelogenin antibody only reacted with the SDS-based extract of the deep enamel layer (Fig. 4D), indicating that the N-terminal amelogenin fragment is not immediately associated with the growing crystal surface.

3.5. Discussion

For the present contribution we have queried the developing enamel matrix using *in vivo* and *in vitro* models as well as amelogenin self-assembly patterns to reconcile seemingly divergent models and proposed mechanisms of mammalian matrix mediated tooth enamel formation. We have revisited electron micrographs of mouse enamel development, carefully analyzed lesser known aspects of enamel matrix reconfiguration and initial crystal growth in organ culture, and characterized amelogenin *in vitro* self-assembly patterns using atomic force microscopy, fluorescence microscopy, and Nickel-labeling of the N-terminal polyhistidine tags at the N-terminus of amelogenin N92 fragments. We have also performed Western blot analyses to determine whether stage-specific changes in enamel matrix configuration were related to the amelogenin posttranslational processing along stages and layers of enamel development using N- and C-terminal amelogenin antibodies. Together, these studies establish the enamel matrix as a dynamic and multifunctional protein assembly involved in all aspects of enamel formation, including vesicular transport, matrix assembly, spacing of crystal nucleation sites, and protein mediated crystal elongation.

Our micrographs indicate substantial differences in matrix subunit dimensions and shapes between secretory vesicles, pre-crystallization enamel protein matrix, and intercrystalline protein matrix during the crystal elongation phase. Specifically, there was a significant difference in matrix subunit compartment size between secretory vesicle assemblies measuring approximately

7 nm in diameter and the extracellular enamel protein matrix subunit compartments with an average diameter of 17.5 nm. Similar changes in subunit dimensions have been reported in earlier molecular cross-linking studies (Brookes et al., 2006). A detailed analysis of matrix dimensions in an earlier transmission electron microscopic study reported 5 nm diameters in secretory vesicles and 20 nm diameters in stippled materials and in the protein coat covering initial enamel crystal deposits (Diekwisch et al., 1995). Estimates of protein assembly dimensions based on transmission electron micrographs are likely to underestimate actual dimensions by a small percentage because of the dehydration involved in sample preparation, suggesting that actual subunit dimensions may be closer to 10 nm in secretory vesicles and 25 nm in the extracellular matrix. Together, these findings indicate that the enamel matrix is reconfigured when the enamel mineral/protein cargo leaves the secretory vesicles and enters the extracellular matrix milieu. Our data are also suggestive of a second change in matrix configuration after initial crystal precipitation. In fact, the structures presented in our transmission electron micrographs somewhat resemble helical structures (Smales, 1975), but more likely consist of ribbon-like assemblies of donut-shaped protein nanospheres (Zhang et al., 2011;Carneiro et al., 2016) in immediate proximity to the elongating crystal needles. Such protein nanoribbons not always display the corresponding crystal needle in the same section because of the ultrathin sectioning technique involved in sample preparation. However, electron micrographs of earlier and later stages illustrate the intimate relationship between each individual electrondense enamel crystal needle and its slightly less electrondense pericrystalline protein coat. Similar images of pre-fusion initial enamel crystals and consecutive stages of apatite fusion into mature enamel crystals have been published earlier (Robinson, 2007;Beniash et al., 2009;Fang et al., 2011).

Organ culture studies revealed four key findings related to our understanding of potential mechanisms involved in enamel crystal growth: (i) granular mineral deposits associated with the enamel matrix framework, (ii) dot-like mineral deposits along elongating initial enamel crystallites, (iii) a mineral free-zone surrounding initial enamel crystal precipitates, and (iv) dramatic changes in enamel matrix configuration following the onset of enamel crystal formation. Organ cultures are unique experimental environments that faithfully mimic the timely progression of physiologic events during embryonic organogenesis (Trowell, 1954;Yamada et al., 1980;Saxen et al., 1983;Evans et al., 1988). However, because of a limited supply in nutrients, limited ion and protein diffusion, isolation from surrounding tissues, and physical separation from long-range signaling events, amelogenesis in organ culture is effectively a time-lapse process that progresses at approximately twice the speed of *in vivo* amelogenesis. The time-lapse progression of events and the slight augmentation of key morphological features due to an accumulation of matrix and mineral allows for the visualization of events and structures that would otherwise remain below the threshold of detection (Diekwisch et al., 1993;Diekwisch et al., 1995;Diekwisch, 1998).

Among the unique findings presented here is the evidence for granular mineral deposits along the stippled materials framework of matrix subunit compartments, suggesting that the stippled materials structure previously thought of as a mineral-free protein zone in fact contains a mixture of mineral ions and proteins. This finding and the detection of dot-like, granular mineral deposits along the elongating apatite crystal surface not only confirm earlier reports of linearly arranged, electron-dense dots and globular subunits (Frank and Nalbandian, 1963;Hohling et al., 1966;Robinson et al., 1981;Robinson et al., 1983), but also lends support to more recent concepts involving co-assembled amelogenin protein/calcium phosphate mineral nanoclusters as the basis

for enamel mineral growth (Beniash et al., 2005;Beniash et al., 2009;Yang et al., 2010;Bromley et al., 2011;Ruan and Moradian-Oldak, 2015). In fact, the presence of an electron lucent zone surrounding initial crystal precipitates with adjacent matrix deposits in organ culture may indicate that protein/mineral nanoclusters had disassembled ("shed") from nanospherical matrix subunits onto the crystal surface and were no longer present at the interface between crystals. One of the most remarkable sights in our electron micrographs of initial enamel mineralization *in vitro* and *in vivo* was the drastic conversion of matrix structure from the stippled materials matrix to the elongated protein and mineral assemblies of initial crystal growth. Such a conversion of matrix organization may be due to the deprotonation of amelogenin histidine residues and simultaneous protonation of crystal surfaces, resulting in the disassembly and shedding of nanosphere substructures (Tarasevich et al., 2009a;Tarasevich et al., 2009b;Bromley et al., 2011;Robinson, 2014;Ruan and Moradian-Oldak, 2015), and the initiation of a cascade of events related to crystal formation, epitaxial crystal growth, and crystal elongation.

Our atomic force micrographs of full-length amelogenin *in vitro* self-assemblies on freshly cleaved mica not only demonstrate that amelogenins have the capacity to form linear protein assemblies but also self-organize into hexagonal rings resembling the subunit compartment organization of the stippled enamel extracellular matrix. As striking as those linear protein assemblies might be, careful examination of these images reveals the large number of hexagonal ring subunits in between rows of globular protein structures. As mentioned earlier, the linear arrangement of protein subunits may be evidence of the unique propensity of amelogenins to form elongated assemblies, which in turn might facilitate longitudinal enamel crystal growth along the crystal c-axis. As to the involvement of individual amelogenin motifs in amelogenin self-assembly, our Nickel labeling of the N92 amelogenin polyhistidine tag confirms

the essential role of the amelogenin N-terminus in the self-assembly of 20 nm diameter aggregates (Zhang et al., 2011). In contrast, our fluorescein labeling studies indicate that the polyproline domain alone results in very limited protein self-assembly and might rather contribute to nanosphere compaction and enamel prism formation (Jin et al., 2009), while the C-terminus has been shown to preferentially bind to the (100) face of apatite crystals when compared to the (001) phase and contribute to c-axis crystal growth (Moradian-Oldak et al., 2002;Pugach et al., 2010;Friddle et al., 2011;Gopinathan et al., 2014).

Our Western blot analysis of sequentially extracted enamel matrix proteins from the enamel organ, superficial and deep enamel matrix layers revealed a 3kDa cleavage of the full-length amelogenin when the protein leaves the enamel epithelium, enters the enamel matrix, and then associates with the crystal surfaces. This finding indicates that the amelogenins of the enamel organ epithelium are of higher molecular weight than the amelogenins in the enamel matrix. Such higher molecular weight (28kDa) amelogenins likely provide the structural framework for the 5-8nm subunit assemblies within the ameloblast secretory vesicles. Once expelled from the ameloblast cell body and upon entry into the enamel matrix, the transition from ameloblast secretory vesicle subunit compartments into 20nm enamel matrix "nanosphere" assemblies is likely accomplished by C-terminal amelogenin cleavage via the matrix metalloproteinase MMP20 (Zhu et al., 2014) into slightly lower molecular weight (25kDa) amelogenins. MMP20 is abundant at the ameloblast/enamel matrix interface and activated in the proton-rich environment of initial apatite crystal formation (Khan et al., 2012). The C-terminal cleavage then results in a reassembly of the enamel protein matrix structure from the 5-8nm subunit assemblies into the 20nm matrix subunit compartments.

The second key finding of our Western blot analysis focuses on the transition from the loosely bound and SDS extractable 25/28kDa amelogenins of the superficial enamel matrix to the crystal associated 8kDa to 16kDa C-terminal amelogenin fragments that were only resolved after subsequent guanidine extraction. In our laboratory, 4M guanidine alone is commonly employed to cause a profound dissolution of the mineral phase, even though addition of EDTA would result in further removal of the enamel mineral. Changes in amelogenin molecular weight from the full-length molecule in the superficial enamel layer to shorter fragments in the crystal-bound phase explains the dramatic change in enamel matrix configuration from "nanosphere"-type supramolecular matrix assemblies to the "crystal ghost"-type organic crystal coverings on the surface of elongating apatite crystals as a result of further enzymatic processing. This finding confirms previous studies on the close proximity of the amelogenin C-terminus to the apatite surface (Tarasevich et al., 2009a;Tarasevich et al., 2009b;Tarasevich et al., 2010;Lu et al., 2013). In contrast to the apatite-associated amelogenin C-terminus, the amelogenin N-terminus was accessible to our SDS solvent based extraction procedure, suggesting that the N-terminal amelogenin resided loosely bound in the intercrystalline space of the deep enamel layer.

In conclusion, our *in vivo*, organ culture, and amelogenin *in vitro* assembly studies have resulted in a dynamic three-phase model of enamel matrix transformation and crystal growth (Fig. 4). Based on our data and other findings presented in this contribution, enamel matrix assembly begins as 5-10 nm subunits formed by full-length amelogenins within ameloblast secretory vesicles (A). Once secreted into the extracellular space, mineral-enriched enamel protein self-assemblies consisting of C-terminally cleaved amelogenins organize into 20-25 nm diameter subunit compartments that provide the structural basis for orderly spaced enamel crystal nucleation (B,C). Proton generation during initial crystallization results in further matrix

reorganization and amelogenin processing, a dissociation of the stippled materials matrix and a "shedding" of C-terminal amelogenin/mineral nanoclusters onto the surfaces of growing enamel hydroxyapatite crystals (E,F).

3.6. References

- Aichmayer, B., Margolis, H., Sigel, R., Yamakoshi, Y., Simmer, J., and Fratzl, P. (2005). The onset of amelogenin nanosphere aggregation studied by small-angle X-ray scattering and dynamic light scattering. *Journal of Structural Biology* 151**,** 239-249.
- Beniash, E., Metzler, R.A., Lam, R.S., and Gilbert, P.U. (2009). Transient amorphous calcium phosphate in forming enamel. *J Struct Biol* 166**,** 133-143.
- Beniash, E., Simmer, J.P., and Margolis, H.C. (2005). The effect of recombinant mouse amelogenins on the formation and organization of hydroxyapatite crystals in vitro. *Journal of Structural Biology* 149**,** 182-190.
- Bonucci, E. (2014). Understanding nanocalcification: a role suggested for crystal ghosts. *Marine Drugs* 12**,** 4231-4246.
- Bonucci, E., Silvestrini, G., and Di Grezia, R. (1988). The infrastructure of the Organic Phase Associated with the Inorganic Substance in Calcified Tissues. *Clinical Orthopaedics and Related Research* 233**,** 243-261.
- Bromley, K.M., Kiss, A.S., Lokappa, S.B., Lakshminarayanan, R., Fan, D., Ndao, M., Evans, J.S., and Moradian-Oldak, J. (2011). Dissecting amelogenin protein nanospheres characterization of metastable oligomers. *Journal of Biological Chemistry* 286**,** 34643-34653.

- Brookes, S.J., Lyngstadaas, S.P., Robinson, C., Shore, R.C., and Kirkham, J. (2006). Intracellular nanosphere subunit assembly as revealed by amelogenin molecular cross-linking studies. *Eur J Oral Sci* 114 Suppl 1**,** 280-284; discussion 285-286, 382.
- Buchanan, L.E., Carr, J.K., Fluitt, A.M., Hoganson, A.J., Moran, S.D., De Pablo, J.J., Skinner, J.L., and Zanni, M.T. (2014). Structural motif of polyglutamine amyloid fibrils discerned with mixed-isotope infrared spectroscopy. *Proceedings of the National Academy of Sciences* 111**,** 5796-5801.
- Carneiro, K.M., Zhai, H., Zhu, L., Horst, J.A., Sitlin, M., Nguyen, M., Wagner, M., Simpliciano, C., Milder, M., and Chen, C.-L. (2016). Amyloid-like ribbons of amelogenins in enamel mineralization. *Scientific Reports* 6.
- Chen, S., Berthelier, V., Hamilton, J.B., O'nuallai, B., and Wetzel, R. (2002). Amyloid-like features of polyglutamine aggregates and their assembly kinetics. *Biochemistry* 41**,** 7391-7399.
- Diekwisch, T., David, S., Bringas, P., Santos, V., and Slavkin, H.C. (1993). Antisense inhibition of AMEL translation demonstrates supramolecular controls for enamel HAP crystal growth during embryonic mouse molar development. *Development* 117**,** 471-482.
- Diekwisch, T.G. (1998). Subunit compartments of secretory stage enamel matrix. *Connective Tissue Research* 38**,** 101-111.
- Diekwisch, T.G., Berman, B.J., Anderton, X., Gurinsky, B., Ortega, A.J., Satchell, P.G., Williams, M., Arumugham, C., Luan, X., and Mcintosh, J.E. (2002). Membranes, minerals, and proteins of developing vertebrate enamel. *Microscopy Research and Technique* 59**,** 373-395.

- Diekwisch, T.G., Berman, B.J., Gentner, S., and Slavkin, H.C. (1995). Initial enamel crystals are not spatially associated with mineralized dentine. *Cell and Tissue Research* 279**,** 149-167.
- Eastoe, J. (1960). Organic matrix of tooth enamel. *Nature* 187**,** 411-412.
- Eastoe, J. (1963). The amino acid composition of proteins from the oral tissues—II: The matrix proteins in dentine and enamel from developing human deciduous teeth. *Archives of Oral Biology* 8**,** 633-652.
- Evans, J., Bringas, P., Jr., Nakamura, M., Nakamura, E., Santos, V., and Slavkin, H.C. (1988). Metabolic expression of intrinsic developmental programs for dentine and enamel biomineralization in serumless, chemically-defined, organotypic culture. *Calcif Tissue Int* 42**,** 220-230.
- Fang, P.-A., Conway, J.F., Margolis, H.C., Simmer, J.P., and Beniash, E. (2011). Hierarchical self-assembly of amelogenin and the regulation of biomineralization at the nanoscale. *Proceedings of the National Academy of Sciences* 108**,** 14097-14102.
- Fearnhead, R. (1963). Organic components of human dental enamel. in: *Journal of Dental Research 1111*.
- Fearnhead, R. (1965). The insoluble organic component of human enamel. *Tooth Enamel***,** 127-131.
- Fincham, A., Moradian-Oldak, J., Diekwisch, T., Lyaruu, D., Wright, J.T., Bringas, P., and Slavkin, H. (1995). Evidence for amelogenin" nanospheres" as functional components of secretory-stage enamel matrix. *Journal of Structural Biology* 115**,** 50-59.
- Fincham, A., Moradian-Oldak, J., and Simmer, J. (1999). The structural biology of the developing dental enamel matrix. *Journal of Structural Biology* 126**,** 270-299.

- Fincham, A., Moradian-Oldak, J., Simmer, J., Sarte, P., Lau, E., Diekwisch, T., and Slavkin, H. (1994). Self-assembly of a recombinant amelogenin protein generates supramolecular structures. *Journal of Structural Biology* 112**,** 103-109.
- Frank, R.M., and Nalbandian, J. (1963). Electron microscopy of the mode of secretion of the ameloblast bodies during amelogenesis. *C R Seances Soc Biol Fil* 157**,** 2297-2298.
- Frank, R.M., Sognnaes, R., and Kern, R. (1960). Calcification of dental tissues with special reference to enamel ultrastructure. *Calcification in Biological Systems***,** 163-202.
- Frank, R.M., Wolff, F., and Gutmann, B. (1964). The organic structure of human fetal enamel in the electron microscope. *Arch Oral Biol* 9**,** 105-110.
- Friddle, R.W., Battle, K., Trubetskoy, V., Tao, J., Salter, E.A., Moradian-Oldak, J., De Yoreo, J.J., and Wierzbicki, A. (2011). Single-Molecule Determination of the Face-Specific Adsorption of Amelogenin's C-Terminus on Hydroxyapatite. *Angewandte Chemie International Edition* 50**,** 7541-7545.
- Fukae, M., Yamamoto, R., Karakida, T., Shimoda, S., and Tanabe, T. (2007). Micelle structure of amelogenin in porcine secretory enamel. *Journal of Dental Research* 86**,** 758-763.
- Glimcher, M.J. (1959). Molecular biology of mineralized tissues with particular reference to bone. *Reviews of Modern Physics* 31**,** 359.
- Gopinathan, G., Jin, T., Liu, M., Li, S., Atsawasuwan, P., Galang, M.-T., Allen, M., Luan, X., and Diekwisch, T.G. (2014). The expanded amelogenin polyproline region preferentially binds to apatite versus carbonate and promotes apatite crystal elongation. *Frontiers in Physiology* 5.

- Hohling, H.J., Hake, T., and Katterbach, R. (1966). Collegen and apatite in healthy and carious dentin. *Adv Fluorine Res* 4**,** 201-212.
- Jin, T., Ito, Y., Luan, X., Dangaria, S., Walker, C., Allen, M., Kulkarni, A., Gibson, C., Braatz, R., Liao, X., and Diekwisch, T.G. (2009). Elongated polyproline motifs facilitate enamel evolution through matrix subunit compaction. *PLoS Biol* 7**,** e1000262.
- Khan, F., Li, W., and Habelitz, S. (2012). Biophysical characterization of synthetic amelogenin C-terminal peptides. *Eur J Oral Sci* 120**,** 113-122.
- Lu, J., Xu, Y., Buchko, G., and Shaw, W. (2013). Mineral association changes the secondary structure and dynamics of murine amelogenin. *Journal of Dental Research* 92**,** 1000-1004.
- Lyaruu, D., Belcourt, A., Fincham, A., and Termine, J. (1982). Neonatal hamster molar tooth development: extraction and characterization of amelogenins, enamelins, and soluble dentin proteins. *Calcified Tissue International* 34**,** 86-96.
- Lyaruu, D., Bronckers, A., and Wöltgens, J. (1984). The Tomes' process: is stippled material a reality? The effect of fixative temperature on the structure of stippled material in enamel, in: *Proceedings of the Second International Conference on Tooth Morphogenesis and Differentiation. Les Colloques de l'INSERM*, 257-272.
- Lyubchenko, Y.L., Krasnoslobodtsev, A.V., and Luca, S. (2012). Fibrillogenesis of huntingtin and other glutamine containing proteins. *Protein Aggregation and Fibrillogenesis in Cerebral and Systemic Amyloid Disease*. Springer, 225-251.
- Margolis, H., Beniash, E., and Fowler, C. (2006). Role of macromolecular assembly of enamel matrix proteins in enamel formation. *Journal of Dental Research* 85**,** 775-793.

- Martinez-Avila, O., Wu, S., Kim, S.J., Cheng, Y., Khan, F., Samudrala, R., Sali, A., Horst, J.A., and Habelitz, S. (2012). Self-assembly of filamentous amelogenin requires calcium and phosphate: from dimers via nanoribbons to fibrils. *Biomacromolecules* 13**,** 3494-3502.
- Martinez-Avila, O.M., Wu, S., Cheng, Y., Lee, R., Khan, F., and Habelitz, S. (2011). Self-assembly of amelogenin proteins at the water–oil interface. *European Journal of Oral Sciences* 119**,** 75-82.
- Moradian-Oldak, J., Bouropoulos, N., Wang, L., and Gharakhanian, N. (2002). Analysis of self-assembly and apatite binding properties of amelogenin proteins lacking the hydrophilic C-terminal. *Matrix Biology* 21**,** 197-205.
- Moradian-Oldak, J., and Goldberg, M. (2005). Amelogenin supra-molecular assembly in vitro compared with the architecture of the forming enamel matrix. *Cells Tissues Organs* 181**,** 202-218.
- Nikiforuk, G., and Simmons, N. (1965). Purification and properties of protein from embryonic bovine enamel. *Journal of Dental Research* 44**,** 1119-1122.
- Nylen, M. (1979). Matrix-Mineral Relationships-A. Morphologist's Viewpoint. *Journal of Dental Research* 58**,** 922-929.
- Paine, M.L., White, S.N., Luo, W., Fong, H., Sarikaya, M., and Snead, M.L. (2001). Regulated gene expression dictates enamel structure and tooth function. *Matrix Biology* 20**,** 273-292.
- Pugach, M.K., Li, Y., Suggs, C., Wright, J.T., Aragon, M.A., Yuan, Z.A., Simmons, D., Kulkarni, A.B., and Gibson, C.W. (2010). The amelogenin C-terminus is required for enamel development. *J Dent Res* 89**,** 165-169.

- Reith, E.J. (1967). The early stage of amelogenesis as observed in molar teeth of young rats. *Journal of Ultrastructure Research* 17**,** 503-526.
- Robinson, C. (2007). Self-oriented assembly of nano-apatite particles: a subunit mechanism for building biological mineral crystals. *J Dent Res* 86**,** 677-679.
- Robinson, C. (2014). Enamel maturation: a brief background with implications for some enamel dysplasias. *Frontiers in Physiology* 5.
- Robinson, C., Briggs, H., and Atkinson, P. (1981). Histology of enamel organ and chemical composition of adjacent enamel in rat incisors. *Calcified Tissue International* 33**,** 513-520.
- Robinson, C., Briggs, H.D., Kirkham, J., and Atkinson, P.J. (1983). Changes in the protein components of rat incisor enamel during tooth development. *Arch Oral Biol* 28**,** 993-1000.
- Robinson, C., Shore, R., Kirkham, J., and Stonehouse, N. (1990). Extracellular processing of enamel matrix proteins and the control of crystal growth. *Journal de Biologie Buccale* 18**,** 355-361.
- Ronnholm, E. (1962). III. The structure of the organic stroma of human enamel during amelogenesis. *J Ultrastruct Res* 6**,** 368-389.
- Ruan, Q., and Moradian-Oldak, J. (2015). Amelogenin and enamel biomimetics. *Journal of Materials Chemistry B* 3**,** 3112-3129.
- Saxen, L., Salonen, J., Ekblom, P., and Nordling, S. (1983). DNA synthesis and cell generation cycle during determination and differentiation of the metanephric mesenchyme. *Dev Biol* 98**,** 130-138.

- Schneider, R., Schumacher, M.C., Mueller, H., Nand, D., Klaukien, V., Heise, H., Riedel, D., Wolf, G., Behrmann, E., and Raunser, S. (2011). Structural characterization of polyglutamine fibrils by solid-state NMR spectroscopy. *Journal of Molecular Biology* 412**,** 121-136.
- Smales, F. (1975). Structural subunit in prisms of immature rat enamel. *Nature* 258**,** 772-774.
- Tanaka, M., Machida, Y., Nishikawa, Y., Akagi, T., Morishima, I., Hashikawa, T., Fujisawa, T., and Nukina, N. (2002). The effects of aggregation-inducing motifs on amyloid formation of model proteins related to neurodegenerative diseases. *Biochemistry* 41**,** 10277-10286.
- Tarasevich, B.J., Lea, S., Bernt, W., Engelhard, M., and Shaw, W.J. (2009a). Adsorption of amelogenin onto self-assembled and fluoroapatite surfaces. *The Journal of Physical Chemistry B* 113**,** 1833-1842.
- Tarasevich, B.J., Lea, S., Bernt, W., Engelhard, M.H., and Shaw, W.J. (2009b). Changes in the quaternary structure of amelogenin when adsorbed onto surfaces. *Biopolymers* 91**,** 103-107.
- Tarasevich, B.J., Lea, S., and Shaw, W.J. (2010). The leucine rich amelogenin protein (LRAP) adsorbs as monomers or dimers onto surfaces. *Journal of Structural Biology* 169**,** 266-276.
- Termine, J., Belcourt, A., Christner, P., Conn, K., and Nylen, M. (1980). Properties of dissociatively extracted fetal tooth matrix proteins. I. Principal molecular species in developing bovine enamel. *Journal of Biological Chemistry* 255**,** 9760-9768.
- Tomson, M., and Nancollas, G. (1978). Mineralization kinetics: a constant composition approach. *Science* 200**,** 1059-1060.

- Travis, D.F., and Glimcher, M.J. (1964). The structure and organization of, and the relationship between the organic matrix and the inorganic crystals of embryonic bovine enamel. *The Journal of Cell Biology* 23**,** 447.
- Trowell, O.A. (1954). A modified technique for organ culture in vitro. *Exp Cell Res* 6**,** 246-248.
- Wallwork, M.L., Kirkham, J., Zhang, J., Smith, D.A., Brookes, S.J., Shore, R.C., Wood, S.R., Ryu, O., and Robinson, C. (2001). Binding of matrix proteins to developing enamel crystals: an atomic force microscopy study. *Langmuir* 17**,** 2508-2513.
- Yamada, M., Bringas, P., Jr., Grodin, M., Macdougall, M., Cummings, E., Grimmett, J., Weliky, B., and Slavkin, H.C. (1980). Chemically-defined organ culture of embryonic mouse tooth organs: morphogenesis, dentinogenesis and amelogenesis. *J Biol Buccale* 8**,** 127-139.
- Yang, X., Wang, L., Qin, Y., Sun, Z., Henneman, Z.J., Moradian-Oldak, J., and Nancollas, G.H. (2010). How amelogenin orchestrates the organization of hierarchical elongated microstructures of apatite. *The Journal of Physical Chemistry B* 114**,** 2293-2300.
- Zhang, X., Ramirez, B.E., Liao, X., and Diekwisch, T.G. (2011). Amelogenin supramolecular assembly in nanospheres defined by a complex helix-coil-PPII helix 3D-structure. *PLoS One* 6**,** e24952.
- Zhu, L., Liu, H., Witkowska, H.E., Huang, Y., Tanimoto, K., and Li, W. (2014). Preferential and selective degradation and removal of amelogenin adsorbed on hydroxyapatites by MMP20 and KLK4 in vitro. *Front Physiol* 5**,** 268.

4. CONCLUSION

Enamel formation is a highly complex process involving multiple events occurring simultaneously throughout the ameloblast cells and the enamel matrix. Our studies provide intimate knowledge about the transportation and posttranslational fate of enamel matrix proteins, mainly amelogenin, during enamel formation. Our first study demonstrated the importance of matrix vesicular protein PHOSPHO1 in enamel mineralization. The significant reduction in enamel mineralization, phosphate content, loss of enamel prism organization and increase in width of incisor enamel in *Phospho1-/-* mice provided us an insight about the role of secretory vesicles in ameloblasts for the preservation of enamel integrity. Future studies are required to identify the different stage at which vesicular protein PHOSPHO1 participates in the enamel development and further trace the entire lifecycle of enamel development.

Our second study correlates the events occurring during the first eight days of enamel formation using a mouse model and illustrates the significant changes in the enamel matrix proteins and identifies the novel key proteins during different stages of enamel formation. At day 2 or the early secretory stage of enamel formation, our proteomics data indicated a significant rise in the matrix proteins, followed by an increase of cytoskeleton proteins from day 4 to day 6 and a continuous increase in amelogenin from day 6 to day 8. We were also able to capture the transformation of mineral from early stages of amorphous calcium phosphate to mature hydroxyapatite which is important for structural rigidity of enamel.

Our third study revealed the fate of amelogenin from the moment it is packaged and transported through the ameloblast cells to the initiation of enamel prisms formation. The subunits changed their size from 5-10nm in secretory vesicles to 20nm once secreted in the extracellular matrix. The configurational change in the enamel protein and our three-dimensional

model summarizes the three stages of matrix assemble, extracellular matrix reorganization, and the fate of protein-mediated crystal growth and amelogenin rich enamel matrix during enamel formation.

Our future studies will focus on a transgenic mouse knockout model for vesicular trafficking research that will provide further substantial insights into the mechanism of protein and mineral transportation through ameloblasts.

Figure 1- Chapter 1 : PHOSPHO1 localization in the ameloblast secretory vesicle walls.
Reprinted with permission from Frontiers editorial office.

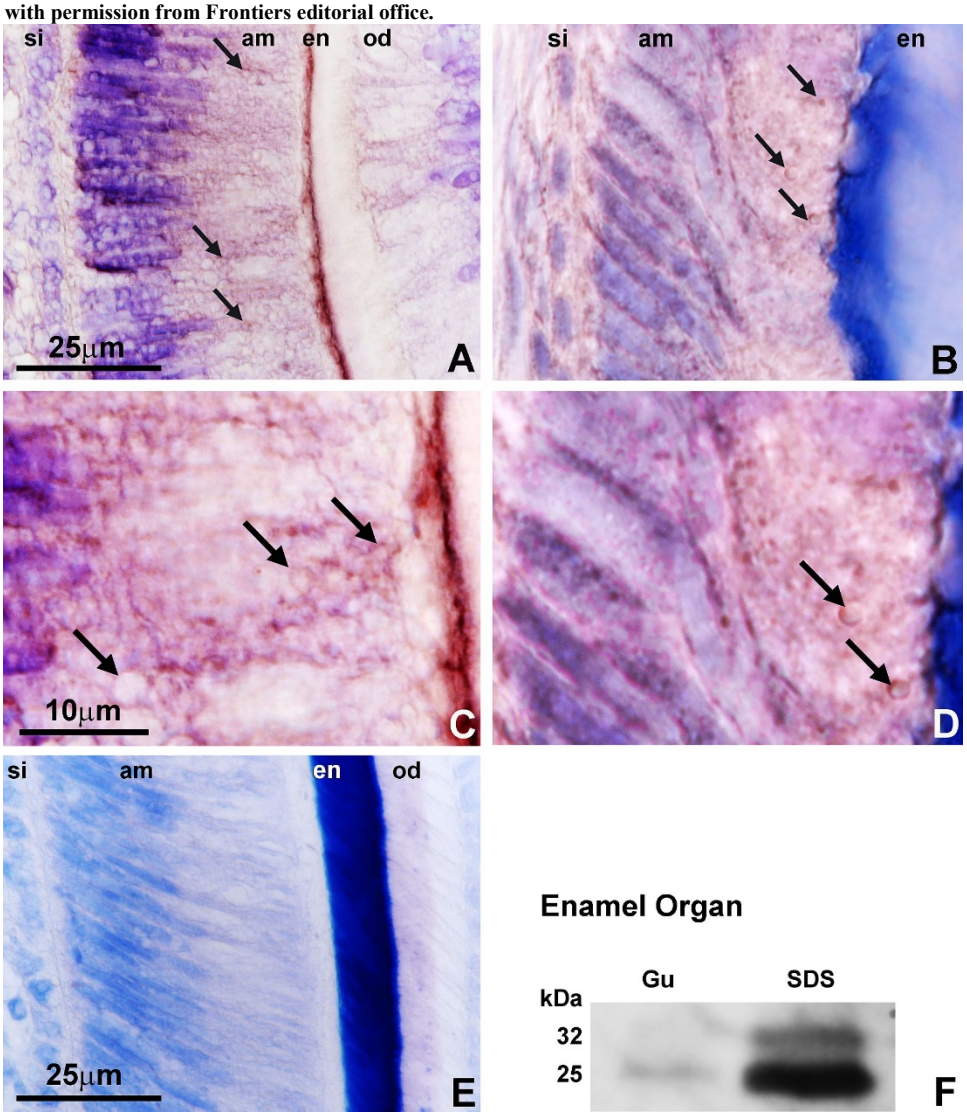

Figure 1 – Chapter 1. PHOSPHO1 localization in the ameloblast secretory vesicle walls.

The first set of immunoreactions (A,C) was generated using a commercial antibody (GTX119275) and the second set was based on the original antibody from the Millán lab (AbD Serotec)(B,D). Immunohistochemical labeling (A-D) located PHOSPHO1 at the periphery of

secretory vesicles (arrows) and in the enamel layer of 3 days postnatal (dpn) WT mouse molars (en). (C,D) are higher magnification images of (A,B) allowing for detailed assessment of Phospho1 localization in ameloblast secretory vesicle walls (arrows). (E) is a same stage mouse molar control in which the primary antibody was replaced with pre-immune serum. (F) is a Western blot demonstrating the characteristic 32KDa full-length PHOSPHO1 band and a 25kDa cleavage product using the AbD Serotec antibody on blotted enamel organ extracts. Gu were 4M guanidine extracts and SDS were SDS extracts of enamel organ tissues. The scale bar was 25μm for A,B,E, and 10μm for C,D.

Figure 2 - Chapter 1 : Decreased mineralization in the enamel layer of 30 days old *Phospho1-/-* mice. Reprinted with permission from Frontiers editorial office.

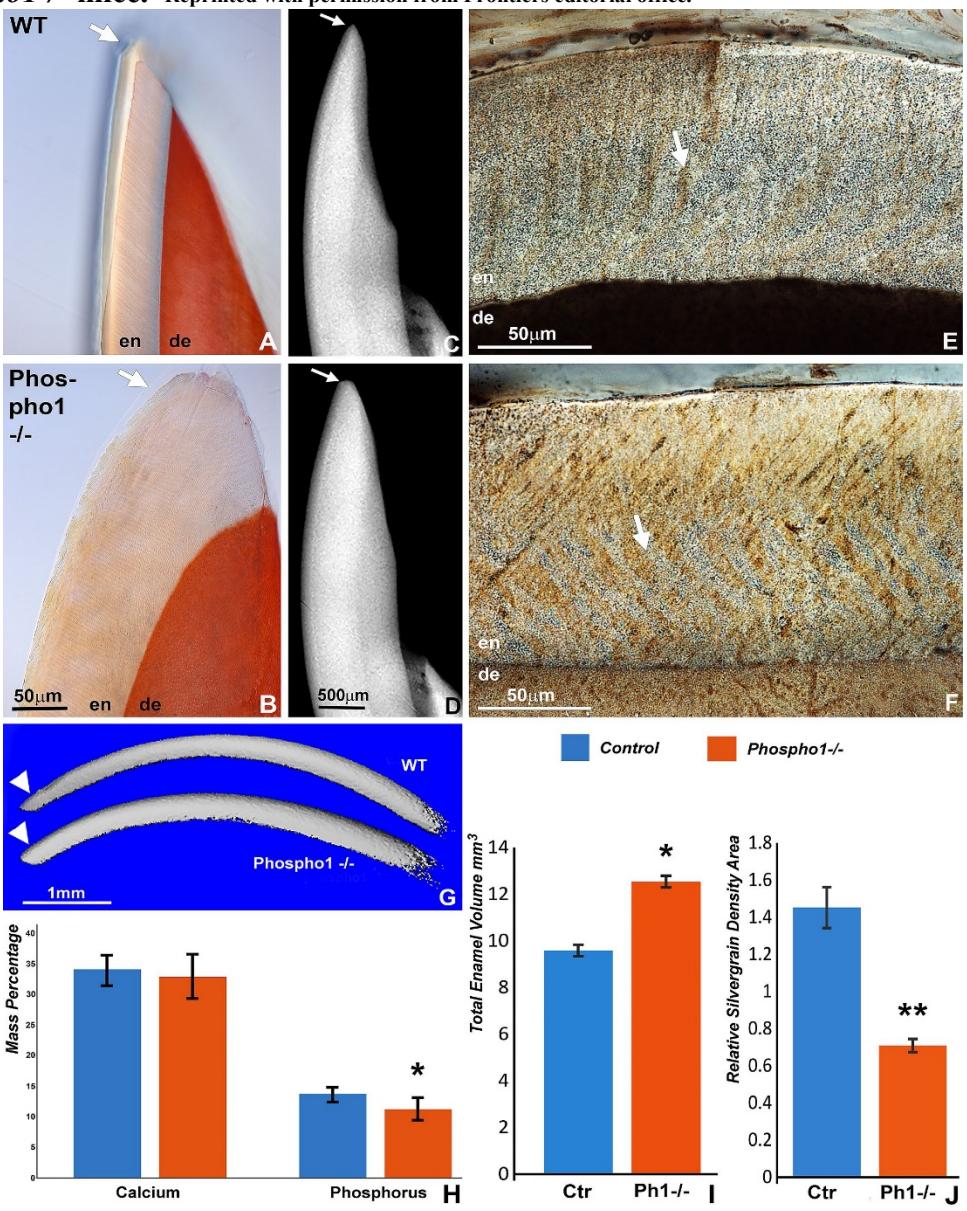

Figure 2 – Chapter 1. Decreased mineralization in the enamel layer of 30 days old *Phospho1-/-* mice. Incisal tips of *Phospho1-/-* mice (B,D) were thicker and rounded (arrows) when compared to those of WT mice. The molar enamel layer of *Phospho1-/-* mice contained

less von Kossa staining and more organic material in the prisms (F) than the WT mice (E). Three-D micro-CT reconstructions of representative WT and *Phospho1-/-* mouse incisors confirm differences in incisal tip contours and in the overall enamel volume (G). Elemental analysis revealed a significant difference in the amount of phosphorus in the *Phospho1-/-* mice when compared to the WT mice as demonstrated by EDS-SEM. The EDS-SEM data were calculated as average mass percent of calcium and phosphorus (H). (I) Statistical analysis of the differences in enamel volume between WT and *Phospho1-/-* mice based on 3D reconstructed micro-CT images. (J) Comparative analysis of differences in mineralization between WT and *Phospho1-/-* mice as revealed by von Kossa stained ground sections using a grain counting algorithm. * = $p < 0.05$, ** = $p < 0.001$. Control values are shown in blue columns and *Phospho1-/-* data are displayed in orange/red colored columns. The scale bar is 50µm for (A,B), 500µm for (C,D), and 50µm for (E,F).

Figure 3 - Chapter 1 : Loss of enamel prism structure and crystal organization in *Phospho1-/-* mouse molars. Reprinted with permission from Frontiers editorial office.

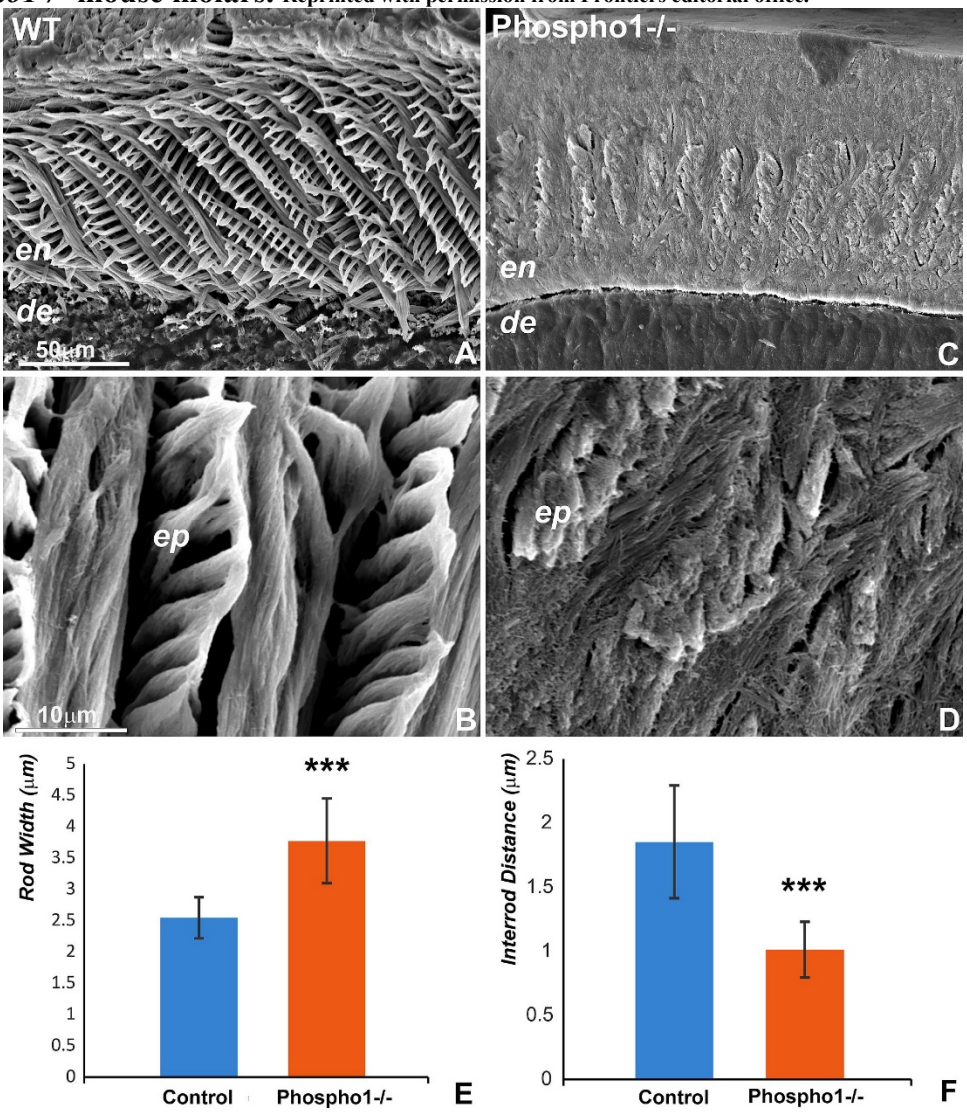

Figure 3 – Chapter 1. Loss of enamel prism structure and crystal organization in *Phospho1-/-* mouse molars. Scanning electron micrographs of 30 days old mouse molars illustrate the arrangement of enamel prims at 750x and 5000x magnifications (A and B respectively) in WT (A, B) and *Phospho1-/-* (C, D) mouse molars. There was a significant loss of enamel prism structure as well as a dramatic change in the organization of the enamel crystals

in the PHOSPHO1 null mice. (E,F) Morphometric comparison of enamel prism width (E) and inter-rod distance (F) between WT and *Phospho1-/-* mice. *** = $p < 0.0001$. The scale bar is 50µm for (A,C) and 10µm (B,D)

Figure 4 - Chapter 1 : PHOSPHO1 as an intravesicular apatite nucleation enzyme in ameloblast secretory vesicles. Reprinted with permission from Frontiers editorial office.

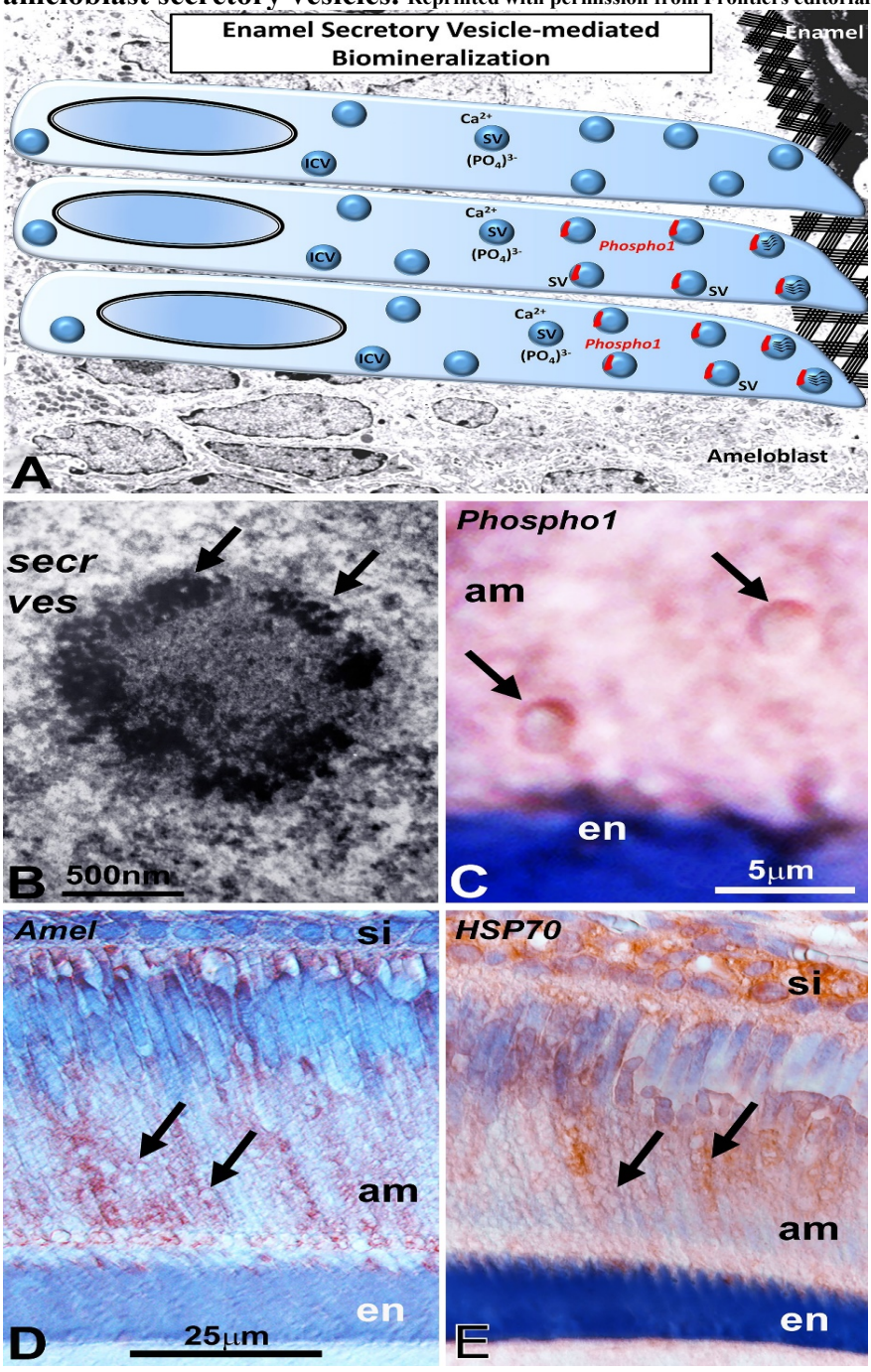

Figure 4 – Chapter 1. PHOSPHO1 as an intravesicular apatite nucleation enzyme in ameloblast secretory vesicles. (A) The presence of PHOSPHO1 as a secretory vesicle (SV)

component in ameloblast secretory vesicles suggests intravesicular mineral/matrix assembly prior to secretion into the ameloblast extracellular matrix. The transmission electron micrograph (B) of ameloblast intracellular secretory vesicles supports the concept of mineral nucleation sites (arrows) within such secretory vesicles (secr ves). This secretory vesicle was localized at the secretory face of the ameloblast. (C) is a high magnification micrograph demonstrating highly specific immunostaining for PHOSPHO1 in the walls of ameloblast secretory vesicles (arrows). (D) and (E) are immunoreactions using either anti-amelogenin (D) or anti-HSP70 antibodies, demonstrating immunoreactivity associated with secretory vesicles (arrows). secr ves = secretory vesicles, am = ameloblasts, si = stratum intermedium, en = enamel. The scale bar is 500nm (B), 5µm for (A,C) and 25µm for (D,E).

Figure 1 - Chapter 2 : First mandibular mouse molar development from postnatal days 1 to 8. **Reprinted with permission from Frontiers editorial office.**

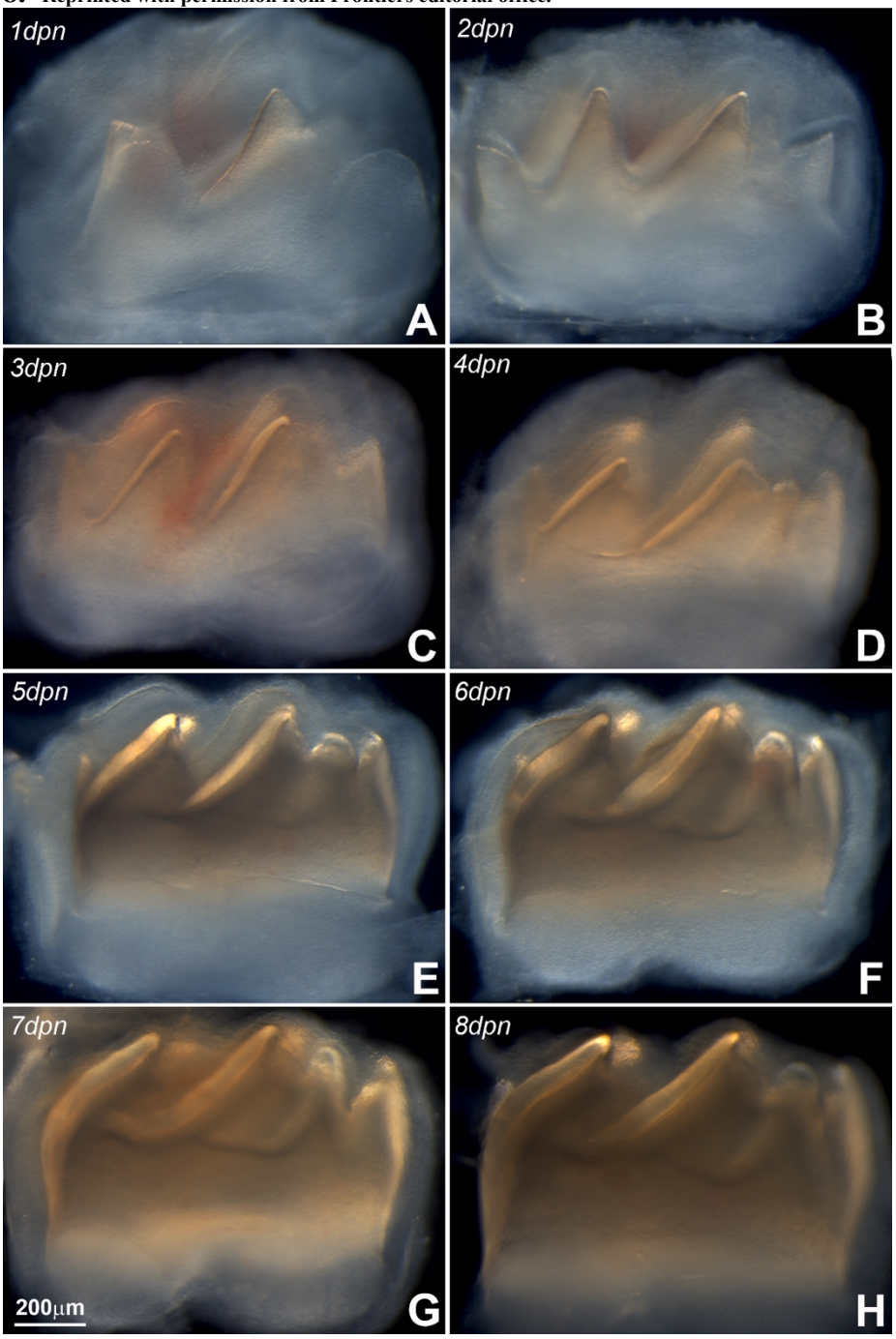

Figure 1 – Chapter 2. First mandibular mouse molar development from postnatal days 1 to 8. During the first eight days of postnatal mouse molar development, the mineralized portion

of the crown dentin continuously increased in height, while the length of the crown remained fairly unchanged. Note the gradual increase in the thickness of the enamel layer (identified in Fig. 2F).

Figure 2 - Chapter 2 : Mouse molar enamel birefringence and enamel matrix layer dissection for mineral and protein analysis. **Reprinted with permission from Frontiers editorial office.**

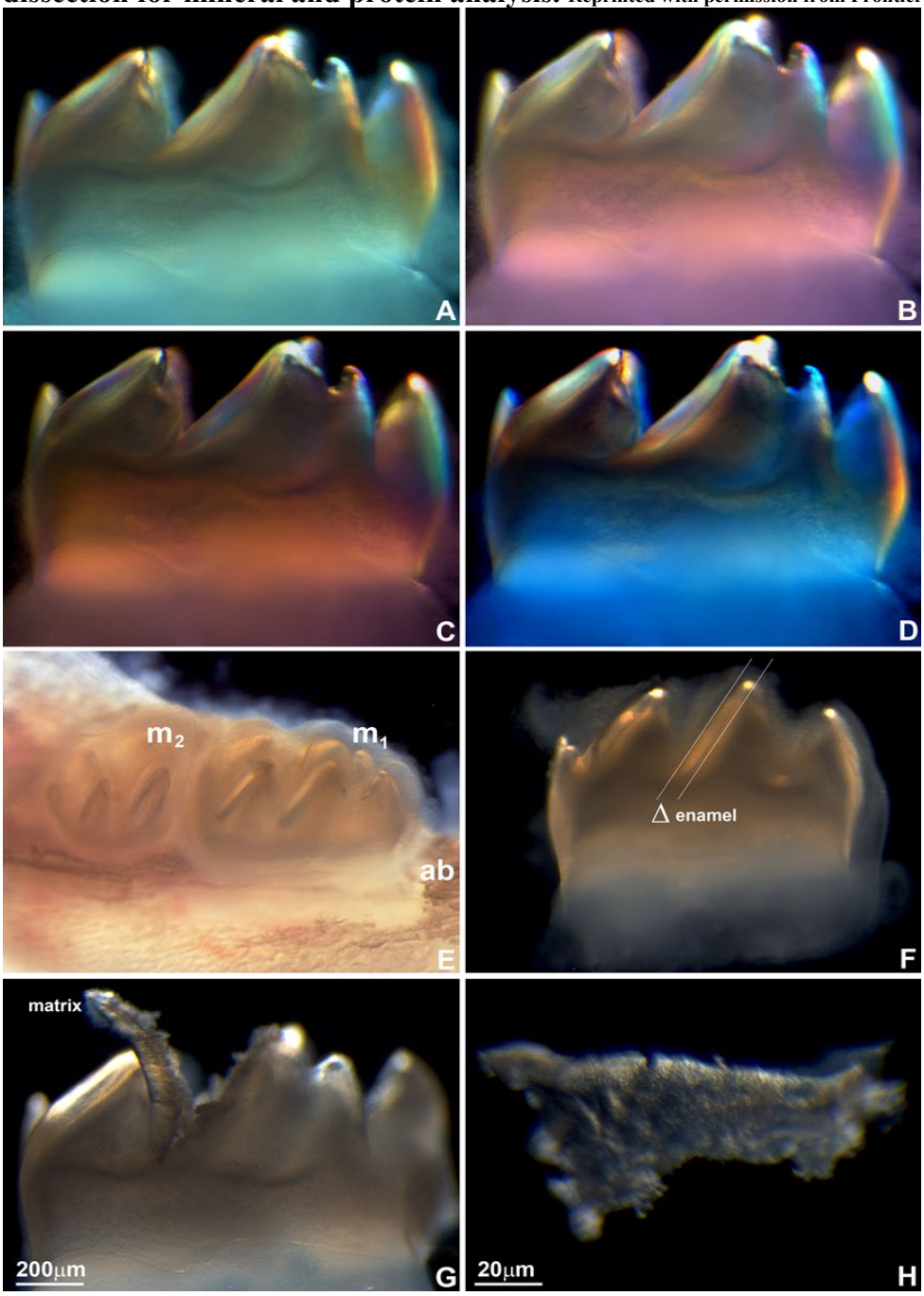

Figure 2 – Chapter 2. Mouse molar enamel birefringence (A-D) and enamel matrix layer dissection for mineral and protein analysis (E-H). (A-D) Mouse molars were dissected from

mouse jaws and placed between crossed polarizers. Polarizers were oriented at the following angles: 0 degrees (A), 90 degrees (B), 180 degrees (C), and 270 degrees (D). (E) Position of the first (m_1) and the second (m_2) mouse mandibular molar relative to the jaw bone and the alveolar bone (ab). (F) Enamel layer on the distal slope of the mesial cusp of the first mandibular mouse molar used for the present analysis. Δ marks the thickness of the enamel layer between two parallel lines. (G) Preparation of the matrix layer from the distal slope of the middle cusp of the first mandibular mouse molar. (H) High magnification light micrograph of the dissected enamel layer.

Figure 3 - Chapter 2 : Analysis of the postnatal mouse molar enamel mineral layer. **Reprinted with permission from Frontiers editorial office.**

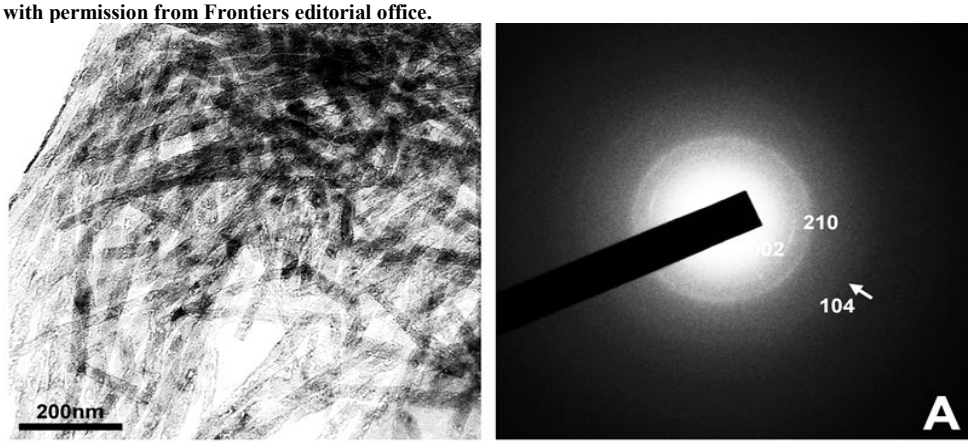

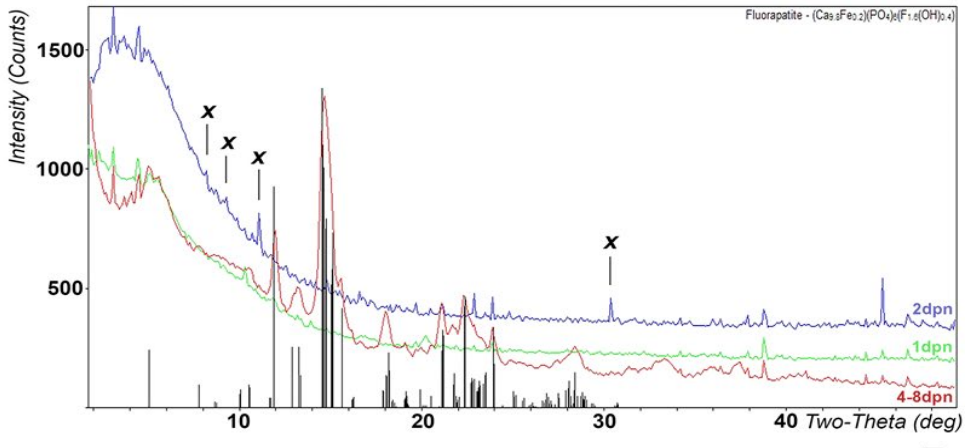

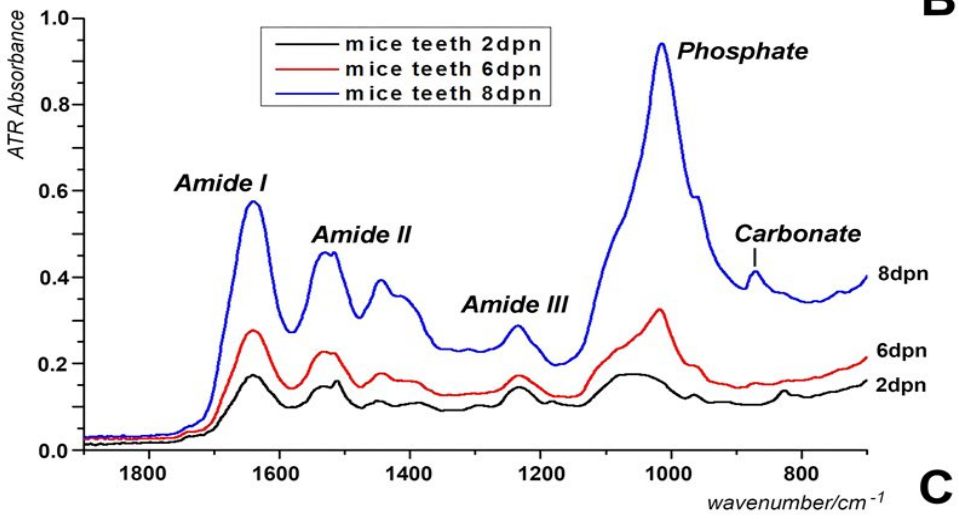

Figure 3 – Chapter 2. Analysis of the postnatal mouse molar enamel mineral layer. (A) Transmission electron microscopy of four days postnatal mouse molar enamel matrix revealed bundles of thick apatite crystals with diffraction rings in the 002 and 210 planes, and a faint diffraction ring in the 104 plane, indicative of hydroxyapatite. (B) X-ray powder diffraction analysis of enamel matrix preparations from the distal slopes of 1 day postnatal (1dpn), 2days postnatal (2dpn), 4 days, 6 days, and 8 days postnatal (4-8dpn) mouse mandibular molars. The vertical bars at the base of the figure illustrate the partially fluoride substituted hydroxyapatite powder diffraction pattern with the height of the bars representing relative peak intensities. Unique unmatched peaks in the spectrum of 2 days postnatal samples were marked by an X. Only the 4-8dpn samples matched hydroxyapatite powder diffraction standards. (C) Fourier-transform infrared spectra of developing enamel matrix preparations from the distal slopes of 2 days postnatal (2dpn), 6 days postnatal (6dpn), and 8 days postnatal (8dpn) mouse mandibular molars. Peaks corresponding to vibrations for phosphate, carbonate, proteoglycan, and amide I-III are labeled individually.

Figure 4 - Chapter 2 : Comparison between spectral counts of individual proteins identified during postnatal mouse molar enamel development. Reprinted with permission from Frontiers editorial office.

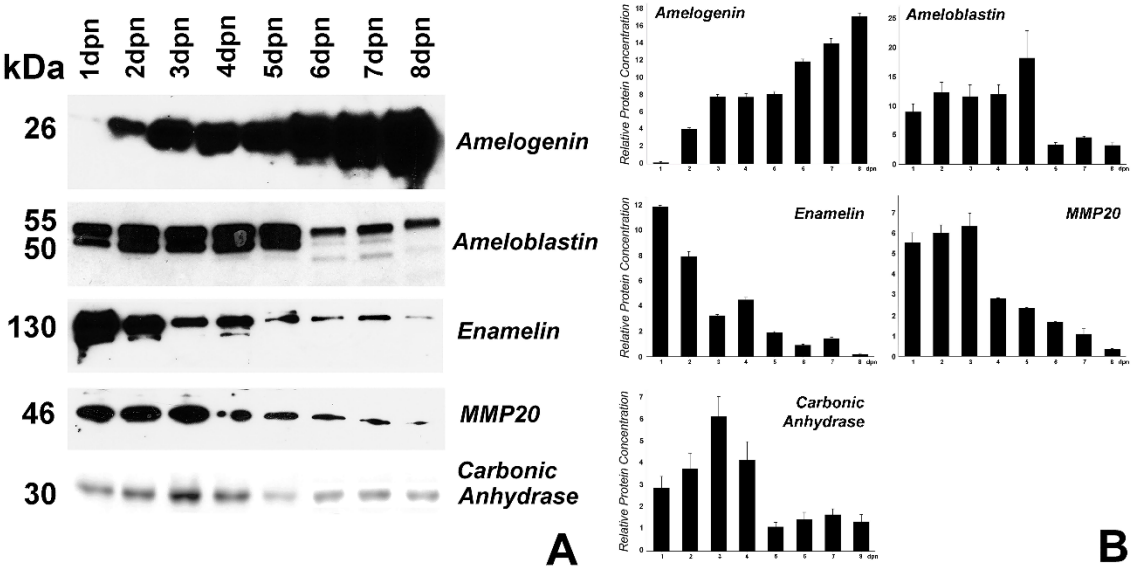

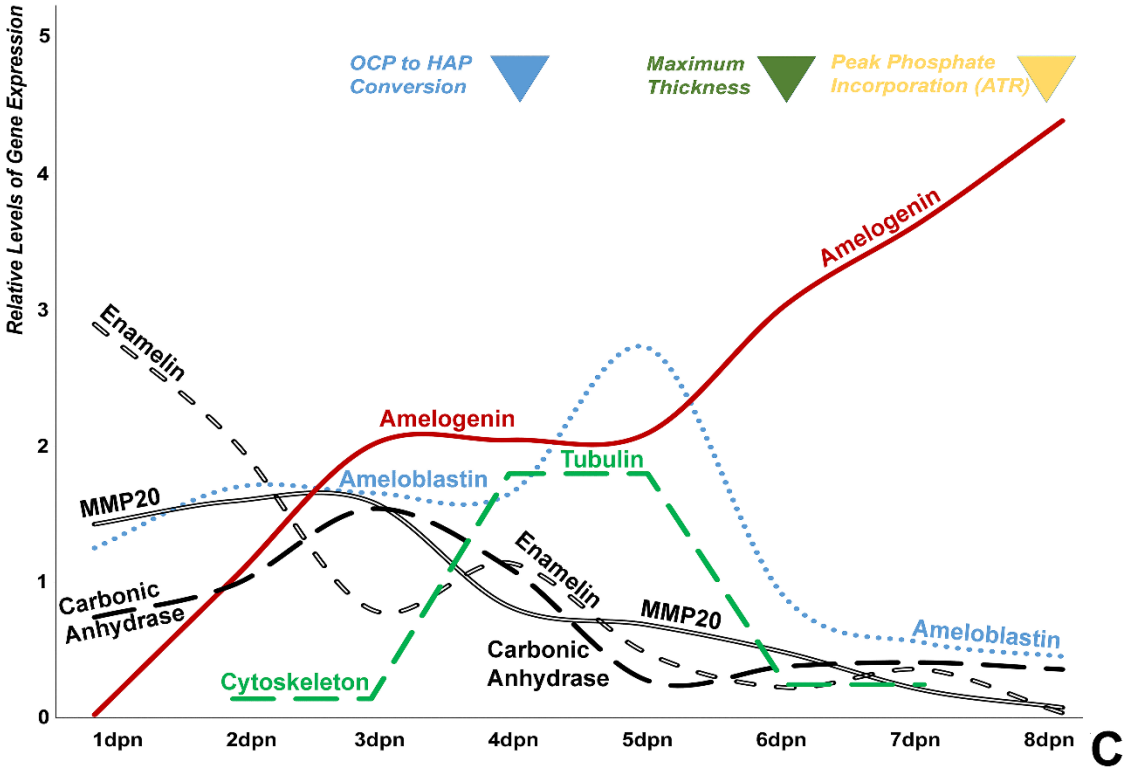

Figure 4 – Chapter 2. Comparison between spectral counts of individual proteins identified during postnatal mouse molar enamel development (days 2dpn, 4dpn, and 6dpn)(99% probability, 2 peptide minimum). Proteins were grouped into four categories: (A) mineralization, (B) cytoskeleton, (C) extracellular matrix/cell surface, and (D) other. Six proteins with highest quantitative values in each group were chosen for display and further analysis. Orbitrap mass spectrometry is inherently biased to exclude hydrophobic proteins (Griffin and Schnitzer, 2011)(Carroll et al. 2007), promoting a methodological focus on hydrophilic proteins at the expense of the hydrophobic proteins that occupy the majority of the developing enamel matrix. Spectral counts of 2dpn (blue), 4dpn (yellow), and 6dpn (gray) enamel matrix were distinguished by color coding, and levels of significance were marked as * = $p<0.05$, ** = $p<0.01$, and *** = $p<0.001$ for comparisons between 2dpn and 4dpn data, and # = 0.05, ## = $p<0.01$, and ### = $p<0.001$ for comparisons between 4dpn and 6dpn data.

Figure 5 - Chapter 2 : Changes in mouse molar enamel matrix protein levels from postnatal day 1 – 8. **Reprinted with permission from Frontiers editorial office.**

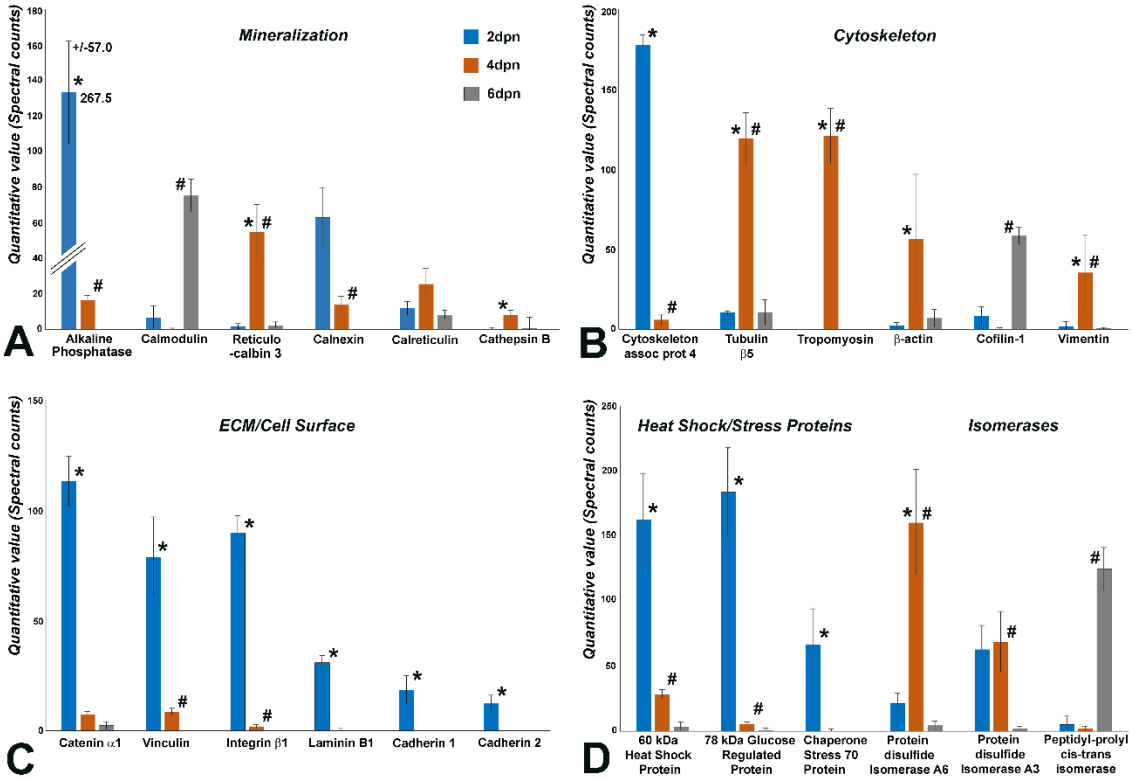

Figure 5 – Chapter 2. Changes in mouse molar enamel matrix protein levels from postnatal day 1 – 8. (A) Changes in amelogenin, ameloblastin, enamelin, MMP20, and carbonic anhydrase II, protein levels in enamel matrix preparations as revealed by Western blot. (B) Densitometric evaluation of protein levels in the Western blot shown in (A). (C) Sketch correlating changes in protein levels with changes in the enamel mineral phase.

Figure 1 - Chapter 3 : Electron micrographs illustrating subunit assembly and structural transformation during initial enamel crystal formation *in vivo*. **Reprinted with permission from Frontiers editorial office.**

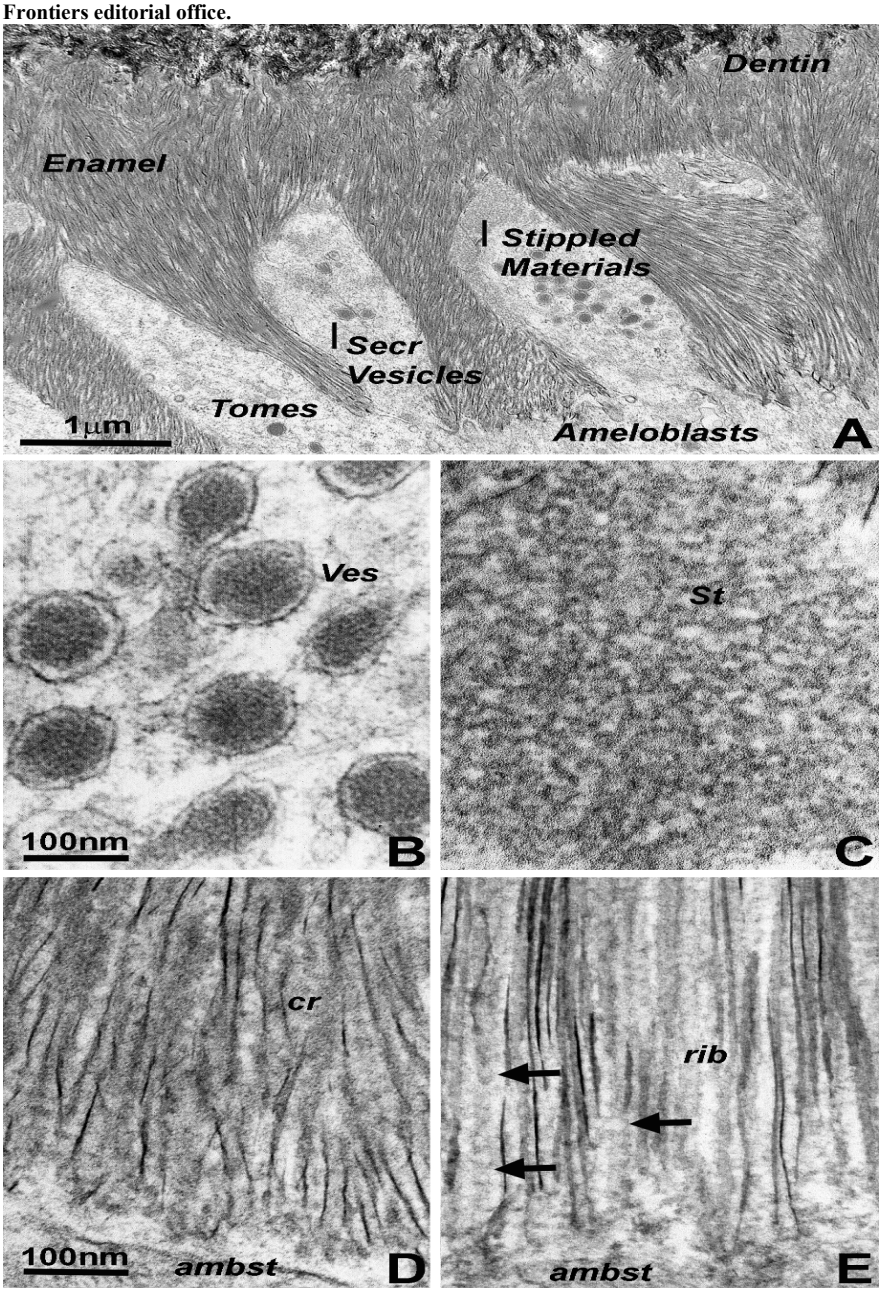

Figure 1 – Chapter 3. Electron micrographs illustrating subunit assembly and structural transformation during initial enamel crystal formation *in vivo*. (A) Interface between

Tomes' processes and early enamel prisms. Note the presence of enamel matrix carrying secretory vesicles (Secr Vesicles) within the Tomes' process (Tomes) at the apical ameloblast pole. Bulk deposits of an extracellular matrix containing stippled materials were recognized between the ameloblast cell membrane and the newly formed enamel crystal layer. The border between enamel (Enamel) and dentin (Dentin) was delineated by differences in crystal structure and organization). (B) High resolution ultrastructure of an ameloblast secretory vesicle (ves). (C) Ultrastructure and subunit organization of the non-mineralized enamel extracellular matrix commonly identified as stippled materials (St). (D, E) Ultramicrographs of early enamel crystals. (D) illustrates the somewhat disorganized arrangement of initial enamel crystals (cr), and (E) reveals ribbon-shaped assemblies (rib, arrows) of organic matter in between highly parallel rows of enamel crystals. Scale bar A = 1μm; B,C = 100nm; D,E = 100nm. The same scale bar applies for figures B – E.

Figure 2 - Chapter 3 : Constituents of first mandibular mouse molar enamel formation in organ culture as revealed by electron microscopy. **Reprinted with permission from Frontiers editorial office.**

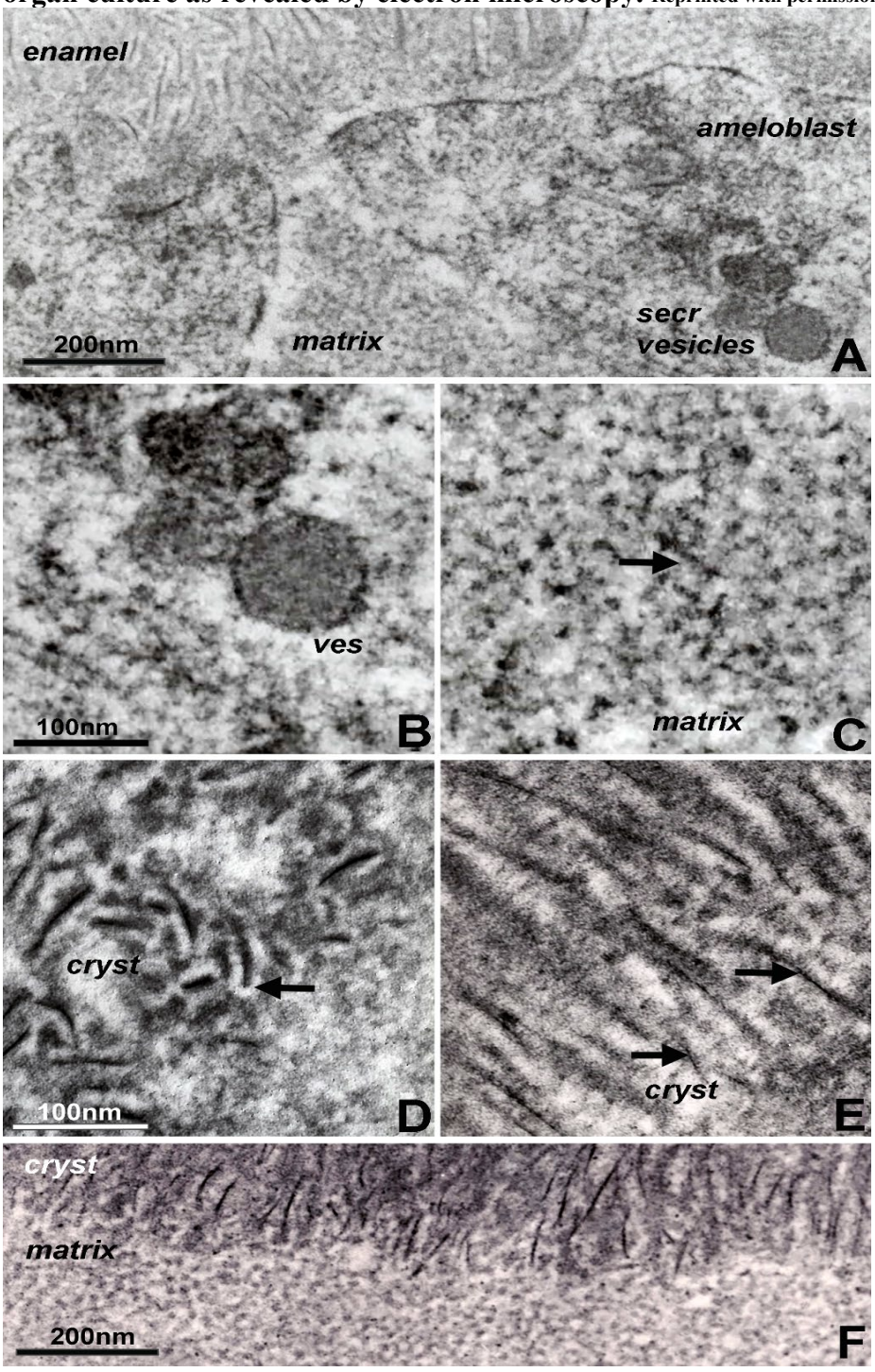

Figure 2 – Chapter 3. Constituents of first mandibular mouse molar enamel formation in organ culture as revealed by electron microscopy. Note the differences between Fig. 1 (*in vivo*) and Fig. 2 (*in vitro*). (A) Interface between apical ameloblast cell membrane (ameloblast), organic extracellular enamel matrix (matrix), and initial enamel crystal deposits (enamel). Note the secretory vesicles (secr vesicles) at the apical ameloblast pole. (B, C) High magnification ultrastructural comparison between enamel matrix structure within secretory vesicles (B) and extracellular matrix (C). The arrow in (C) points to electron dense mineral deposits as part of the supramolecular matrix framework. (D, E) Initial stages of enamel crystal (cryst) formation in organ culture. Note the electron opaque coat (arrow) surrounding initial crystal precipitates (D) and the electron dense particles (arrow) in immediate proximity of the elongated crystals (E). (F) Sharply delineated interface between non-crystallized organic matrix (matrix) and the initial crystallized enamel layer (cryst). Scale bar A = 200nm; B,C = 100nm; D,E = 100nm; F = 200nm. The same scale bar applies for figures B – E.

Figure 3 - Chapter 3 : Amelogenin protein self-assembly *in vitro*. **Reprinted with permission from Frontiers editorial office.**

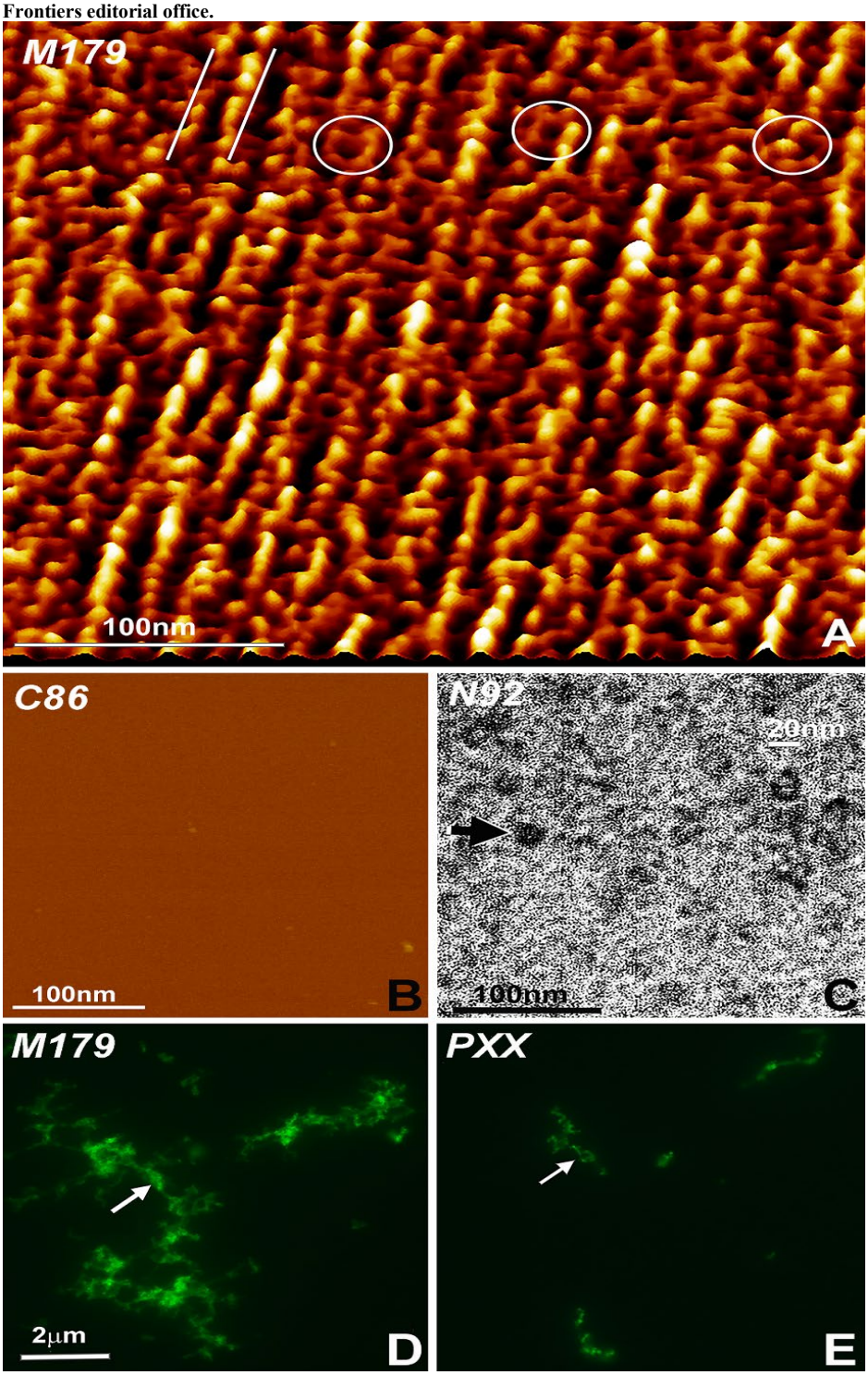

Figure 3 – Chapter 3. Amelogenin protein self-assembly *in vitro*. (A) AFM image of M179 amelogenin on freshly cut mica. Note the parallel rows of self-assembled amelogenin spheres (parallel white lines) next to hexagon-shaped, ring-like assemblies (white circles). (B) In contrast, C86 amelogenin on freshly cut mica did not reveal any prominent structural entities. (C) Oval shaped, N-terminal His-tagged amelogenin N92 assemblies (arrow) as revealed by Nickel-stain. (D) Fluorescently labeled, self-assembled full-length amelogenins in aqueous solution. (E) Fluorescently labeled, self-assembled amelogenin PXX33 polyproline repeat peptides in aqueous solution. The arrow points to elongated amelogenin structures (D,E). The same scale bar applies for figures D and E.

Figure 4 - Chapter 3 : Localization of amelogenin fragments in enamel organ, superficial, and deep enamel layers based on fractionated protein extraction and antibody recognition site. **Reprinted with permission from Frontiers editorial office.**

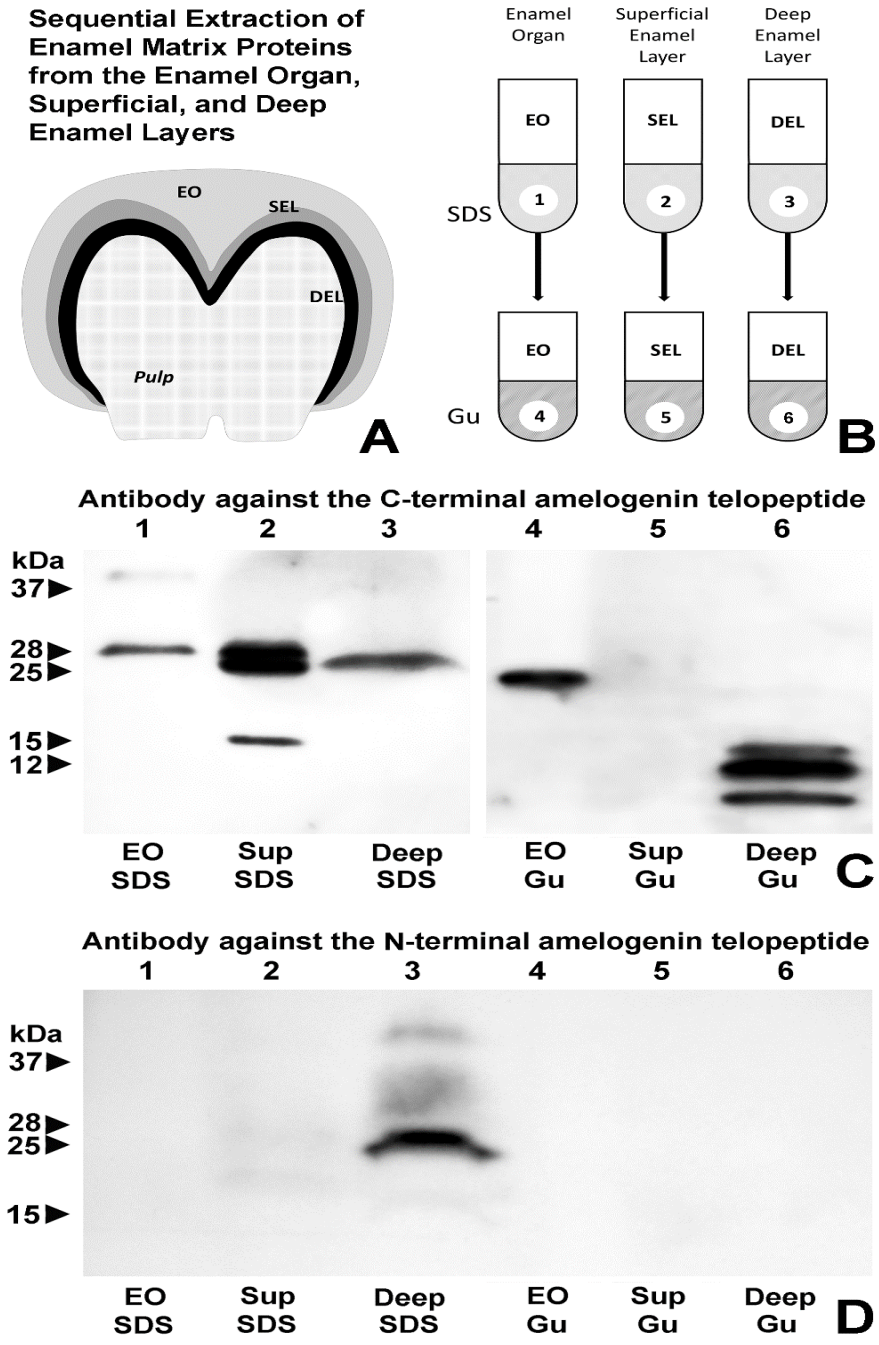

Figure 4 – Chapter 3. Localization of amelogenin fragments in enamel organ, superficial, and deep enamel layers based on fractionated protein extraction and antibody recognition site. (A) Porcine enamel organ dissection and preparation scheme. Enamel organ (EO), superficial enamel layer (SEL), and deep enamel layer (DEL) were separately collected for further analysis. (B) Fractionated enamel protein extraction procedure using sodium dodecylsulfate (SDS) as a first step and 4M guanidine HCl for subsequent extraction of the SDS-insoluble residue as a second step. (C) C-terminal amelogenin peptide antibody based Western blots of SDS extracts (SDS) or SDS residue guanidine extracts (Gu) of EO, SEL, and DEL enamel organ/enamel layer protein preparations. (D) N-terminal amelogenin peptide antibody based Western blot of SDS extracts (SDS) or SDS residue guanidine extracts (Gu) of EO, SEL, and DEL enamel organ/enamel layer protein preparations.

Figure 5 - Chapter 3 : Model explaining enamel crystal formation through matrix assembly and processing. Reprinted with permission from Frontiers editorial office.

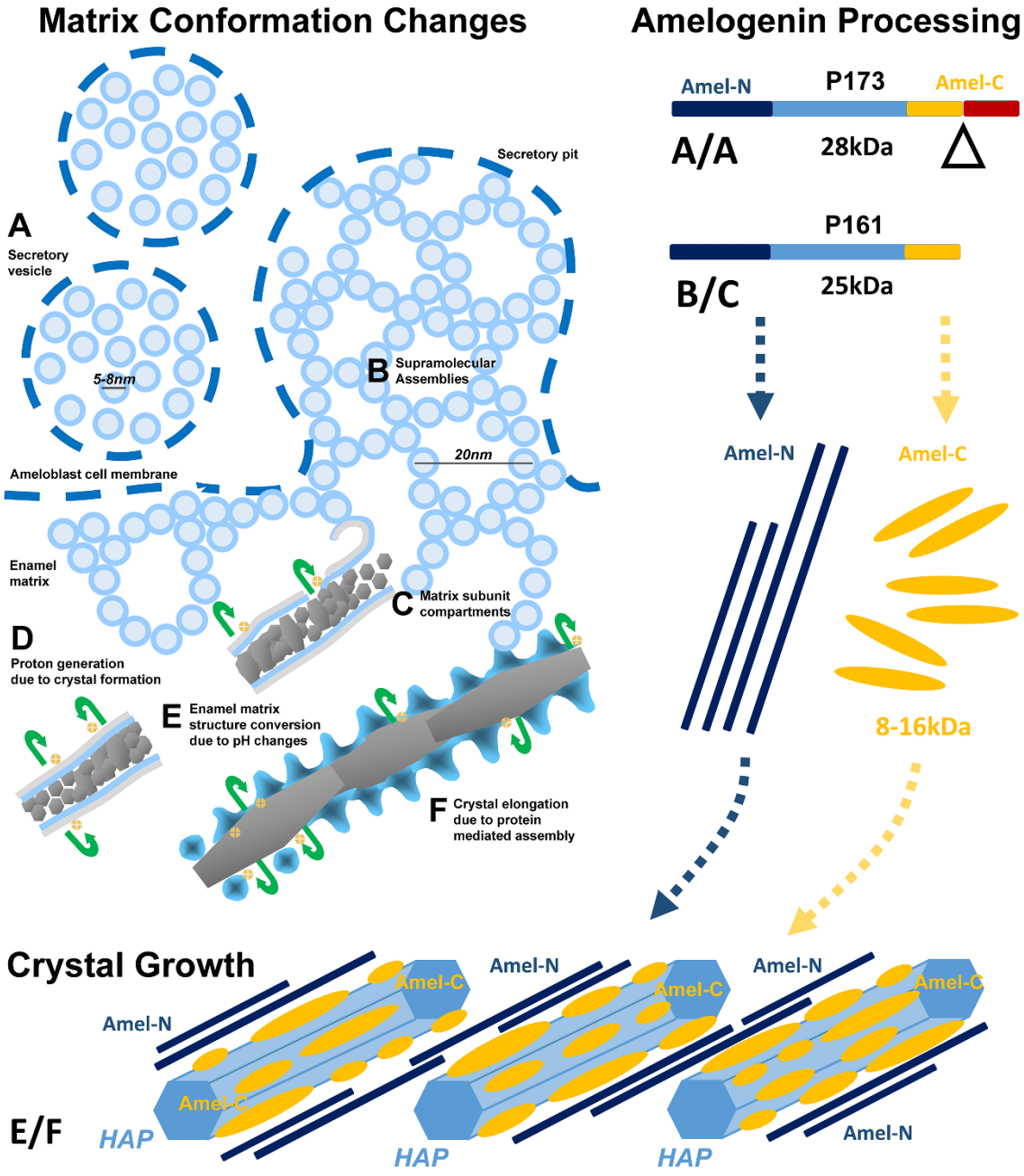

Figure 5 – Chapter 3. Model explaining enamel crystal formation through matrix assembly and processing. (A-F) Changes in matrix conformation. Enamel matrix assembly begins as 5-7 nm subunits within ameloblast secretory vesicles (A). Once secreted into the extracellular space, mineral-rich enamel proteins self-assemble as 20 nm diameter subunit compartments that provide the structural basis for orderly spaced enamel crystal nucleation (B,C). Proton generation during initial crystallization results in a dissociation of the stippled materials matrix and a "shedding" of enamel protein assemblies onto the surfaces of growing enamel hydroxyapatite crystals (E,F). **(A/A – B/C) Temporo-spatial amelogenin processing during enamel maturation.** (A/A) Full-length P173 amelogenins are exclusive to the enamel organ (Fig. 4C lane 1), where they are packaged into 5-8nm subunits within secretory vesicles (Figs. 1A,B, 2A,B). Upon entry into the enamel extracellular matrix, cleavage of the hydrophilic C-terminus generates P161 amelogenins (Fig. 4C lanes 2,3), and resulting hydrophobic interactions between P161 amelogenins trigger the formation of 20nm sized subunit compartments ("nanospheres", Figs. 1C, 2C) for the spacing of enamel crystal nucleation sites. **(E/F) N- and C-terminal amelogenins during enamel crystal formation and elongation.** Further processed amelogenin C-terminal fragments (Fig. 4C lane 6, 8-16kDa) are tightly associated with the elongating crystal surface (Figs. 1E, 2D-E) as revealed by guanidine extracts. In contrast, N-terminal amelogenins likely float in between elongating apatite crystals as they were only detected in SDS detergent extracts and not in the guanidine fraction (Fig. 4D).